



National Library
of Canada

Bibliothèque nationale
du Canada

Canadian Theses Service

Services des thèses canadiennes

Ottawa, Canada
K1A 0N4

CANADIAN THESES

THÈSES CANADIENNES

NOTICE

The quality of this microfiche is heavily dependent upon the quality of the original thesis submitted for microfilming. Every effort has been made to ensure the highest quality of reproduction possible.

If pages are missing, contact the university which granted the degree.

Some pages may have indistinct print especially if the original pages were typed with a poor typewriter ribbon or if the university sent us an inferior photocopy.

Previously copyrighted materials (journal articles, published tests, etc.) are not filmed.

Reproduction in full or in part of this film is governed by the Canadian Copyright Act, R.S.C. 1970, c. C-30. Please read the authorization forms which accompany this thesis.

THIS DISSERTATION
HAS BEEN MICROFILMED
EXACTLY AS RECEIVED

AVIS

La qualité de cette microfiche dépend grandement de la qualité de la thèse soumise au microfilmage. Nous avons tout fait pour assurer une qualité supérieure de reproduction.

S'il manque des pages, veuillez communiquer avec l'université qui a conféré le grade.

La qualité d'impression de certaines pages peut laisser à désirer, surtout si les pages originales ont été dactylographiées à l'aide d'un ruban usé ou si l'université nous a fait parvenir une photocopie de qualité inférieure.

Les documents qui font déjà l'objet d'un droit d'auteur (articles de revue, examens publiés, etc.) ne sont pas microfilmés.

La reproduction, même partielle, de ce microfilm est soumise à la Loi canadienne sur le droit d'auteur, SRC 1970, c. C-30. Veuillez prendre connaissance des formules d'autorisation qui accompagnent cette thèse.

LA THÈSE A ÉTÉ
MICROFILMÉE TELLE QUE
NOUS L'AVONS REÇUE



National Library of Canada

Bibliothèque nationale du Canada

Ottawa, Canada
K1A 0N4

TC -
IS 0-315-23297-8

CANADIAN THESES ON MICROFICHE-SERVICE - SERVICE DES THÈSES CANADIENNES SUR MICROFICHE

PERMISSION TO MICROFILM - AUTORISATION DE MICROFILMER

• Please print or type - Écrire en lettres moulées ou dactylographier

AUTHOR - AUTEUR

Full Name of Author - Nom complet de l'auteur

STARBUCK, Gordon R. Macdonald

Date of Birth - Date de naissance

30/12/1939

Canadian Citizen - Citoyen canadien

Yes No

Country of Birth - Lieu de naissance

Canada

Permanent Address - Residence fixe

104 Avenue D.G.
East London, Ont.
Canada

THESIS - THÈSE

Title of Thesis - Titre de la thèse

Thesis on the role of the...
Masters Thesis

Degree for which thesis was presented
Grade pour lequel cette thèse fut présentée

M.Sc.

Year this degree conferred
Année d'obtention de ce grade

1985

University - Université

U. of Alberta

Name of Supervisor - Nom du directeur de thèse

Dr. John A. ...

AUTHORIZATION - AUTORISATION

Permission is hereby granted to the NATIONAL LIBRARY OF CANADA to microfilm this thesis and to lend or sell copies of the film.

L'autorisation est, par la présente, accordée à la BIBLIOTHÈQUE NATIONALE DU CANADA de microfilmer cette thèse et de prêter ou de vendre des exemplaires du film.

The author reserves other publication rights, and neither the thesis nor extensive extracts from it may be printed or otherwise reproduced without the author's written permission

L'auteur se réserve les autres droits de publication, ni la thèse ni de longs extraits de celle-ci ne doivent être imprimés ou autrement reproduits sans l'autorisation écrite de l'auteur

ATTACH FORM TO THESIS - VEUILLEZ JOINDRE CE FORMULAIRE À LA THÈSE

Signature

[Handwritten Signature]

Date

01/15/95

THE UNIVERSITY OF ALBERTA

FEASIBILITY STUDIES FOR A HIGH EFFICIENCY MEDIUM ENERGY
DEUTERON POLARIMETER

by



KENTON RICHARD STARKO

A THESIS

SUBMITTED TO THE FACULTY OF GRADUATE STUDIES AND RESEARCH IN
PARTIAL FULFILMENT OF THE REQUIREMENTS FOR THE DEGREE OF
MASTER OF SCIENCE
IN
NUCLEAR PHYSICS

DEPARTMENT OF PHYSICS

EDMONTON, ALBERTA

FALL 1985

THE UNIVERSITY OF ALBERTA
RELEASE FORM

NAME OF AUTHOR: KENTON RICHARD STARKO
TITLE OF THESIS: FEASIBILITY STUDIES FOR A HIGH EFFICIENCY
MEDIUM ENERGY DEUTERON POLARIMETER
DEGREE: MASTER OF SCIENCE
YEAR THIS DEGREE GRANTED: 1985

Permission is hereby granted to the UNIVERSITY OF ALBERTA LIBRARY to reproduce single copies of this thesis and to lend or sell such copies for private, scholarly, or scientific research purposes only.

The author reserves other publication rights, and neither the thesis nor extensive extracts from it may be printed or otherwise reproduced without the authors written permission.

.....
Signature

Date

Permanent Address: 104 Laurier Drive
Edmonton, Alberta
Canada T5R-5P6

THE UNIVERSITY OF ALBERTA
FACULTY OF GRADUATE STUDIES AND RESEARCH

The undersigned certify that they have read and recommend to the Faculty of Graduate Studies and Research for acceptance a thesis entitled FEASIBILITY STUDIES FOR A HIGH EFFICIENCY MEDIUM ENERGY DEUTERON POLARIMETER submitted by Kenton Richard STARKO in partial fulfilment of the requirements for the degree of MASTER OF SCIENCE in Nuclear Physics.

John M. Cameron
.....
Supervisor

Douglas M. Sheppard
.....
John ...
.....
Richard ...
.....
External Examiner

Date :

Abstract

Spherical tensor analyzing powers iT_{11} , T_{20} , and T_{22} , have been measured for polarized deuteron inclusive scattering from targets of ${}^6\text{Li}$, ${}^{12}\text{C}$, ${}^{58}\text{Ni}$, ${}^{208}\text{Pb}$, and polarized deuteron elastic scattering from ${}^1\text{H}$, ${}^2\text{H}$, ${}^6\text{Li}$, ${}^{58}\text{Ni}$, and ${}^{208}\text{Pb}$ at energies of 191 and 395 MeV. Cartesian tensor analyzing powers A_y and A_{yy} as well as differential cross section have been measured for polarized deuterons scattered from ${}^{58}\text{Ni}$ at energies of 200, 400, and 700 MeV.

Values of the analyzing power T_{20} have been found to be of sufficient magnitude that a high efficiency medium energy deuteron polarimeter may be built based upon d-p elastic scattering. A large negative peak in the T_{20} curve between scattering angles of 85° and 148° in the center of momentum frame reaches nearly -0.6 at 191 MeV. The polarimeter, designed to measure deuteron tensor polarizations t_{20} , t_{21} , and t_{22} , at deuteron energies between 80 and 200 MeV, would have an efficiency of approximately 10^{-3} and a figure of merit for T_{20} of approximately 2×10^{-2} .

The vector analyzing powers iT_{11} are relatively large for nearly all measured elastic scatterings seen in this work.

Acknowledgements

I would first like to express my gratitude and appreciation to my supervisor Dr. John Cameron for his guidance and encouragement throughout the course of my work on this thesis. His attitude towards physics and producing successful results made this project a very satisfying one to be involved in.

I would also like to express my appreciation to Dr. Helmy Sherif for his guidance and assistance with my coursework and understanding of some theoretical aspects of nuclear physics which made it possible for me to complete this degree.

The many informative discussions with my colleagues Jon Johansson, Ronald Mitchell, Richard Tkachuk, Gerhard Lotz, Carl Chan, and Geoffry Edwards, proved to be invaluable to my education and I wish to express my appreciation to these people.

I would like to thank Dr. Michel Garçon for all his time spent assisting me with understanding the finer details of the experiments involved in this work.

Gratitude is also directed to my special friends outside of the physics community who on countless occasions helped relieve the pressures of the day.

Last but not least I would like to express my sincere appreciation to my parents for their consistent support during the course of my work on this degree.

Table of Contents

Chapter	Page
I Introduction	1
II Formalisms for the Description of Elastically Scattered Polarized Deuterons	5
1. Vector Polarization	5
2. Tensor Polarization	7
3. Polarized Deuteron Beams	10
4. Reaction Efficiency and Figure of Merit	15
III Experimental Methods and Analyses	19
1. The Radiography Experiment - June 1984	20
a). Method	20
b). Analysis	22
2. The SPES I Experiment	27
a). Method	27
b). Analysis	28
3. The Radiography Experiment - November 1983	29
a). Method	29
b). Analysis	30
IV Experimental Results	39
1. The Radiography Experiment - June 1984	39
2. The SPES I Experiment	40
3. The Radiography Experiment - November 1983	40
V Deuteron Tensor Polarimeters	71
1. Method of Determination of Deuteron Polarization	71
2. Low Energy Deuteron Polarimeters	75

3. Medium Energy Deuteron Polarimeter	77
Bibliography	86
References	87
Appendix 1	89
Appendix 2	90
Appendix 3	91
Appendix 4	92
Appendix 5	94

IV-14 :	d + Li	191 MeV	Inclusive Scattering	No Absorber	55
IV-15 :	d + Li	395 MeV	Inclusive Scattering	5.5 cm Fe Absorber	56
IV-16 :	d + Ni	200 MeV	$d\sigma/d\Omega$	2^+ State	57
IV-17 :	d + Ni	200 MeV	A_y	2^+ State	58
IV-18 :	d + Ni	200 MeV	A_{yy}	2^+ State	59
IV-19 :	d + Ni	400 MeV	$d\sigma/d\Omega$	2^+ State	60
IV-20 :	d + Ni	400 MeV	A_y	2^+ State	61
IV-21 :	d + Ni	400 MeV	A_{yy}	2^+ State	62
IV-22 :	d + Ni	700 MeV	$d\sigma/d\Omega$	2^+ State	63
IV-23 :	d + Ni	700 MeV	A_y	2^+ State	64
IV-24 :	d + Ni	700 MeV	A_{yy}	2^+ State	65
IV-25 :	d + d	191 MeV	Elastic Scattering		66
IV-26 :	d + d	395 MeV	Elastic Scattering		67
IV-27 :	d + p	191 MeV	Elastic Scattering		68
IV-28 :	d + p	395 MeV	Elastic Scattering		69
IV-29 :	d + p	differential cross section for various energies			70
V-1 :	d + p	80 MeV	Elastic Scattering		81
V-2 :	d + p	Elastic scattering kinematics			82
V-3 :	Deuteron energy distribution at the scattering point. Mean incident deuteron energy = 120 MeV				83
V-4 :	a) Distribution of all scattered particles as a function of θ (c.m.)				84
	b) Distribution of all detected events as a function of θ (c.m.)				
V-5 :	d + p	80 MeV			85
	a) Inclusive proton spectrum for laboratory proton angle = 15°				
	b) A_{yy} for breakup protons, inelastic, and elastic events				

Chapter I - Introduction

Since its discovery in 1932 the deuteron has been at the focus of much research. To justify this statement one has merely to remember that a complete knowledge of the deuteron's properties is required in order to determine the particle's wave function. Being the only stable two nucleon system, understanding the deuteron wave function is of primary importance in understanding the nuclear force.

Two angular momentum states are possible in the deuteron and they are the 3S_1 and 3D_1 states. The wave function is known to be predominantly S state, with about 4% D state. The percentage of D state (P_D) is a controversial figure, and many calculations have been done using different values for P_D . Inconsistency in these calculations as well as disagreement with experimental findings indicates that further information is needed in order to obtain a more reliable representation of the wave function. Some of this information is contained in the deuteron form factors.

There are two form factors needed to describe the non spherical deuteron. These are the electric and magnetic form factors, which are denoted by $A(q)$ and $B(q)$ respectively. Appendix 1 shows the relationships between these form factors and their constituent charge monopole, charge quadrupole and magnetic dipole form factors which are denoted $F_C(q)$, $F_Q(q)$, and $F_M(q)$. Each of these three functions of momentum transfer are Fourier transforms involving the S and D states of the deuteron wave function, and relevant nucleon form factors. $A(q)$ and $B(q)$ are defined such that the $q \rightarrow 0$ limits of $F_C(q)$ and $F_M(q)$ are the deuteron charge and magnetic moment. Explicit expressions for the deuteron form factors, along with a summary of deuteron properties, may be found in Appendix 1.

Deuteron form factors may be determined by measuring reaction observables in electron deuteron elastic scattering over a particular range of momentum transfer. Appendix 1 gives the relationship between the e-d reaction cross section and form factors A and B. From this relation it is seen that A and B may be determined easily by measuring the

From this relation it is seen that A and B may be determined easily by measuring the angular dependence of the reaction cross section, and that F_M is determined uniquely. To separate the form factors F_C and F_Q , it is however necessary to determine one additional linear combination. This may be done by a measurement of recoil deuteron polarization from the scattering.

Since deuterons are spin 1 particles, their polarization is described by a set of polarization tensors. Two of these sets will be described in detail in Chapter II. The set of such tensors which is convenient for determining deuteron form factors is the spherical tensors. Relationships between deuteron form factors and spherical tensor polarization parameters for electron deuteron scattering are given in Appendix 2.

As seen in Appendix 2, determination of tensor polarization observables from electron deuteron scattering is essential to allow separation of monopole charge and quadrupole charge form factors. Polarizations t_{20} and t_{21} are of particular interest due to the fact that if one of these is measured successfully, the previously unseparable product $F_C F_Q$ becomes separable. A method of determining these tensor polarizations is developed in Chapters II and III and involves first considering a reaction of the form $d + A \rightarrow d + A$. As deuteron beam polarizations are given by tensors, tensor analyzing powers must also be defined as is done in Chapter II. The cross section of a reaction of the above form is characterized partly by its unpolarized cross section and its tensor analyzing powers. To measure the initial deuteron beam tensor polarization it is necessary that the tensor analyzing powers of the target be known. Finding a target with sufficiently large analyzing power to measure the polarization of the deuteron from e-d scattering in an efficient manner is the essence of this work. It is the analyzing power T_{20} that is emphasized in the case of this experiment. Tensor analyzing powers for several targets were determined using the well known tensor polarized deuteron beam at Laboratoire National Saturne (LNS).

Chapter II also presents two quantities known as reaction efficiency and figure of merit. The reaction efficiency is directly related to the reaction cross section and target thickness, and the figure of merit gives a quantitative evaluation of how efficiently a particular target will measure a particular component of beam polarization.

The facility at LNS consists of a synchrotron capable of accelerating tensor polarized deuterons to energies ranging from 100 MeV to 2340 MeV. The duty cycle of the machine varies from 40% at 1 GeV to 15% at 2.7 GeV. On the site there are 7 experimental bunkers. Three of these contain magnetic spectrometers (named SPES), one of which is employed for some of the experiments dealt with in this work. The experimental facilities will be discussed in greater detail in chapter III.

The targets tested were ^{58}Ni , ^6Li , ^{12}C , ^{207}Pb , ^1H , and ^2H . Previous measurements of elastic scattering showed that ^{58}Ni may have large spherical tensor analyzing power because of its relatively large cartesian tensor analysing power. Experimental techniques and the methods of analysis for determining spherical tensor analyzing powers for deuteron - nucleus scattering are explained in detail in Chapter III. Determination of cartesian analyzing powers, and determination of spherical analyzing powers for d-d and d-p scattering will be briefly covered in this chapter. The results of the analyses for all targets tested will be presented in Chapter IV.

As another prerequisite to the understanding of operating principles of deuteron polarimeters, the method of decoding the collected data and determination of the deuteron beam tensor polarization is described in detail in Chapter V.

Several low energy deuteron tensor polarimeters have been constructed based upon the $d(d,p)t$ and $^3\text{He}(d,p)^4\text{He}$ reactions, however for energies greater than 100 MeV difficulties have previously been encountered in finding a suitable analyzing reaction. In Chapter V, tensor polarization analyzing reactions and deuteron polarimeters for low energies will be briefly discussed. Also included in this chapter is the outline of the

operating principles, requirements, and limitations of a medium energy deuteron polarimeter. Based on the results of d-p scattering at 200 MeV, it is shown that such a polarimeter may be successfully implemented in the e-d scattering experiment which is to take place at the Bates Linear Accelerator Center in 1986/87.

Chapter II - Formalisms for the Description of Elastically Scattered Polarized Deuterons.

1. Vector Polarization

When discussing polarization of particle beams or targets, spin 1/2 are most commonly dealt with. The polarization of such an ensemble of particles is characterized by a magnitude and direction, which is just the average value of the spin of the ensemble. It is clear that for spin 1/2 particles a vector is sufficient to describe the polarization.

The discussion [1] of polarization of spin 1/2 particles begins with the spin wave function

$$\chi = c_1 \alpha + c_2 \beta \quad \text{where } \alpha^t = [1 \ 0] \text{ and } \beta^t = [0 \ 1].$$

The superscript t represents the transposed matrix. c_1 and c_2 are complex constants, such that for normalization purposes, $|c_1|^2 + |c_2|^2 = 1$.

When dealing with an ensemble of particles in N different states, a density matrix is defined by $\rho = \sum_1^N \chi_i \chi_i^\dagger / N$. χ_i is the wave function of a particle in state τ . From the definition of the expectation value of an operator \mathbf{a} , $\langle \mathbf{a} \rangle = \chi^\dagger \mathbf{a} \chi$, it can be shown that for an ensemble of particles the expectation value of \mathbf{a} is given by $\langle \mathbf{a} \rangle = \text{tr}(\rho \mathbf{a})$.

The general density matrix for a beam of some polarization is given by:

$$\rho = [1 + \mathbf{P} \cdot \underline{\sigma}] / 2.$$

Here $\underline{\sigma} = \sigma_x \mathbf{i} + \sigma_y \mathbf{j} + \sigma_z \mathbf{k}$, σ_i are the Pauli spin 1/2 matrices, \mathbf{i} , \mathbf{j} , and \mathbf{k} are the cartesian unit vectors, and \mathbf{P} is an expansion parameter. If one considers $\langle \underline{\sigma} \rangle$:

$$\langle \underline{\sigma} \rangle = \text{tr}(\rho \underline{\sigma}) = \text{tr}((1 + \mathbf{P} \cdot \underline{\sigma}) \underline{\sigma}) / 2$$

Then $\langle \underline{\sigma} \rangle = \mathbf{P}$, as $\text{tr}(\underline{\sigma}) = 0$ and $\text{tr}(\mathbf{P} \cdot \underline{\sigma}) \underline{\sigma} = 2\mathbf{P}$. This suggests that \mathbf{P} is the polarization of the beam, and the density matrix for a beam of polarization \mathbf{P} is:

$$\rho = [1 + \mathbf{P} \cdot \underline{\sigma}] / 2 = \begin{bmatrix} (1 + P_z) / 2 & (P_x - iP_y) / 2 \\ (P_x + iP_y) / 2 & (1 - P_z) / 2 \end{bmatrix}$$

When a spin 1/2 particle undergoes an elastic scattering in the center of momentum (c.m.) frame, the only 2 things that may change are the direction and spin state of the particle. The final spin state $\chi_{(f)}$ is related to the initial spin state $\chi_{(i)}$ by the scattering matrix M :

$$\chi_{(f)} = M \chi_{(i)}$$

Consider the most general form of the scattering matrix for scattering from a spinless target. First define the coordinate system where

$$\mathbf{n} = (\mathbf{K} \times \mathbf{K}') / |\mathbf{K} \times \mathbf{K}'|, \mathbf{p} = (\mathbf{K} + \mathbf{K}') / |\mathbf{K} + \mathbf{K}'|, \text{ and } \mathbf{q} = (\mathbf{K} - \mathbf{K}') / |\mathbf{K} - \mathbf{K}'|$$

\mathbf{K} and \mathbf{K}' are the directions of the momentum of the incident particle before and after the scattering. The matrix is written:

$$M(\theta) = T + U \underline{\sigma} \cdot \mathbf{n}$$

This matrix is obtained by considering a complete set of basis matrices ($\mathbf{I}, \underline{\sigma}$), and combining these with the direction unit vectors \mathbf{n} , \mathbf{p} , and \mathbf{q} , in various ways in order to find the most general sum of tensors which may describe the scattering. Parity invariance is then incorporated to reduce the number of contributing terms.

The most general form of the scattering matrix for spin 1/2 scattering off spin 1/2 particles is:

$$M(\theta) = V + W \underline{\sigma}_1 \cdot \mathbf{n} \underline{\sigma}_2 \cdot \mathbf{n} + X (\underline{\sigma}_1 \cdot \mathbf{n} + \underline{\sigma}_2 \cdot \mathbf{n}) + Y \underline{\sigma}_1 \cdot \mathbf{p} \underline{\sigma}_2 \cdot \mathbf{p} + Z \underline{\sigma}_1 \cdot \mathbf{q} \underline{\sigma}_2 \cdot \mathbf{q}$$

where subscript i represents particle i . Incident and target particles are represented by $i = 1$ and 2 respectively. $V - Z$ are functions of θ . For this matrix, parity invariance and time reversal invariance are used to reduce the number of terms.

A final state density matrix is defined

$$\rho^{(f)} = \sum_1^N \chi_{\tau}^{(f)} \chi_{\tau}^{(f)\dagger} / N$$

$$= \sum_1^N (M \chi_{\tau}^{(i)}) (M \chi_{\tau}^{(i)\dagger}) / N$$

$$= \sum_1^N M \chi_{\tau}^{(i)} \chi_{\tau}^{(i)\dagger} M^{\dagger} / N$$

$$= M \rho^{(i)} M^{\dagger}, \text{ where } \rho^{(i)} \text{ is the initial state density matrix.}$$

For an unpolarized beam, $\rho^{(f)} = \mathbf{M}\mathbf{M}^\dagger / (2s_1 + 1)(2s_2 + 1)$, s_1 and s_2 are the values of the spins of incident and target particles. It may be shown further that the differential cross section for the elastic scattering is given by:

$$(\frac{d\sigma}{d\Omega})_0 = \text{tr}(\rho^{(f)})$$

For a polarized beam incident on an unpolarized target, the differential cross section may be written:

$$\begin{aligned} (\frac{d\sigma}{d\Omega})_p &= \text{tr}(\rho^{(f)}) \\ &= \text{tr}[\mathbf{M}(1 + \mathbf{P} \cdot \underline{\sigma}_1)\mathbf{M}^\dagger] / (2s_1 + 1)(2s_2 + 1) \\ &= [\text{tr}(\mathbf{M}\mathbf{M}^\dagger) + \mathbf{P} \cdot \text{tr}(\mathbf{M}\underline{\sigma}_1\mathbf{M}^\dagger)] / (2s_1 + 1)(2s_2 + 1) \end{aligned}$$

$$(\frac{d\sigma}{d\Omega})_p = (\frac{d\sigma}{d\Omega})_0 + \mathbf{P} \cdot \mathbf{A} (\frac{d\sigma}{d\Omega})_0$$

The vector \mathbf{A} is defined as the analyzing power of the reaction and is calculated from the scattering matrix as:

$$\mathbf{A} = \text{tr}(\mathbf{M}\underline{\sigma}_1\mathbf{M}^\dagger) / \text{tr}(\mathbf{M}\mathbf{M}^\dagger)$$

Note also that the polarization of a scattered beam may be written:

$$\mathbf{P} = \text{tr}(\mathbf{M}\mathbf{M}^\dagger\underline{\sigma}_1) / \text{tr}(\mathbf{M}\mathbf{M}^\dagger)$$

2. Tensor Polarization

When dealing with spin 1 particles the description of polarization requires second rank tensors. This is due to the three possible spin projections spin 1 particles have on a given quantization axis. Expressions similar to the spin 1/2 operators are defined for spin 1 particles, and the treatment of the spin 1 case will follow closely the framework of the spin 1/2 case. The discussion begins with the spin 1 wave function

$$\lambda = a_1\alpha + a_2\beta + a_3\delta$$

where $\alpha^t = [1\ 0\ 0]$, $\beta^t = [0\ 1\ 0]$, and $\delta^t = [0\ 0\ 1]$, and the a_i are complex constants.

For a spin 1 beam a density matrix is defined as in the spin 1/2 case:

$$\rho = \sum_t \lambda_t \lambda_t^\dagger / N$$

Note that there are nine quantities in this matrix, and the normalization requirement reduces the number of independent quantities to eight.

The spin operators used are the Pauli spin 1 operators and the 3 x 3 identity matrix. These operators do not however form a complete basis for the general 3 x 3 density matrix, and it is therefore necessary to define a complete set of tensors. The first set to be defined are the cartesian tensor operators [2]:

$$v_i = S_i \quad i = x, y, z \quad \text{II-1 a)}$$

$$v_{ij} = (3/2)(S_i S_j + S_j S_i) - 2\delta_{ij} \mathbf{1} \quad i, j = x, y, z \quad \text{II-1 b)}$$

$$S_x = \begin{bmatrix} 0 & 1/\sqrt{2} & 0 \\ 1/\sqrt{2} & 0 & 1/\sqrt{2} \\ 0 & 1/\sqrt{2} & 0 \end{bmatrix} \quad S_y = \begin{bmatrix} 0 & -i/\sqrt{2} & 0 \\ 1/\sqrt{2} & 0 & -i/\sqrt{2} \\ 0 & -i/\sqrt{2} & 0 \end{bmatrix} \quad S_z = \begin{bmatrix} 1 & 0 & 0 \\ 0 & 0 & 0 \\ 0 & 0 & -1 \end{bmatrix}$$

Note that

$$v_{xx} + v_{yy} + v_{zz} = 0,$$

as

$$\sum(S_i^2) = S(S+1) = 2 \mathbf{1}.$$

The expectation values of these tensors are defined in terms of the density matrix and represent polarizations of the spin 1 beam:

$$p_i = \text{tr}(\rho v_i) / \text{tr}(\rho) \quad \text{vector polarization}$$

$$p_{ij} = \text{tr}(\rho v_{ij}) / \text{tr}(\rho) \quad \text{tensor polarization}$$

It is desirable and more convenient for the purposes of this work to express this polarization in terms of tensors which transform under rotation like the spherical harmonics. A set of such tensors is presented by Lakin [3]:

$$\tau_{00} = \mathbf{1} \quad \text{II-2 a)}$$

$$\tau_{10} = \sqrt{3/2} S_z \quad \text{II-2 b)}$$

$$\tau_{11} = -\sqrt{3} (S_x + iS_y)/2 \quad \text{II-2 c)}$$

$$\tau_{20} = (3S_z^2 - 2\mathbf{1})/\sqrt{2} \quad \text{II-2 d)}$$

$$\tau_{21} = -\sqrt{3} \{ (S_x + iS_y)S_z + S_z (S_x + iS_y) \}/2 \quad \text{II-2 e)}$$

$$\tau_{22} = \sqrt{3} (S_x + iS_y)^2/2 \quad \text{II-2 f)}$$

and $\tau_{k-q} = (-1)^q \tau_{kq}^\dagger$ for $k = 0,1,2$ and $|q| \leq k$.

The polarizations ρ_{kq} are again defined in terms of the density matrix:

$$\rho_{kq} = \text{tr}(\rho \tau_{kq}) / \text{tr}(\rho)$$

Vector polarization is described by the above tensors ρ_{kq} when $k = 1$, and tensor polarization is the case of $k = 2$.

The cartesian and spherical polarization tensors are related by the the equations given in Appendix 2.

Analogous to the spin 1/2 case, a scattering matrix \mathbf{M} is defined and tensor analyzing powers are described in terms of this matrix and the density matrix. The algebra for this formalism will not be presented here due to its similarity to the spin 1/2 case.

The analyzing powers are denoted by A_i and A_{ij} in cartesian coordinates, and T_{kq} in spherical coordinates:

$$A_i = \text{Tr}(\mathbf{M} \mathbf{v}_i \mathbf{M}^\dagger) / \text{Tr}(\mathbf{M} \mathbf{M}^\dagger) \quad i = x, y, z$$

$$A_{ij} = \text{Tr}(\mathbf{M} \mathbf{v}_{ij} \mathbf{M}^\dagger) / \text{Tr}(\mathbf{M} \mathbf{M}^\dagger) \quad i, j = x, y, z$$

or

$$T_{kq} = \text{Tr}(\mathbf{M} \tau_{kq} \mathbf{M}^\dagger) / \text{Tr}(\mathbf{M} \mathbf{M}^\dagger) \quad k = 0, 1, 2, \quad |q| \leq k$$

3. Polarized Deuteron Beams

In the case of this work, the ensemble of particles is a polarized deuteron beam. Like the polarized deuteron beam at LNS, most polarized deuteron sources produce spin systems with cylindrical symmetry. This is the type of system which will be studied in this chapter. In designing a device which measures tensor polarization of a beam without symmetry, well known beams like the one at LNS are necessary for calibration, and for determining a suitable analyzer. These topics will be discussed in subsequent chapters.

The axially symmetric system is represented in Figure II-1 by N_+ particles having their spin projections oriented along a quantization axis ξ , N_- particles have their spin projections along $-\xi$ and N_0 particles have spin projections distributed axially symmetrically around, and perpendicular to ξ . The expectation values of the spins of particles in each orientation are for

$$N_0 / N_S, \quad \langle S_z \rangle = 0,$$

$$N_+ / N_S, \quad \langle S_z \rangle = +1,$$

$$N_- / N_S, \quad \langle S_z \rangle = -1,$$

where $N_S = N_0 + N_+ + N_-$.

Consider the above expectation values in determining the values of the spherical polarization tensors. Assuming normalization, the average value of the z component of spin is

$$\langle S_z \rangle = (N_+ - N_-) / N_S.$$

Terms containing $(S_x + iS_y)$ are zero due to the cylindrical symmetry. When these terms are substituted into the tensor relations, only two terms are different from zero:

$$\rho_{10} = \sqrt{3/2} \langle S_z \rangle = \sqrt{3/2} (N_+ - N_-) / N_S$$

$$\rho_{20} = \langle (3 S_z^2 - 2 \mathbf{1}) \rangle / \sqrt{2} = (N_S - 3N_0) / N_S \sqrt{2}$$

To investigate further the meaning of vector and tensor polarization, consider first the case where $\rho_{20} = 0$ (tensor polarization is zero). N_0 is required to be $N_S/3$. In this case

beam is purely vector polarized with

$$-\sqrt{2/3} \leq \rho_{10} \leq \sqrt{2/3}.$$

When $\rho_{10} = 0$, this is the case of pure tensor polarization. Here either $N_+ = N_-$ or $N_+ = N_- = 0$.

These two conditions result in

$$-\sqrt{2} \leq \rho_{20} \leq 1/\sqrt{2}.$$

The Madison Convention [4] has defined the coordinate to be system used throughout the remainder of this work. In this right handed coordinate system the positive z axis is taken along the direction of the momentum of the incoming particles, and the positive y axis is along $\mathbf{k}_{in} \times \mathbf{k}_{out}$.

Now consider a polarized beam of deuterons with quantization axis ξ aligned along the z axis of a cartesian coordinate system as in Figure 2. When ξ is rotated relative to z, the result will be a change in the values of ρ_{kq} . If ξ is rotated through the spherical polar angles β and ϕ , the new values of ρ_{kq} may be found using rotation **D** matrices as in Appendix 3. The results give values of the new spherical tensors which will be denoted

t_{kq} .

$$t_{00} = 1 \quad \text{II-3 a)}$$

$$t_{10} = \rho_{10} \cos(\beta) \quad \text{II-3 b)}$$

$$i t_{11} = \rho_{10} \sin(\beta) e^{i\phi} / \sqrt{2} \quad \text{II-3 c)}$$

$$t_{20} = \rho_{20} (3 \cos^2(\beta) - 1) / 2 \quad \text{II-3 d)}$$

$$t_{21} = -i \sqrt{3/2} \rho_{20} \sin(\beta) \cos(\beta) e^{i\phi} \quad \text{II-3 e)}$$

$$t_{22} = -\sqrt{3/8} \rho_{20} \sin^2(\beta) e^{i2\phi} \quad \text{II-3 f)}$$

Having developed the above relations, determination of the t_{kq} 's for the polarized deuteron beam at LNS follows. At LNS the quantization axis ξ is oriented such that $\beta = \pi/2$. The above tensors become:

$$t_{00} = 1 \quad \text{II-4 a)}$$

$$t_{10} = 0 \quad \text{II-4 b)}$$

$$i t_{11} = \rho_{10} [\cos(\phi) + i \sin(\phi)] / \sqrt{2} \quad \text{II-4 c)}$$

$$t_{20} = \rho_{20} / 2 \quad \text{II-4 d)}$$

$$t_{21} = 0 \quad \text{II-4 e)}$$

$$t_{22} = \sqrt{3}/8 \rho_{20} [\cos(2\phi) + i \sin(2\phi)] \quad \text{II-4 f)}$$

The cross section for a reaction in which tensor polarized particles are incident upon an unpolarized target is given by:

$$\sigma(\theta) = \sigma_0(\theta) \sum_{kq} t_{kq} T_{kq}^*(\theta)$$

where σ_0 is the unpolarized cross section, and θ is the angle that the scattered particle makes with the incident beam direction. Expanding this equation, observing parity conservation (see Appendix 4), one obtains:

$$\begin{aligned} \sigma(\theta) = \sigma_0(\theta) \{ & 1 + 2iT_{11}(\theta) \operatorname{Re}(it_{11}) + T_{20}(\theta) t_{20} \\ & + 2T_{21} \operatorname{Re}(t_{21}) + 2T_{22}(\theta) \operatorname{Re}(t_{22}) \} \quad \text{II-5 a)} \end{aligned}$$

From equations II-3 the above equation becomes the general cross section expression for a deuteron beam with axis ξ rotated through arbitrary spherical polar angles θ and ϕ :

$$\begin{aligned} \sigma(\theta) = \sigma_0(\theta) \{ & 1 + 2i\rho_{10} T_{11}(\theta) \sin(\theta) \cos(\phi) / \sqrt{2} \\ & + T_{20}(\theta) \rho_{20} (3\cos^2(\theta) - 1) / 2 \\ & + \sqrt{6} T_{21}(\theta) \rho_{20} \sin(\theta) \cos(\theta) \sin(\phi) \\ & - \sqrt{3}/2 T_{22}(\theta) \rho_{20} \sin^2(\theta) \cos(2\phi) \} \quad \text{II-5 b)} \end{aligned}$$

Using equations II-4 for the polarized beam at LNS, the cross section becomes:

$$\sigma(\theta) = \sigma_0(\theta) \{ 1 + 2iT_{11}(\theta) (\rho_{10} \cos(\phi) / \sqrt{2}) + \rho_{20} T_{20}(\theta) / 2 + 2T_{22} \sqrt{3}/8 \rho_{20} \cos(2\phi) \}$$

Which may be written:

$$\sigma(\theta) / \sigma_0(\theta) = 1 + \sqrt{2} i \rho_{10} T_{11} \cos(\phi) + \rho_{20} [T_{20} / 2 + \sqrt{3}/2 T_{22} \cos(2\phi)] \quad \text{II-5 c)}$$

This very important result allows the tensor analyzing powers T_{20} and T_{22} to be calculated. This is true because at LNS, the beam polarizations, ρ_{10} and ρ_{20} , may be made

to vary. The ion source has the capability of doing this through the application of various sets of 3 radio frequency (RF) transitions.

Selection of these states begins by using a sextupole magnetic field to select the electronic states $m_e = +1/2$ for deuterium atoms. After this is done, RF transitions are applied in order to produce switching between magnetic sublevels. This switching is done in a fashion that produces the desired nuclear polarization. The transitions are:

PT). A low field triple transition at 10.5 MHz:

1. $|1/2, 1\rangle \leftrightarrow |1/2, 1\rangle$
2. $|1/2, 0\rangle \leftrightarrow |1/2, 1\rangle$
3. $|-1/2, 1\rangle \leftrightarrow |-1/2, 1\rangle$

MT). A medium field double transition at 343 MHz:

4. $|1/2, 0\rangle \leftrightarrow |-1/2, 0\rangle$
5. $|1/2, -1\rangle \leftrightarrow |-1/2, 1\rangle$

GT). A high field single transition at 415 MHz:

6. $|1/2, 0\rangle \leftrightarrow |-1/2, 1\rangle$

The above states represent $|e^- \text{ spin state}, d \text{ spin state}\rangle$. The following table summarizes the state populations and maximum attainable values of polarization for all possible transition combinations. For maximum polarization to be obtained, the RF switching must be done in the order PT(\pm), MT(\pm), GT(\pm). The \pm sign represents RF on or off.

Beam Pulse No.	RF Transition			N_+	N_-	N_0	$(\rho_{10})_{\max}$	$(\rho_{20})_{\max}$
	PT	MT	GT					
1	-	-	+	1/3	0	0	$+1/\sqrt{6}$	$+1/\sqrt{2}$
2	+	-	+	1/3	2/3	0	$-1/\sqrt{6}$	$+1/\sqrt{2}$
3	-	+	+	1/3	0	2/3	$+1/\sqrt{6}$	$-1/\sqrt{2}$
4	+	+	+	0	1/3	2/3	$-1/\sqrt{6}$	$-1/\sqrt{2}$

Beam Pulse No.	RF Transition			N_1	N	N_0	$(\rho_{10})_{\max}$	$(\rho_{20})_{\max}$
	PT	MT	GT					
5	-	-	-	1/3	1/3	1/3	0	0
6	+	-	-	0	2/3	1/3	-2/√6	0
7	-	+	-	2/3	0	1/3	+2/√6	0
8	+	+	-	1/3	1/3	2/3	0	0

Note that the maximum possible values polarization shown here do not correspond to the theoretical maximums. The available RF transitions do not allow the maximum values to be achieved.

For this experiment, four of the eight possible polarization modes were to be pulsed consecutively as the deuteron beam was operated. If the cross section for beam pulse i is denoted by $\sigma_i(\theta)$, the cross section expression II-5 c) becomes:

$$\sigma_i(\theta)/\sigma_0(\theta) = 1 + \epsilon_{vi} \sqrt{2} \rho_{10} T_{11} \cos(\phi) + \epsilon_{ti} \rho_{20} [T_{20}/2 + \sqrt{3}/2 T_{22} \cos(2\phi)] \quad \text{II-6}$$

Where $\epsilon_{vi} = (-1)^{i+1}$, $\epsilon_{ti} = 1$ for $i = 1, 2$, and $\epsilon_{ti} = -1$ for $i = 3, 4$. Also defined for reasons to be seen is $\epsilon_{0i} = 1$ for $i = 1, 4$ and $\epsilon_{0i} = -1$ for $i = 2, 3$.

Note that it is possible to find the unpolarized cross section by the following:

$$(\sum_i \sigma_i) / \sigma_0 = 4.$$

Consider the combination

$$\begin{aligned} & (\sum_i \epsilon_{ti} \sigma_i) / \sigma_0 && \text{II-7} \\ & = 4 \rho_{20} [T_{20}/2 + \sqrt{3}/2 T_{22} \cos(2\phi)] \\ & = -2\sqrt{2} \rho_{20} A_{yy}. \end{aligned}$$

It is clear that the cartesian analyzing tensors are easily determined by measuring cross section as a function of beam polarization mode. If the cross sections are known as a function of ϕ and beam polarization mode, the above relation gives a straight line in

$\cos(2\phi)$, and from the slope and intercept of the line T_{22} and T_{20} may be determined.

Similarly

$$\begin{aligned} & (\sum_i \epsilon_{vi} \sigma_i) / \sigma_0 \\ & 4\sqrt{2} \rho_{10} iT_{11} \cos(\phi) \\ & - 4\sqrt{3/2} \rho_{10} A_y \end{aligned} \quad \text{II-8}$$

Also in this case, knowing the ϕ dependence makes it possible to determine iT_{11} from the slope of this line. A convenient relation involves a similar expression:

$$(\sum_i \epsilon_{0i} \sigma_i) / \sigma_0 = 0 \quad \text{II-9}$$

The next chapter deals with the experiments and experimental philosophies considered in carrying out these measurements.

2. Reaction Efficiency and Figure of Merit

When searching for a reaction analyzer at a certain energy as in the deuteron scattering dealt with in this work, it must be ensured that the reaction cross section is sufficiently large that enough data may be obtained in a reasonable amount of time. As the target thickness also influences the reaction rate, the efficiency ϵ of a scattering reaction is given by the product of the target thickness e (nuclei/cm²) and the differential cross section (cm²) for the reaction at that scattering angle. When considering a reaction where a range of scattering angle is used the efficiency clearly becomes

$$\epsilon = e \int_{\theta} (d\sigma/d\Omega)_{cm} d\Omega \quad \text{II-10}$$

where $d\Omega = 2\pi \sin(\theta) d\theta$.

The figure of merit is a quantity which gives some representation as to the accuracy in which an initial polarization may be measured from a given scattering experiment. Upon integration of equation II-5 b) over ϕ , a relation for the number of particles reacting as a function of θ may be found:

$$N(\theta) = N_0(0) (1 + t_{20} T_{20}(\theta))$$

Where N_0 is the number of particles reacting in the unpolarized case. Rearranging the above equation and differentiating, the error in t_{20} is found to be

$$\Delta t_{20} = 1 / T_{20}(\theta) \sqrt{N_0}$$

assuming the product $t_{20} T_{20}(\theta)$ is small. However N_0 is also given by

$$N_0 = N_{inc} e^{-\sigma} = N_{inc} F$$

N_{inc} is the number of particles incident on the target. This leads to the definition of the figure of merit for T_{20} at a given angle θ :

$$F_{20} = \sqrt{F} T_{20}$$

The error in t_{20} then becomes

$$\Delta t_{20} = 1 / F_{20} \sqrt{N_{inc}}$$

The value $\sqrt{N_{inc}}$ for this purpose may be treated as a constant and made as large as possible. Notice that Δt_{20} is inversely proportional to the figure of merit. This relation demonstrates the necessity for large F_{20} . If the value is to be calculated for a range of θ a simple integration is performed:

$$F_{20}^2 = e \int_{\theta} (d\sigma/d\Omega)_{cm} T_{20}^2 d\Omega \quad \text{II-11}$$

Similar calculations are done to find the other F_{kq} 's.

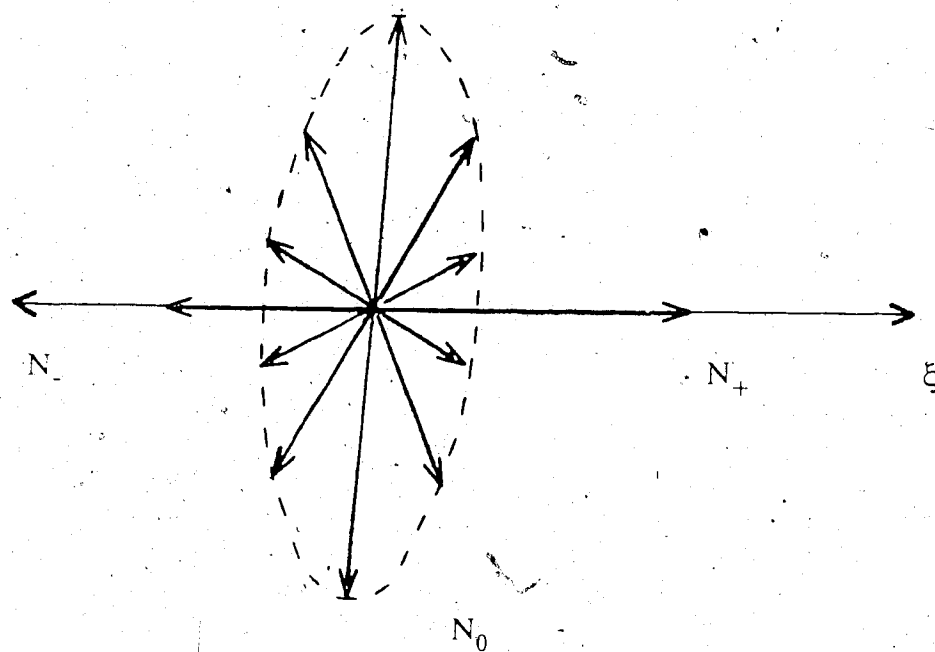


Figure II-1 : Possible orientations of spin projection for spin 1 particles

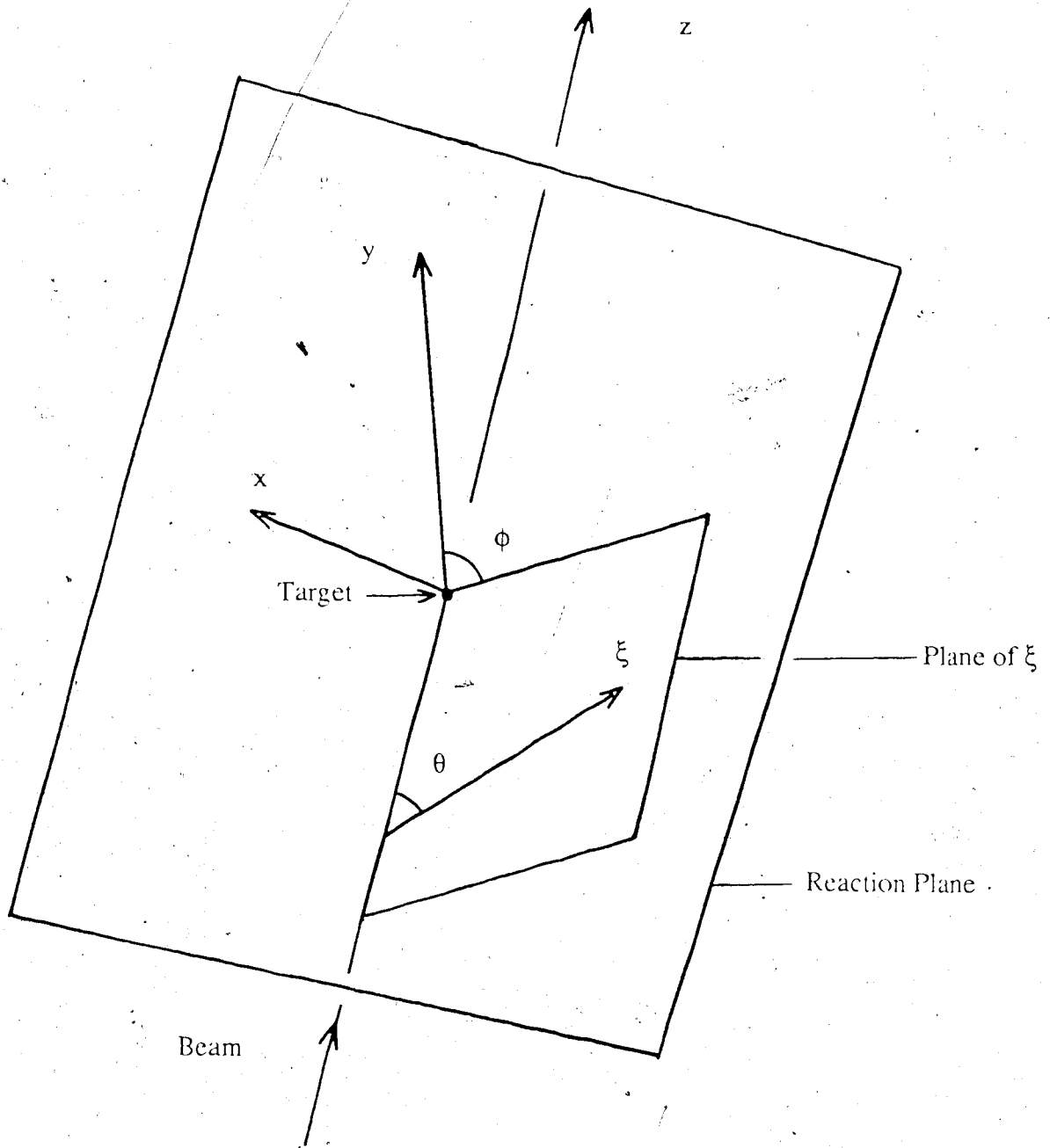


Figure II-2 : Rotation of axis ξ through spherical polar angles ϕ and β relative to z .

Chapter III - Experimental Methods and Analyses

Experiments to measure cartesian analyzing powers (A_y, A_{yy}) and spherical analyzing powers ($iT_{11}, T_{20},$ and T_{22}) were carried out separately at LNS over the course of 1983,84. The A's were determined for 200, 400, and 700 MeV tensor polarized deuterons on targets of $^{40}\text{Ca}, ^{58}\text{Ni},$ and ^{16}O using the SPES I magnetic spectrometer. These cartesian analyzing powers were determined for the elastic scattering off each nucleus, and inelastic scattering (2^+ state) off ^{58}Ni . The tensor analyzing powers were measured for 191 and 395 MeV polarized deuterons incident on targets of $^6\text{Li}, ^{12}\text{C}, ^{58}\text{Ni}, ^{207}\text{Pb}, ^2\text{H},$ and ^1H . The scattering for these measurements was inclusive and the experiment utilized the "radiography device". Figure III-1 shows a layout of the experimental facility at LNS, including SPES I and the radiography area. The emphasis of this chapter is on the details and analysis of the run in June 1984 which utilized the radiography device. Brief descriptions of the other experimental runs and their analyses are also found in this chapter.

For each of the above experiments, the polarized beam was produced in the atomic beam source "Hyperion". The source produces a 385 keV beam, which is accelerated to 10 MeV in a linac, then injected into the Saturne synchrotron ring. Hyperion is capable of producing a beam which is approximately 82% tensor polarized and nearly 100% vector polarized. The values of $(\rho_{10})_{\text{max}}$ and $(\rho_{20})_{\text{max}}$ for these experiments have been determined to be 0.394 and 0.581 respectively. This measurement was done at 385 keV using a low energy polarimeter which is described in Chapter V. Studies [5] have shown that the depolarization effects during the subsequent acceleration are negligible. For more information on the polarized deuteron source see Reference [6].

1. The Radiography Experiment - June 1984

a). Method

The radiography device was designed by a group at LNS primarily for use in tomography. Presented in this work are some aspects of the components of the system and system operating modes, however for greater detail see reference [2]. The device is a combination of wire chambers and plastic scintillators set in the configuration of Figure III-2.

Front end wire chambers WC1 and WC2 have x and y planes of 160 wires each. The wire spacing is 1.27 mm and the resolution for each plane is 0.635 mm. Chambers WC3 and WC4 also have x and y planes of 512 wires each. Here the wire spacing is 2 mm and the position resolution for each plane is 1.5 mm. In each chamber the gas mixture is 35% ethane and 65% argon. The wire chambers give particle trajectory coordinates which are of course essential in determining the cross section θ and ϕ dependence. Raytracing procedures which determine the origin of the scattered particle within the target are also employed in order to eliminate particles which have undergone excessive multiple scattering. This will be discussed in detail in the following section.

Iron absorbers of variable thickness were available for the purpose of eliminating data contaminating protons produced from deuteron breakup. The range of 100 MeV protons in iron is 1.42 cm, and the range of 200 MeV deuterons is approximately twice this. At incident deuteron energies of 200 MeV sheets of iron 1.5 cm or 1.8 cm thick were placed between WC4 and S3 for certain runs depending upon on line results. This would have the effect of cutting out breakup protons and reducing the deuteron energy to about 110 MeV. The range data is obtained from Reference [8]. Note that the degradation of the deuteron energy occurs after the scattering and therefore has no effect on determination of the analyzing powers. Similarly for the 400 MeV run a 5.5 cm thick sheet of iron was

available. The range of 200 MeV protons in iron is 4.7 cm. and deuterons passing through the absorber will exit with an energy of about 240 MeV. It is also important to note that the absorber is located downstream of the wire chambers so that multiple scattering which has occurred in the iron is not significant to position measurements.

Scintillators S1 and S2 are 5 mm thick and each of S3, S4 and S5 are 10 mm thick. Multiple scattering through the apparatus upstream of WC4, and the position resolution of the wire chambers are both expected to have negligible contributions to the error in the analyzing powers compared to the statistical errors in the experiment.

The parts of the system not designed by the Saclay group are the four large plastic scintillators (denoted "Alberta detectors" in Figure III-2) at the downstream end of the arrangement. Each NE 102 scintillator block is coupled to two RCA 4522 5" photomultiplier tubes and set in a metal housing. The solid angle covered by all four detectors added up to 0.5125% of the total solid angle or 0.0644 steradians and the positions of these detectors are illustrated in Figure III-3. The scintillators were used for energy determination, and were calibrated relative to each other by adjusting the 2 associated photomultiplier voltages V1 and V2 for each scintillator. The calibration was done such that for a ^{90}Sr source (2.27 MeV β) set on the surface of the counter, the phototube gains were made constant. Figure III-4 shows the calibration curves for the Alberta detectors. The energy resolution of these scintillators is about 3%. A typical energy spectrum for 191 MeV deuterons is shown in Figure III-5. The detectors are denoted D (droit), G (gauche), B (bas), and H (haut), for right, left, bottom, and top positions. The photomultiplier voltages are denoted D1, D2, G1, G2, etc. The output signals from each photomultiplier tube are added, sent to an ADC, then to the Saclay designed electronic signal processing system [7].

The electronics trigger utilizes some or all of the plastic scintillators. It is possible to include or exclude the Alberta detectors in the triggering mode. In either case trigger

requirements were coincidence between S1, S2, S3 or S4, and not S5.

b). Analysis

Software for data acquisition and analysis for the radio experiment was written by the group at Saclay. The computer used was a machine designed and built by DPh-N/ME of Saclay known as the Satellite d'Acquisition Rapide (SAR). This computer is a relatively fast unit having a cycle time of 280 nS, which makes for more efficient data acquisition and processing. The data acquisition software was written in machine language for use on the SAR. During each beam-pulse data events were accumulated in block memory in the form of a scaler block of 13 words followed by an event block of an undetermined number of words. Between beam bursts these data were transferred to the SAR and then on to Magnetic tape. The scaler and event blocks are processed by the analyzing software either on or off line as described in the following text. Further information on the data acquisition system and methodology is given in Reference [7].

The main program for the off line analysis, referred to here as "FORDEP", was also written in machine language for use on the SAR. The on line analysis is similar to the off line analysis and will not be discussed in this work. The main function of FORDEP is to read the blocks on the data tapes and control the calling of Fortran subroutines which process the data. Immediately after FORDEP reads the first scaler block, the subroutine "SUBECH" is called. This routine examines the scalers and decides whether to use the following event block or not, based upon several tests and comparisons made. The pertinent scalers from the scaler block are:

- run number
- beam polarization state = i
- number of energy words from Alberta detectors

- S1 S2 coincidence = S1S2
- S1 S2 accidental coincidence = S1S2AC
- number of events which satisfy trigger requirements = NTR
- number of events read by electronics after dead time = NATM
- number of events rejected by electronics
- number of events accepted by electronics
- number of events passed to the SAR

The first test is to see if the run number on the tape matches the run number expected. The next tests check that the trigger rate is not too great nor too low, and that the electronics dead time, TM (temps mort), is not too large. TM is calculated by dividing the number of events which satisfy the trigger requirements by the number of events actually processed by the electronics. Further checks include testing to ensure that the beam polarization is correct. If a scaler block passes all these tests, scalers recording number of accepted events are incremented, and control returns to FORDEP. If one of these tests fails, a certain scaler referring to that test is incremented by 1 immediately after the test is failed, and control returns to FORDEP.

If FORDEP finds that the previous scaler block has passed all the tests, the following event block is read and the event processing routine "ISABELLE" is called to use the data from that event block. ISABELLE is called once per event in the event block and manipulates the event data only once each time it is called. If the previous scaler block has not passed all the tests, the next event block is read but ISABELLE is not called. Reading the next scaler block continues the cycle.

The function of ISABELLE is to increment histograms of certain parameters determined from data which has been read from the event block. The parameters are related to positions of the trajectories of incident and scattered particles and are determined from

raytracing procedures. Since this particular experiment deals with deuteron nucleus scattering only one particle, the deuteron, is expected to be detected at the rear wire chambers. The first parameter, DDM, is the value of the shortest distance between incident and scattered particle trajectories. This value gives a representation of the total multiple scattering incurred by the incident and scattered particles. Using the unprocessed wire chamber coordinates to find the actual wire chamber coordinates, DDM may be calculated. When calculating the actual coordinates from the raw values, corrections are made only for the physical offsets of the wire chambers. The actual wire chamber coordinates are used to find the partial derivatives of x and y with respect to z for incident and scattered particles. These derivatives are used along with the wire chamber coordinates to find the x and y values of the particle trajectories at the target plane $z = 0$. Simple analytic geometry then combines all of this information to find DDM. Once this value is calculated, histograms of it are incremented and a comparison between this value and a maximum acceptable value for multiple scattering is made. For this analysis the maximum acceptable value of DDM was 4 mm.

The midpoint of the segment DDM is then calculated and the three dimensions of position within the target where the scattering took place are determined. Histograms of these positions are also incremented. Comparisons with minimum values and maximum values are then made. The final histograms produced are the number of events occurring as functions of the scattering angles θ and ϕ .

The final segment of the subroutine ISABELLE increments one cell of a 3 dimensional array A, which is the array which makes calculation of the analyzing powers feasible. In Chapter II it was shown that if the relative cross sections for scattering for different polarizations were known as a function of ϕ , analyzing powers could be determined. If the 360° of ϕ are divided into equal segments (bins), graphs of relative cross sections versus ϕ may be plotted in order to determine the ϕ dependence for different angles of θ . For this

run ϕ was divided into 10° bins and θ was divided into 4° bins. The dimensions of A are polarization mode i, θ bin, and ϕ bin. Only events which are not cut out by comparisons made throughout ISABELLE actually increment A. After this segment is complete, control returns to FORDEP.

After the histograms are produced, it is possible to reset the comparison values if necessary and rerun through FORDEP, SUBECH, and ISABELLE.

Once all the events in every event block are read, FORDEP then may call the subroutine DEPOU which is the actual analyzing routine that calculates the analyzing powers. As well as manipulating the data in array A in order to calculate the analyzing powers, this subroutine also summarizes information such as run number, scalers from SUBECH, and where the histogram cuts have been placed.

In order to determine the analyzing powers some simple preliminary calculations must be done. First is the calculation of the total S1S2 coincidence rate for real events which requires subtracting the accidentals rate from the measured S1S2 coincidence. The calculation of total electronics dead time TM follows. In order to normalize the calculations to account for systematic asymmetries in electronics dead time or accidentals rate as a function of beam polarization, the constant F_i is determined for each polarization mode. It is defined as:

$$F_i = (S1S2) (NTR_i) / 4 (TM) (NATM_i) \dagger [S1S2_i - S1S2AC_i]$$

where the subscripted variables refer to the the value of that variable for polarization mode i (recall i = 1 - 4). This constant is designed to remove systematic errors as a function of polarization mode, and is used in subsequent calculations.

Since cross sections for different polarization modes are not directly measured, relative numbers of counts (normalized) for each state are used to find the necessary ratios. The following ratios are defined:

$$R_\alpha = \sum_i \epsilon_{\alpha i} F_i N_i / \sum_i F_i N_i$$

$\epsilon_{\alpha i}$ refers to the constant as defined for equation II 6, and $\alpha = v, t, \text{ or } 0$.

So

$$R_v = 12.229 T_{11} \cos(\phi),$$

$$R_t = 2.324 [T_{20}/2 + \sqrt{3}/2 T_{22} \cos(2\phi)],$$

and $R_0 = 0$.

The ratios R_{α} and their errors are then calculated for each ϕ bin. Note that the utilization of 10° ϕ bins was shown to be optimum by the LNS group before the run. Once R_{α} and ΔR_{α} are calculated, χ^2 linear regression is implemented to calculate the slope and intercept of R_v and R_t in order to determine the T_{ij} 's. The linear regression uses the average value of $\cos(\phi)$ or $\cos(2\phi)$ for a ϕ bin as the x coordinate to be plotted for that particular ϕ bin. The errors in T_{ij} are determined as well as the correlation of the errors in T_{20} and T_{22} . The χ^2 value is also calculated for each T_{ij} to determine the closeness of fit. The procedure for doing these calculations is demonstrated in Appendix 5.

The determination of the T_{ij} 's was done separately for each θ bin. The number of counts are recorded as a function of θ for each bin. A weighted average of counts is taken in order to determine the best value of θ for that bin.

A separate analysis utilized the data from the Alberta detectors in order to attempt to select elastic scattering events. The detectors, located at $\phi = 0^\circ, 90^\circ, 180^\circ,$ and 270° , occupied the ϕ range of $\pm 12^\circ$ on either side of these positions. They were located in the θ segment between approximately 17° and 28° . This analysis used the same method as in the inclusive scattering, however the detector positioning allows calculation of the analyzing powers using only four ϕ bins. The data from these energy counters was used to form energy spectra for the reactants. After formation of these histograms, windows which included the elastic peak were selected. The data which fell within the windows was then used for the analysis. No compensation was made for inelastic events which were accumulated in the selected region. The amount of data recorded was limited by the

relatively small solid angle occupied by the Alberta detectors, and is also presented in Chapter IV.

2. The SPES I Experiment

a). Experimental Method

This experiment was performed in order to determine the cartesian tensor analyzing powers and differential cross sections for deuteron scattering off the forementioned nuclei. The spectrometer has a solid angle acceptance of 3 msr, and can move over an angular field from $\theta = 0^\circ$ to 80° . It will accept a maximum momentum of 2.3 GeV, and analyze a range of momentum $\Delta p/p = 4\%$. The dispersion for a momentum range $\Delta p/p = 1\%$ is 15 cm. The momentum resolution of the machine is 0.7×10^{-4} . A schematic of the SPES I line is shown in Figure III-6. For further details on SPES I see Reference [9].

The lack of ability of SPES I to measure ϕ dependence is why spherical analyzing powers cannot be measured. However as seen from the relations in Appendix 2 it is possible to measure values proportional to $iT_{11} \cos(\phi)$ and $[T_{20}/2 + \sqrt{3}/2 T_{22} \cos(2\phi)]$ (proportional to A_y and A_{yy}) for a constant value of ϕ . In the case of this experiment, $\phi = 0^\circ$.

In order to monitor the beam intensity as a function of energy, polarization mode, or any other factor, a monitor known as M1 is used. This monitor is a scintillator placed at an appropriate angle above, and facing the target. It is absolutely calibrated by doing a run with a ^{12}C disk placed in the beam upstream of the target for a measured length of time. After this short run, ^{11}C production in the target is measured through the ^{11}C positron decay. The cross section of the $^{12}\text{C}(d, ^{11}\text{C})X$ reaction is well known, therefore the beam intensity may be calculated.

b). Analysis

Again for this experiment the data acquisition software was written by the LNS group for use on the SAR. Only the method of processing the raw data into analyzing powers and cross sections will be outlined here. The same software was used in analyzing the elastic scattering data as was used in the analysis of the 2^+ state.

The analysis begins by accumulating the data in several histograms for each of the 4 different polarization modes. The histograms include time of flight (TOF), scattering angle, and momentum. There are selection windows within the software which cause the noninclusion of certain data in the momentum histograms if the data falls in an unselected region in the other 2 histograms. For example if the TOF window falls over a certain region, when the data tape is read by the software, the counts which fall in the TOF window will not increment the momentum histogram. The opposite is true for the scattering angle window. This implies that the data tapes should be read once to set the windows and once to accumulate the momentum histograms.

Once the momentum histograms are accumulated the actual determination of the analyzing powers may commence. As done several times to this point, combinations of the normalized number of counts must be added in the prescribed manner to find the values of the appropriate tensors.

Normalization of the number of counts is done by the following calculation:

$$N_i' = N_i \cdot TM_i / M1_i^{COR}$$

where

$$M1_i^{COR} = M1_i / (1 + \epsilon_{vi}\alpha + \epsilon_{ti}\beta)$$

also ϵ_{vi} and ϵ_{ti} are the vector and tensor polarization constants as given in equation II-6.

Determination of dead time TM for each polarization mode is calculated in the LNS software from electronics dead time. $M1_i$ is the time normalized M1 monitor count for beam polarization i , and $M1_i^{COR}$ is the corrected value of the M1 monitor reading due to

effects on this monitor due to beam polarization. The values of α and β are dependent upon target and beam energy, and were determined by a group from L'Institut des Sciences Nucleaires, Grenoble, France.

The quantity N_i in the above expression is the raw number of counts for polarization mode i . This number is found by counting the number of counts in the peak of interest on the momentum histogram. This is easily accomplished for elastic scattering or any of the first few excited states from the available software. Figure III-7 shows an example of the momentum histograms and the selection window. It is clear that the high resolution of the spectrometer leaves no room for ambiguity in separating the peaks of any given state.

Given the maximum available beam polarizations,

$$A_{yy} = -2.434 \frac{\sum_i \epsilon_{ti} N_i'}{\sum_i N_i'}$$

and

$$A_y = 2.072 \frac{\sum_i \epsilon_{vi} N_i'}{\sum_i N_i'}$$

In order to determine the differential cross section, the following relationship is used:

$$d\sigma_0/d\Omega_{cm} = [\sum_i N_i' TM_i / M1_i^{cor}] [130/\Delta\phi] [2.71/\Delta\theta] [JAC / 4 d\Omega TGT CAL]$$

where $1 / [130/\Delta\phi] [2.71/\Delta\theta]$ = fraction of available solid angle used

$d\Omega / [130/\Delta\phi] [2.71/\Delta\theta]$ = solid angle used,

TGT = target thickness (nuclei / cm²)

CAL = relationship between 1 count from M1 and no. of particles
(from ¹²C(d,11C)X calibration)

JAC = $\Delta\Omega_{cm}(\theta) / \Delta\Omega_{lab}(\theta)$

3. The Radiography Experiment - November 1983

a). Experimental Method

This run was the first attempt to measure spherical tensor analyzing powers at LNS.

The apparatus used in this run was similar to the run of June 1984, however the one difference in the setup was that the target was placed closer to the large wire chambers WC3 and WC4. This difference allowed larger scattering angles to be measured for the dd and dp scattering. For dp or dd scattering it is necessary to measure both scattered and recoil particles. The read out electronics have been designed such that when two particle trajectories fall within a 32 mm wide read out section, only one particle will be seen. As seen in the next section, this fact implies that some inefficiencies will occur at angles of $\phi = 0^\circ, 90^\circ, 180^\circ, \text{ and } 270^\circ$.

The Alberta energy detectors were absent for this run.

b). Analysis

The analysis for this run was also very similar to the analysis of the June 1984 run. The difference between the analyses of the two runs was that for dd and dp scattering the requirement of coplanarity of incident, scattered, and recoil particles was incorporated. When only one particle was detected, the event was rejected. The inability to detect 2 particles near $\phi = 0^\circ, 90^\circ, 180^\circ, \text{ and } 270^\circ$, resulted in any good events in these regions being rejected.

1.6° was the maximum acceptable value that the scattered and recoil planes could make with each other. The angular bin sizes were set at $\theta = 8^\circ$ for dd scattering, and $\theta = 12^\circ$ for dp scattering. The ϕ bins were 10° .

The kinematical angular correlation is necessary for the identification of elastically scattered deuterons and protons, however at 30° , deuterons and protons cannot be distinguished. This results in an ambiguity between ϕ and $\phi + \pi$. This ambiguity renders determination of iT_{11} impossible, however has no effect on calculation of the tensor analyzing powers.

Background due to carbon content in the CH_2 and CD_2 targets, and deuteron breakup

were subtracted from each θ and ϕ bin for each beam polarization. Estimated background was 2 - 15% for dp scattering and 10 - 30% for the dd case.

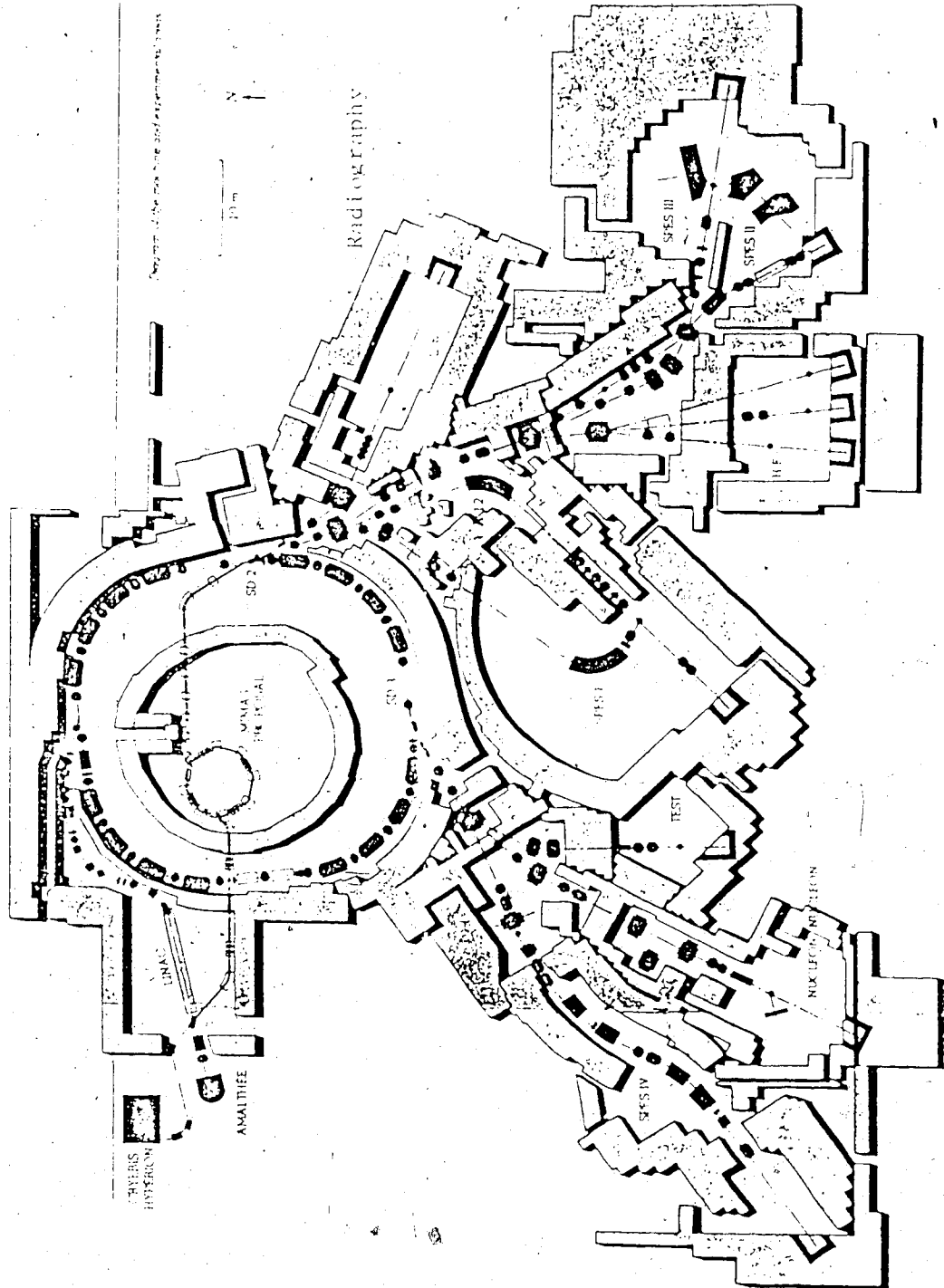


Figure III-1 : Layout of experimental facilities at LNS.

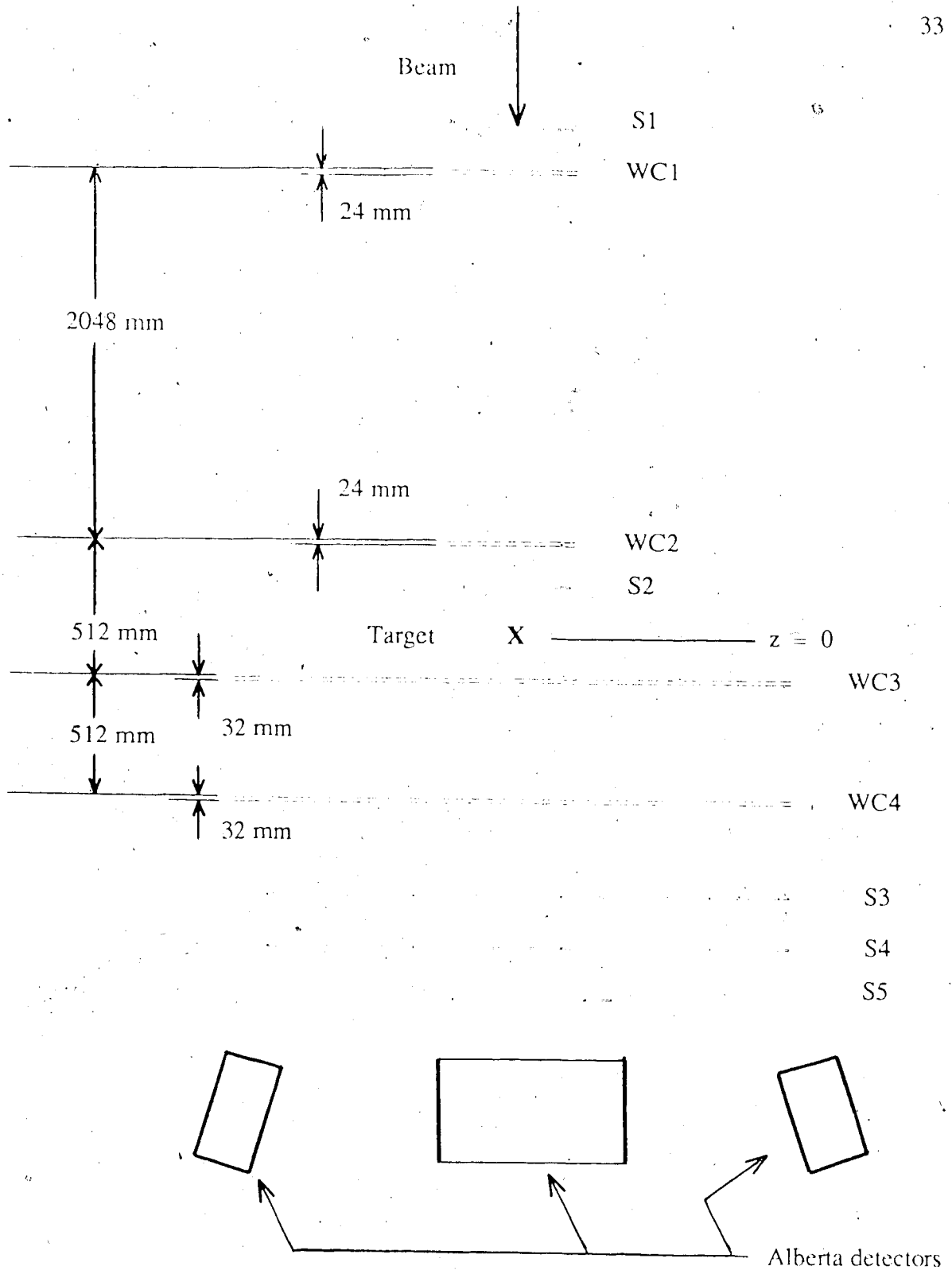


Figure III-2 : Radiography device - Top and side view.

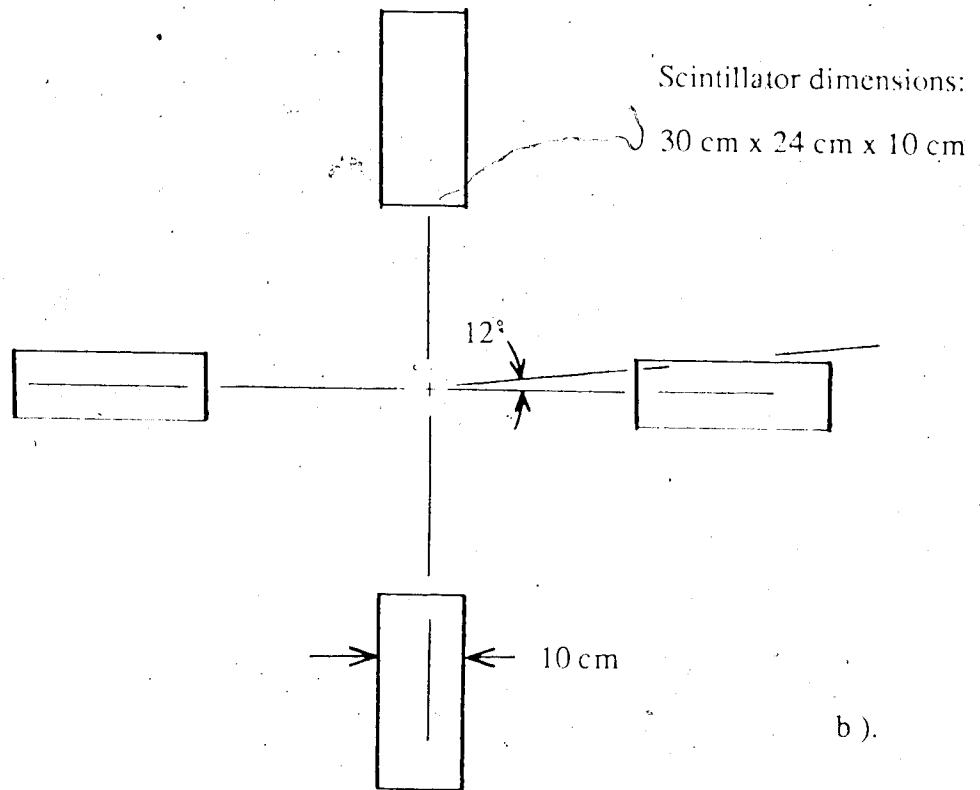
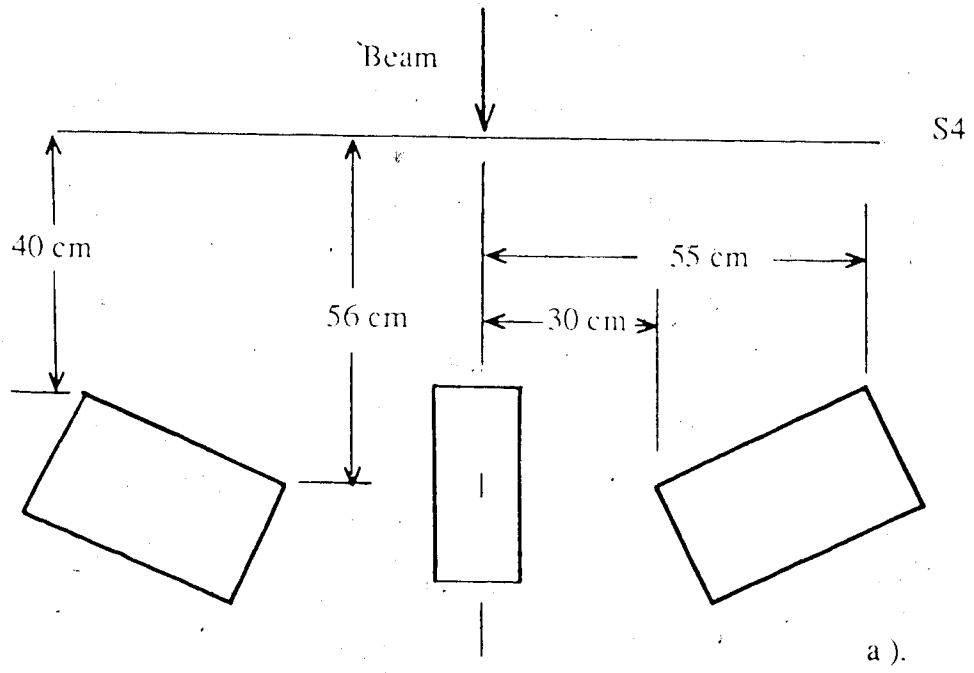


Figure III-3 : Positions of Alberta detectors. a) Top view. b) Looking into beam.

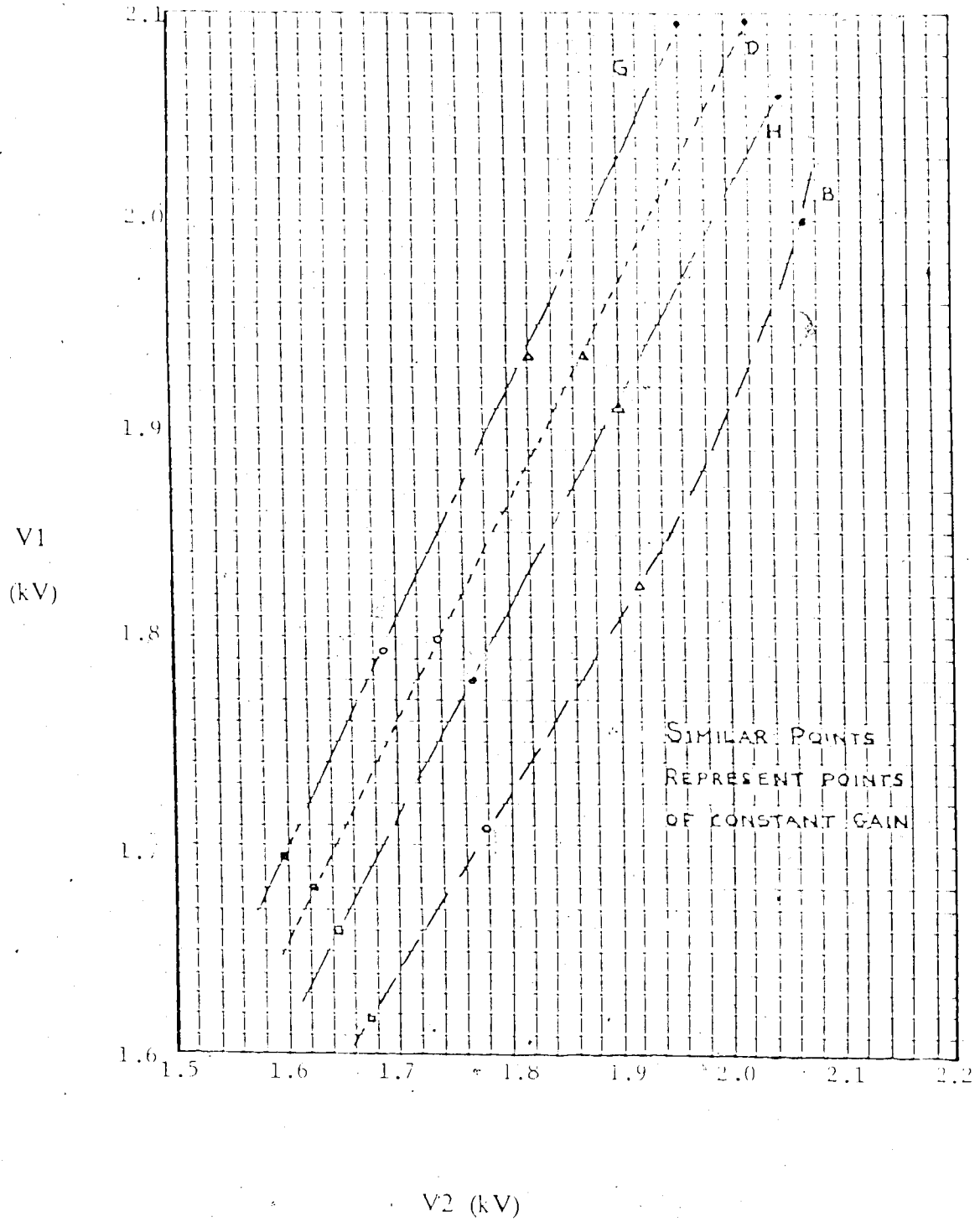


Figure III 4 : Calibration curves for Alberta detectors.

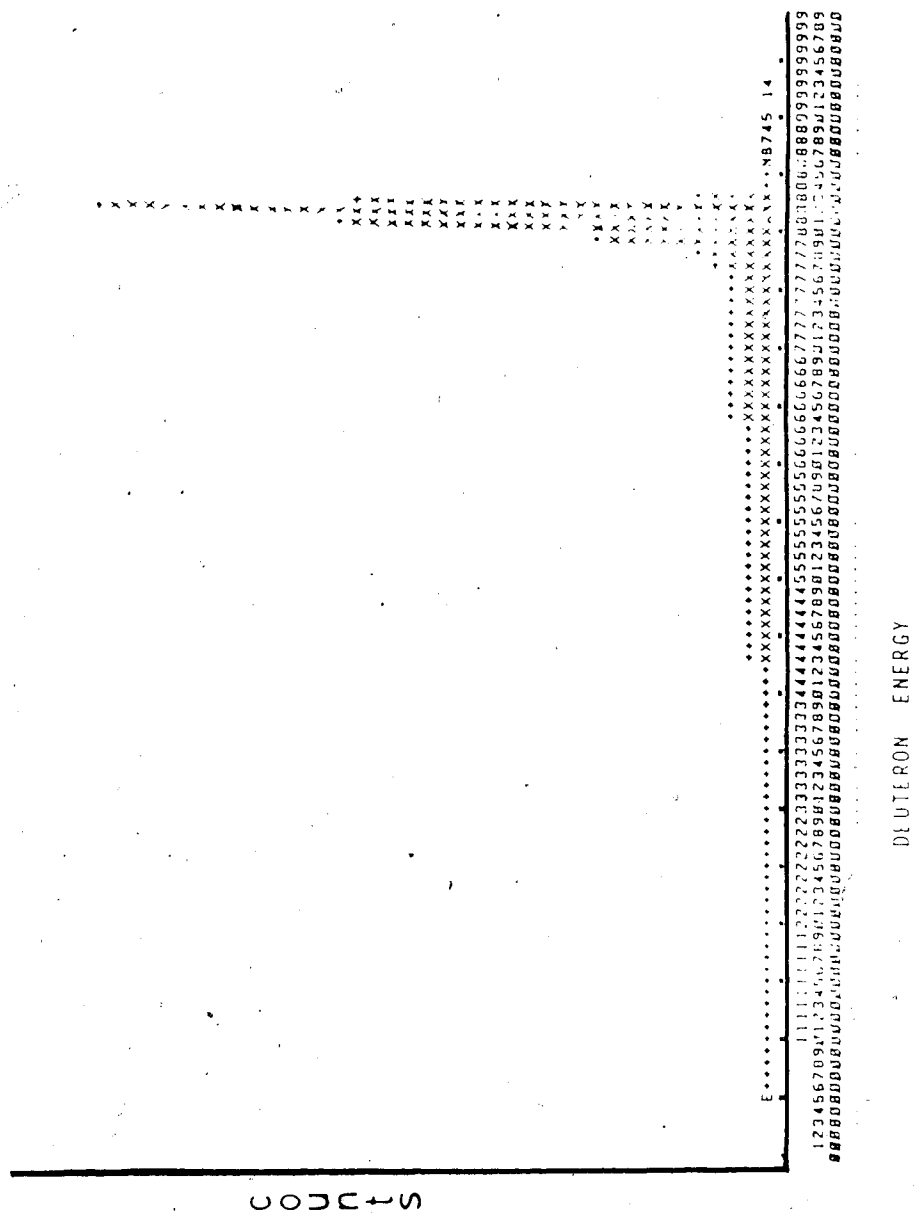


Figure III-5: Alberta detector energy spectrum for 190 MeV deuterons.

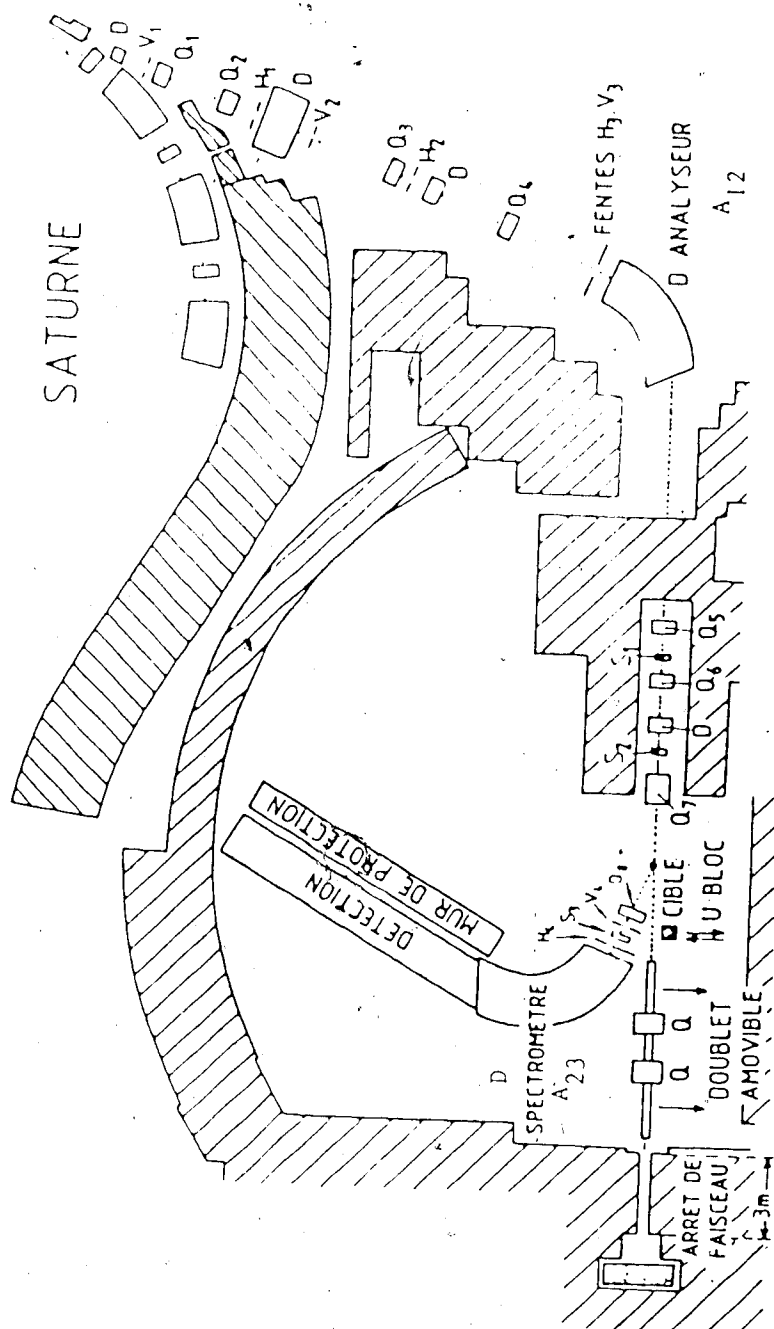


Figure III-6 : Schematic of SPES I beam line.

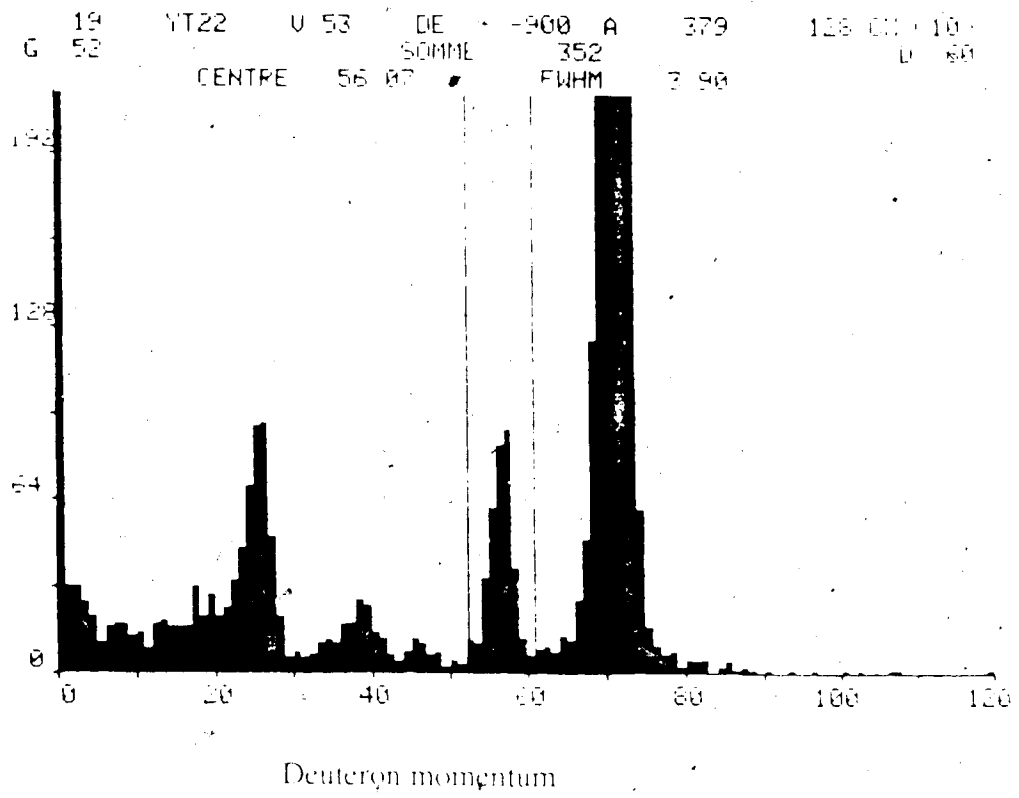


Figure III-7 : SPES 1 momentum spectrum for 200 MeV deuterons scattered from ^{58}Ni .

Chapter IV - Experimental Results

I. The Radiography Experiment - June 1984

Presented here are the results of the deuteron nucleus scattering. These results are shown in Figures IV-1 to IV-15 for 191 MeV and 395 MeV incident deuteron energy with and without the iron absorber in position.

For the 191 MeV case the analyzing powers clearly increased with the inclusion of the iron absorber. In the case where the 1.5 and 1.8 cm slabs were used, the largest values were found for the thicker slabs. The absorber decreases the count rate, and this is reflected in larger statistical errors for this energy. In some of the graphs the error bars are increased by nearly a factor of 2. The values of iT_{11} are also in general greater than the values of T_{20} or T_{22} . As a measure of the goodness of fit for the linear regression performed, the χ^2 values for the measured analyzing powers values were calculated and found to be between 0.3 and 2.5. The small amount of data for the spherical tensor analyzing powers for the elastic channel is plotted in the cases of Ni, Li, and Pb at 191 MeV. The values of all the analyzing powers are significantly larger for the elastic channels. For all the nuclei tested, the T_{20} values proved to be too small to be a viable choice for an analyzer. The largest F_{20} values found are for ^{58}Ni or ^{12}C which are the order of 10^{-3} . The vector analyzing powers however were relatively large for carbon and nickel, and they could be used as a deuteron vector polarimeter target.

For the case of 395 MeV incident deuterons, the inclusion of the iron absorber had a similar effect on the analyzing powers as in the lower energy case. However for this energy the error bars are smaller for the runs with the absorber due to the thicker target used, and the longer running time. The χ^2 values for calculations at this energy ranged from 0.3 to 2. The values of T_{20} and T_{22} were generally greater for this energy than for

the 191 MeV case. The correlations of the errors of T_{20} and T_{22} were less than 0.1.

2. The SPES I Experiment

The cartesian analyzing powers and the cross sections for d - Ni inelastic scattering for the 2^+ state at 200, 400, and 700 MeV are shown in Figures IV-16 to IV-24. The errors for the analyzing powers are large, however definite structure is observed. The structure in the cross sections and analyzing powers is very similar to the elastic scattering data. The elastic scattering data for ^{58}Ni , ^{16}O , and ^{40}Ca may be found in references [10] and [11].

For the d-nucleus scattering discussed in this chapter, it is important to note that when comparing the values of $\sqrt{2} [T_{20}/2 + \sqrt{3}/2 T_{22}]$ to A_{yy} and $i2/\sqrt{3} T_{11}$ to A_y as in Appendix 2, the tensor analyzing powers from elastic scattering must be used. As opposed to the inclusive data, the small amount of data for the spherical analyzing powers from elastic scattering is found to agree with the cartesian analyzing powers found from SPES I.

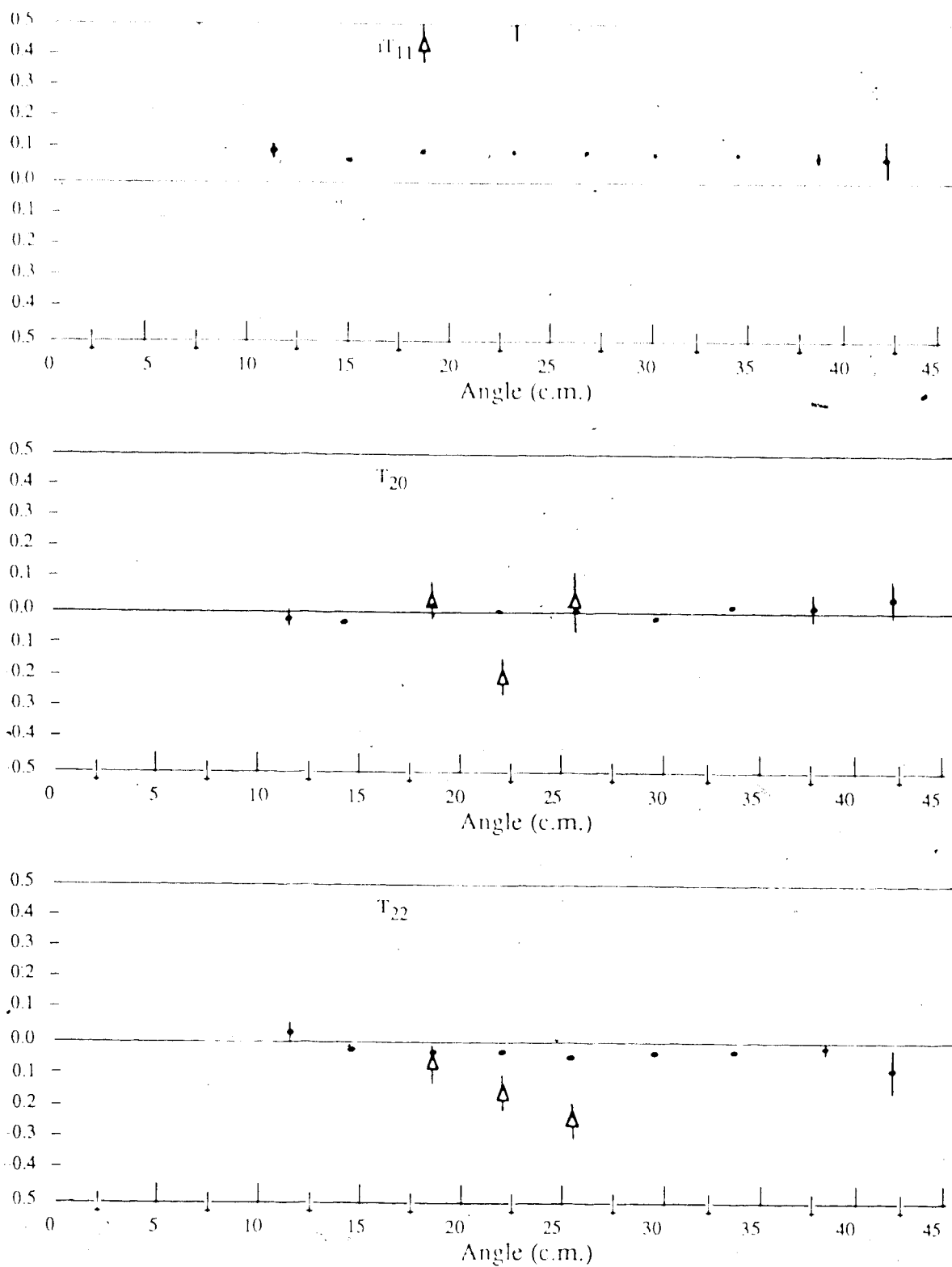
3. The Radiography Experiment - November 1983

Presented in Figures IV-25 to IV-26 are the asymmetries for dd scattering. The analyzing power T_{20} is small for the 191 MeV energy case, but appears to be appreciable for the higher energy measurements. T_{22} and iT_{11} are relatively small for either case. The statistics here are poor, particularly in the 395 MeV case. The χ^2 values for the fits are between 1 and 3.5.

Figure IV-27 illustrates the results for dp elastic scattering at 191 MeV. The tensor analyzing power T_{20} dips down to about -0.6 and is always negative between 85° and 148° in the center of momentum frame. Figure IV-29 shows the cross section for the dp reaction in this angular range. Using equation II-11 and numerical integration, the figure of merit

for T_{20} is determined to be $2 \times 10^{-3} \text{ cm}^{-1/2}$. Equation II-10 gives a conservative estimate of the efficiency at this energy to be 10^{-3} using a liquid hydrogen target. The T_{22} curve is always negative in the region of interest and appears only to dip below -0.2 at about 150° . The vector asymmetry values are large as in most of the other figures shown, however it is noted that the negative lobe is slightly out of phase with the T_{20} curve.

For the 395 MeV case the error bars are larger than for the lower energy tests. The values of iT_{11} seem to be nearly unchanged, where the values of T_{22} have increased dramatically. T_{22} seems to have shifted in the positive sense, with a much less well defined region of possible interest. These curves are shown in Figure IV-28.

Figure IV-1: $d + Ni$ 191 MeV

• Inclusive Scattering - No Absorber
 ▲ Elastic Scattering

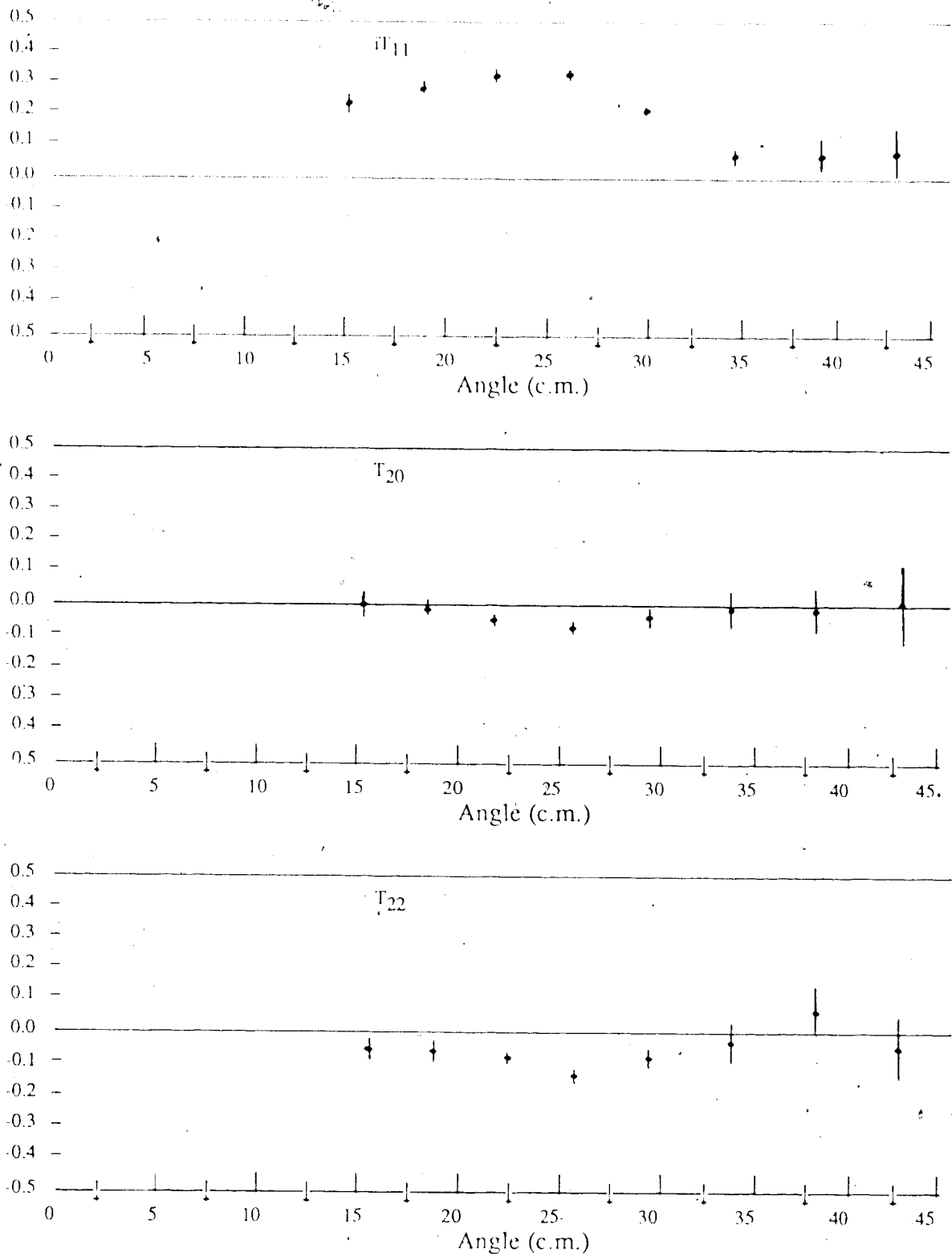


Figure IV-2 : d + Ni 191 MeV

• Inclusive Scattering - 1.5 cm Fe Absorber

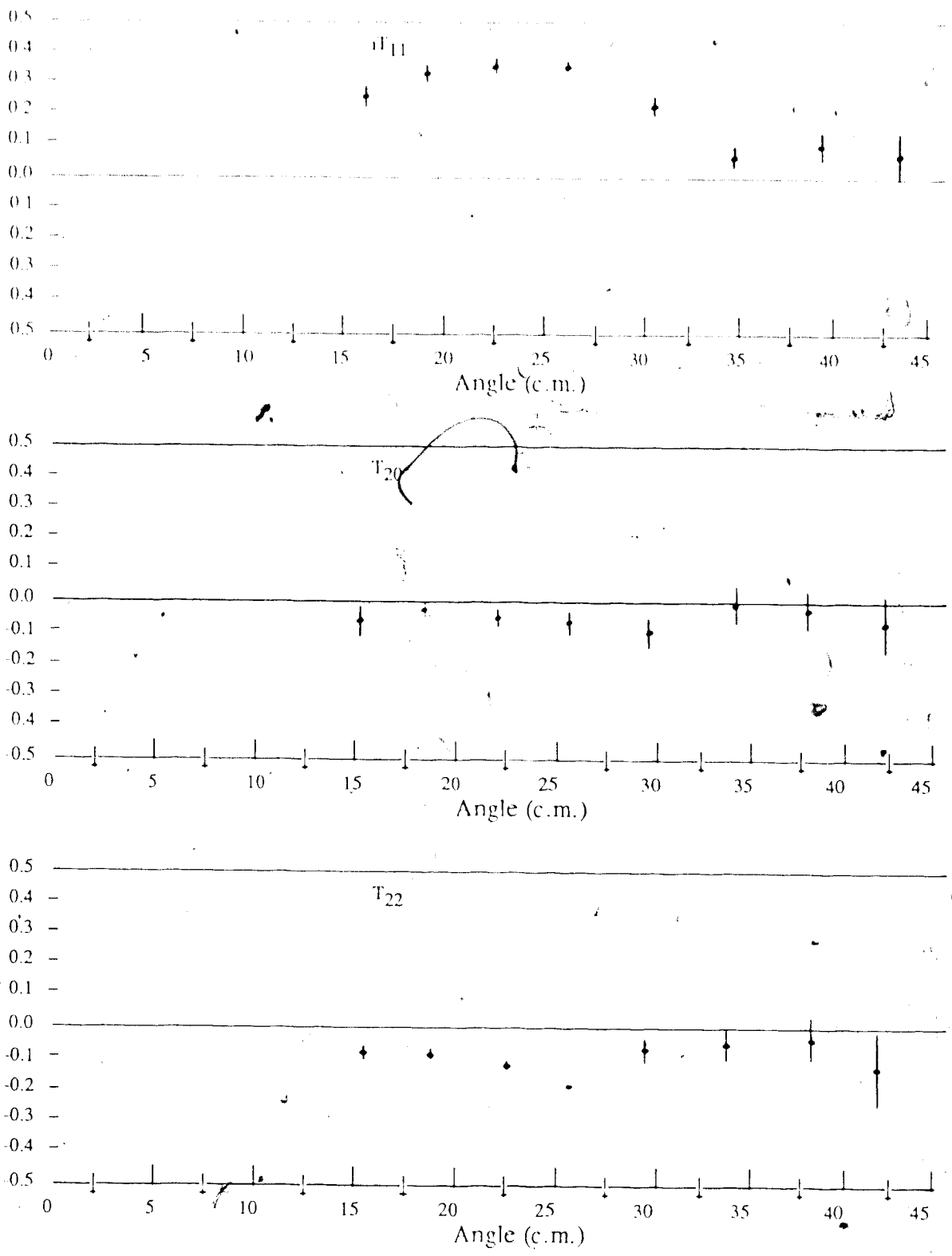


Figure IV-3 : d + Ni 191 MeV • Inclusive Scattering - 1.8 cm Fe Absorber

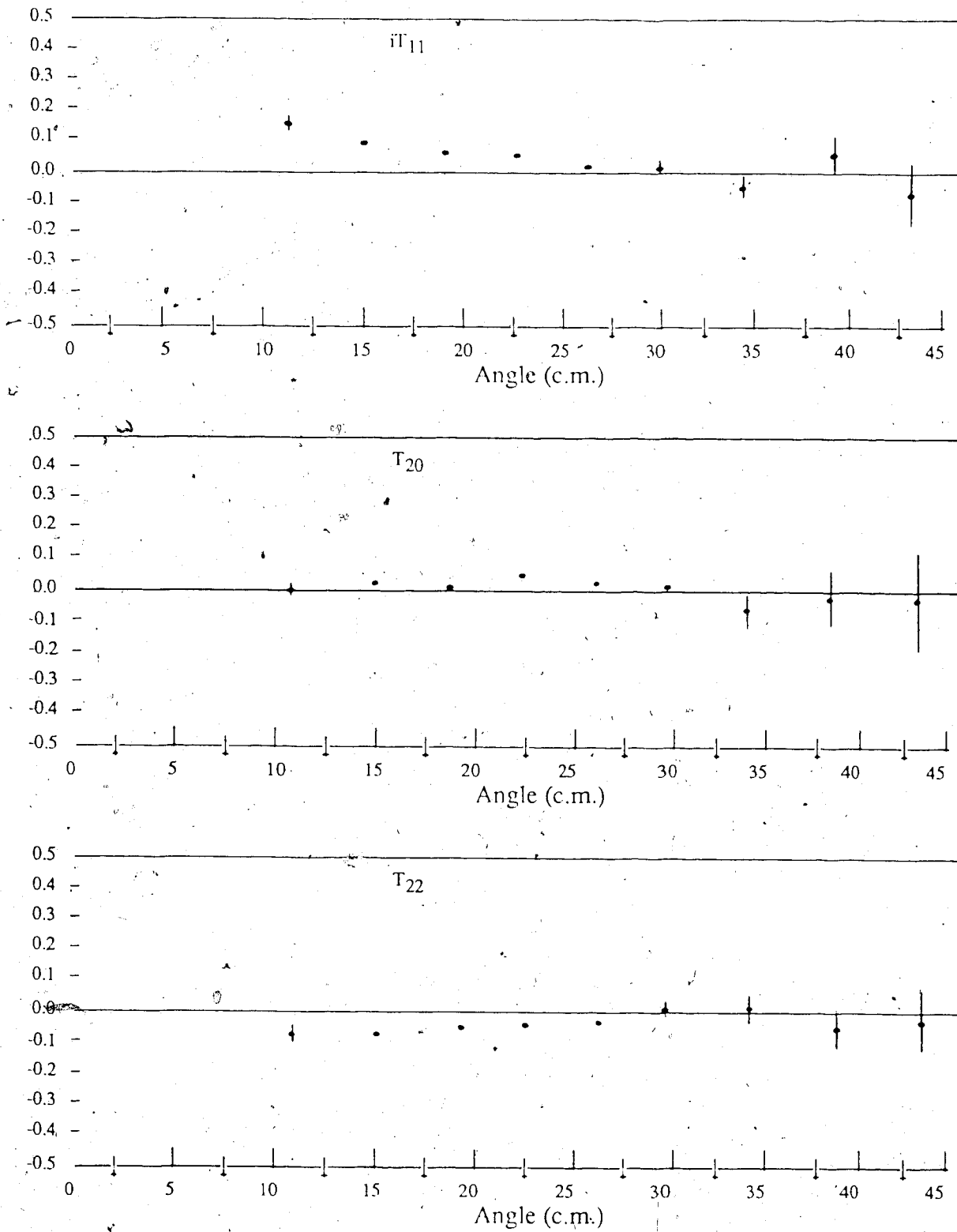


Figure IV-4 : d + Ni 395 MeV • Inclusive Scattering - No Absorber

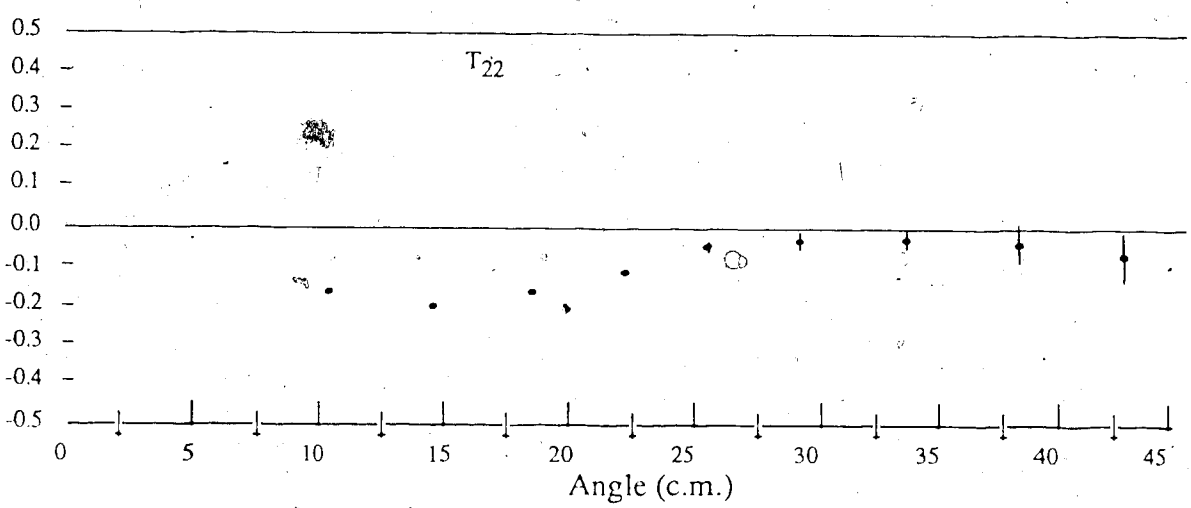
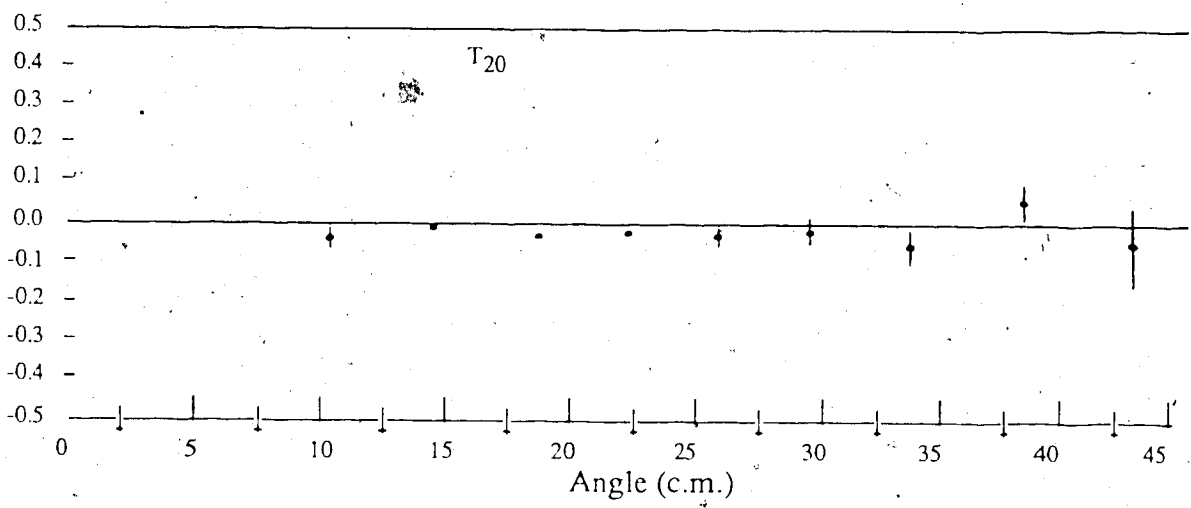
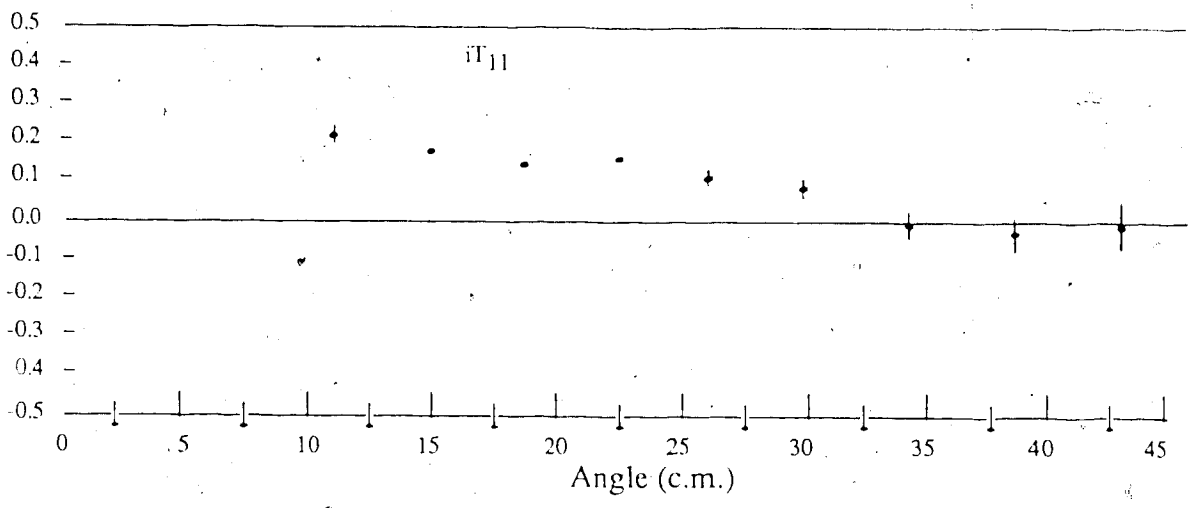


Figure IV-5 : d + Ni 395 MeV

• Inclusive Scattering - 5.5 cm Fe Absorber

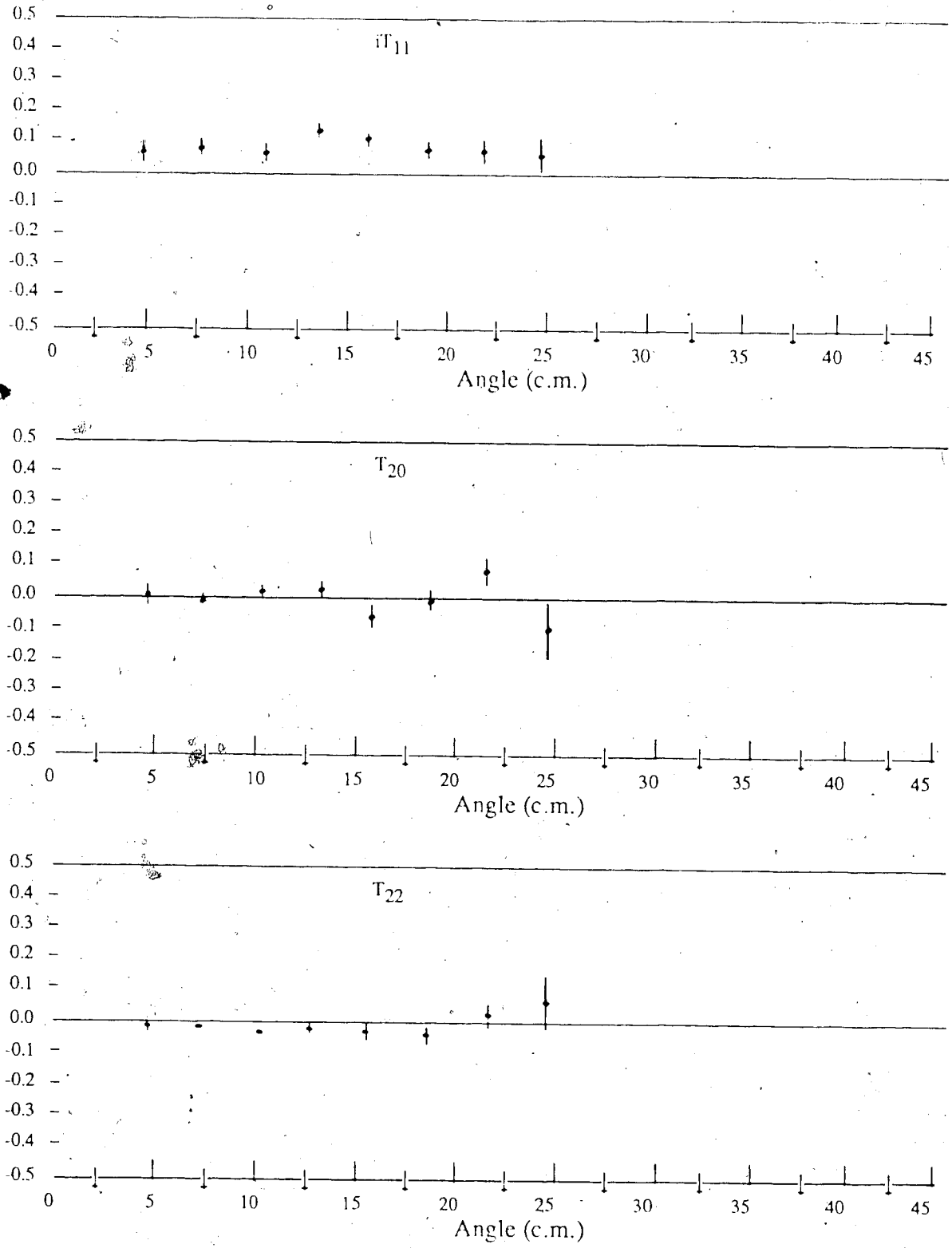


Figure IV-6: $d + C$ 191 MeV • Inclusive Scattering - No Absorber

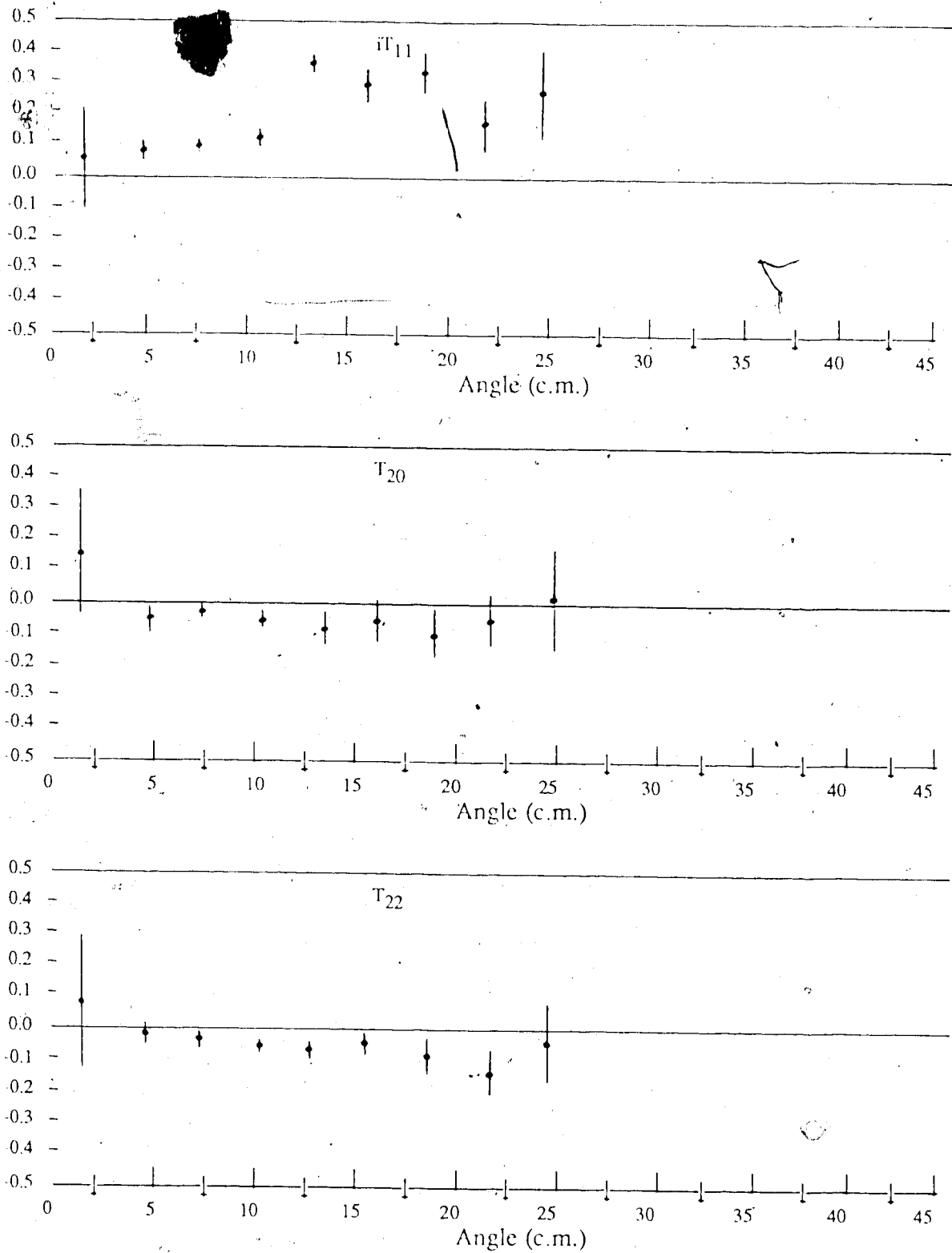


Figure IV-7: $d + C$ 191 MeV. • Inclusive Scattering - 2 cm Fe Absorber

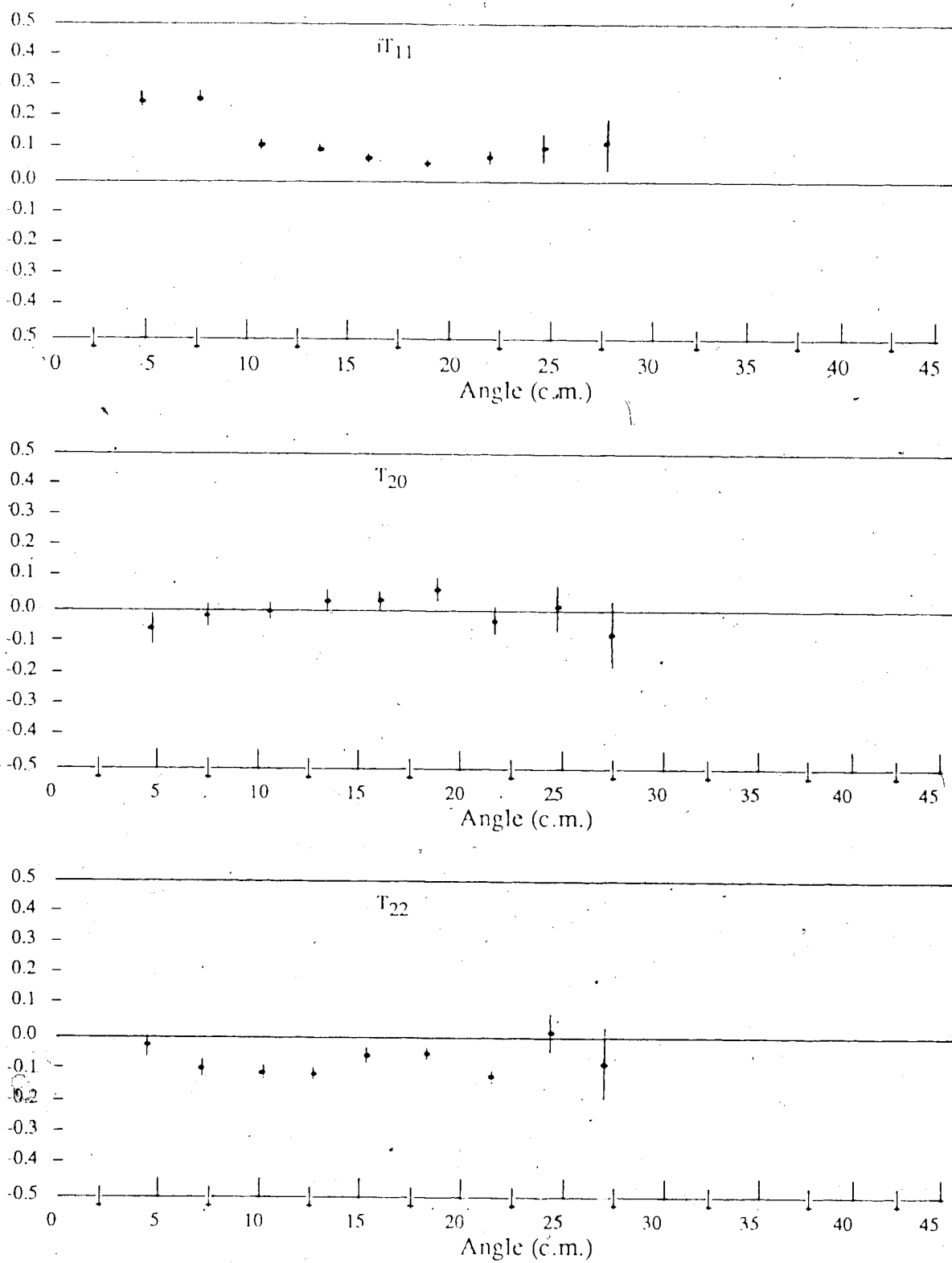


Figure IV-8 : $d + C$ 395 MeV • Inclusive Scattering - No Absorber

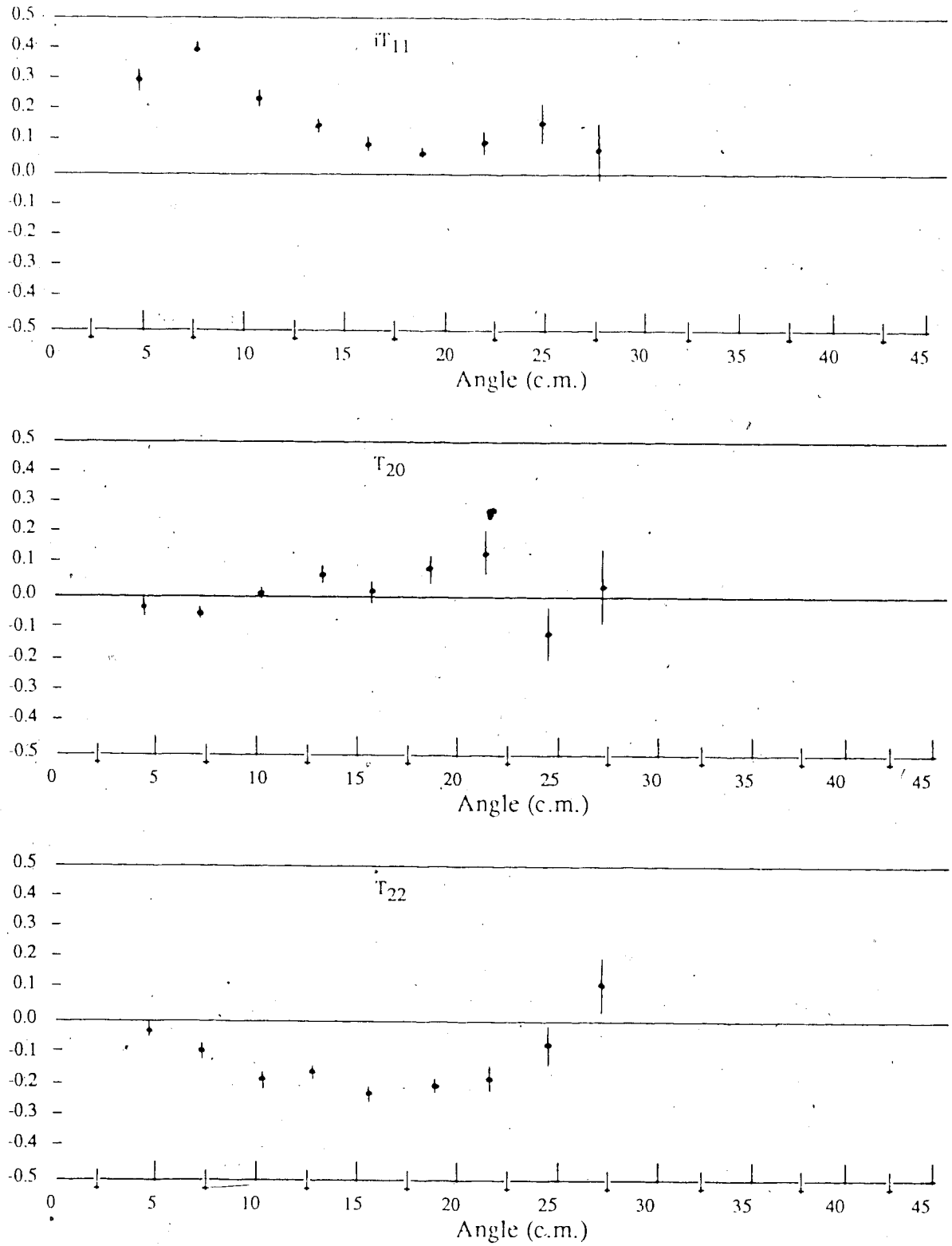


Figure IV-9: $d + C$ 395 MeV • Inclusive Scattering - 5 cm Fe Absorber

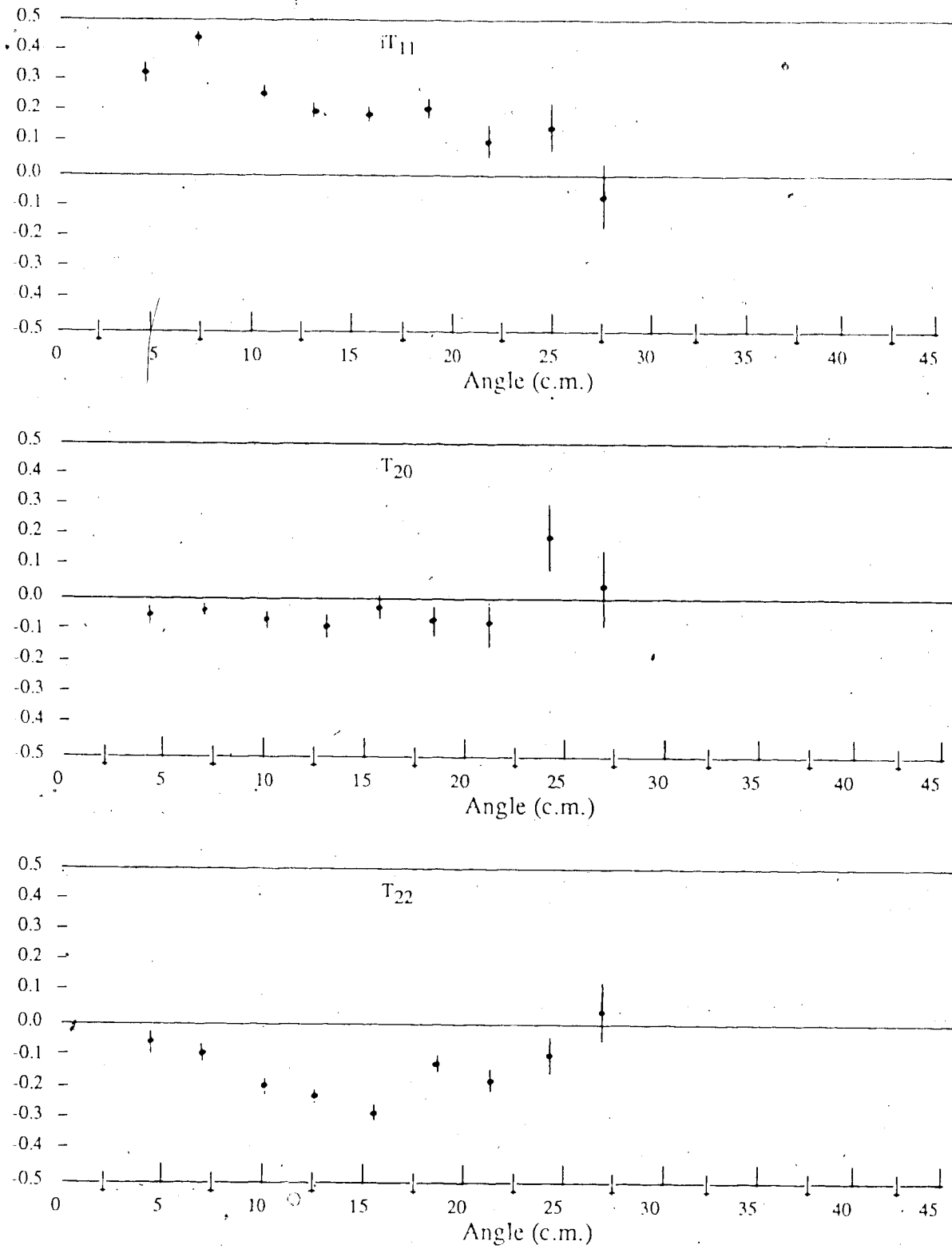
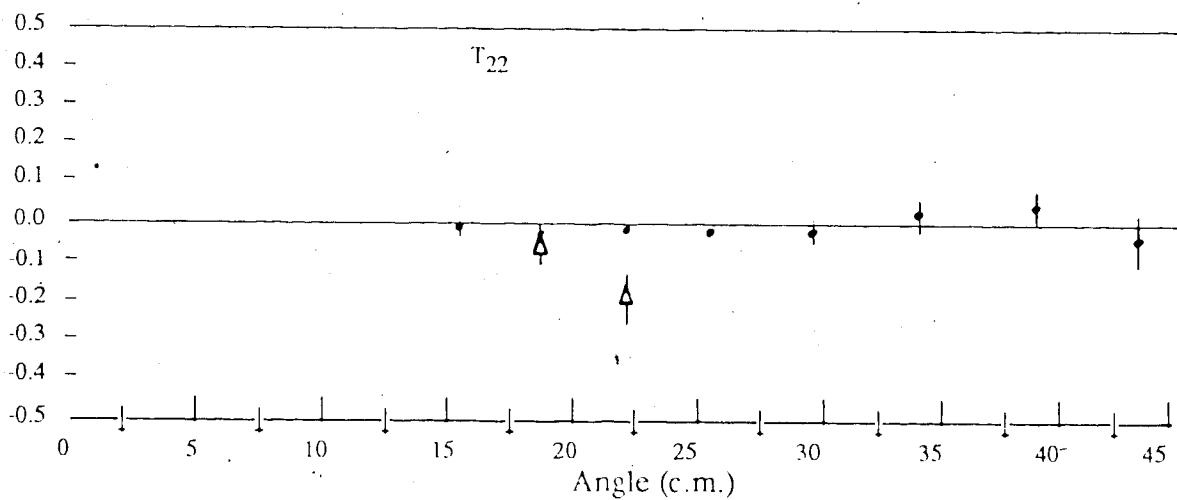
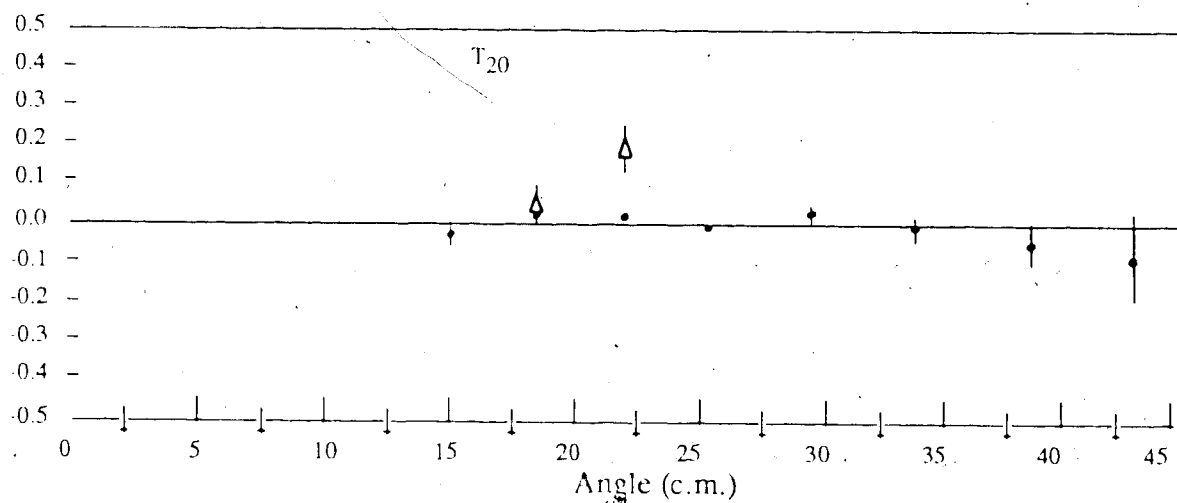
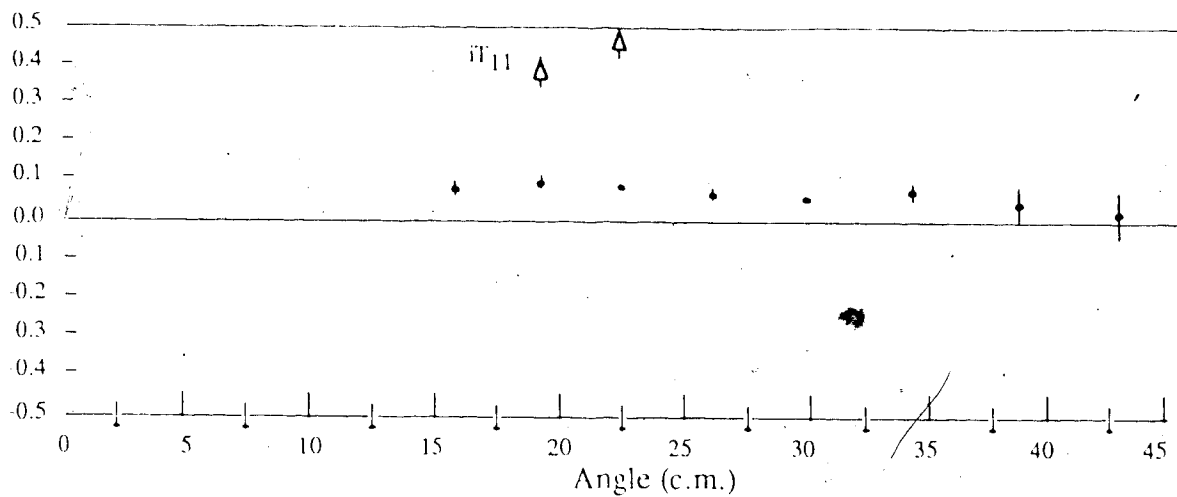


Figure IV-10: $d + C$, 395 MeV. • Inclusive Scattering - 7 cm Fe Absorber

Figure IV-11: $d + Pb$ 191 MeV

• Inclusive Scattering - No Absorber
 Δ Elastic Scattering

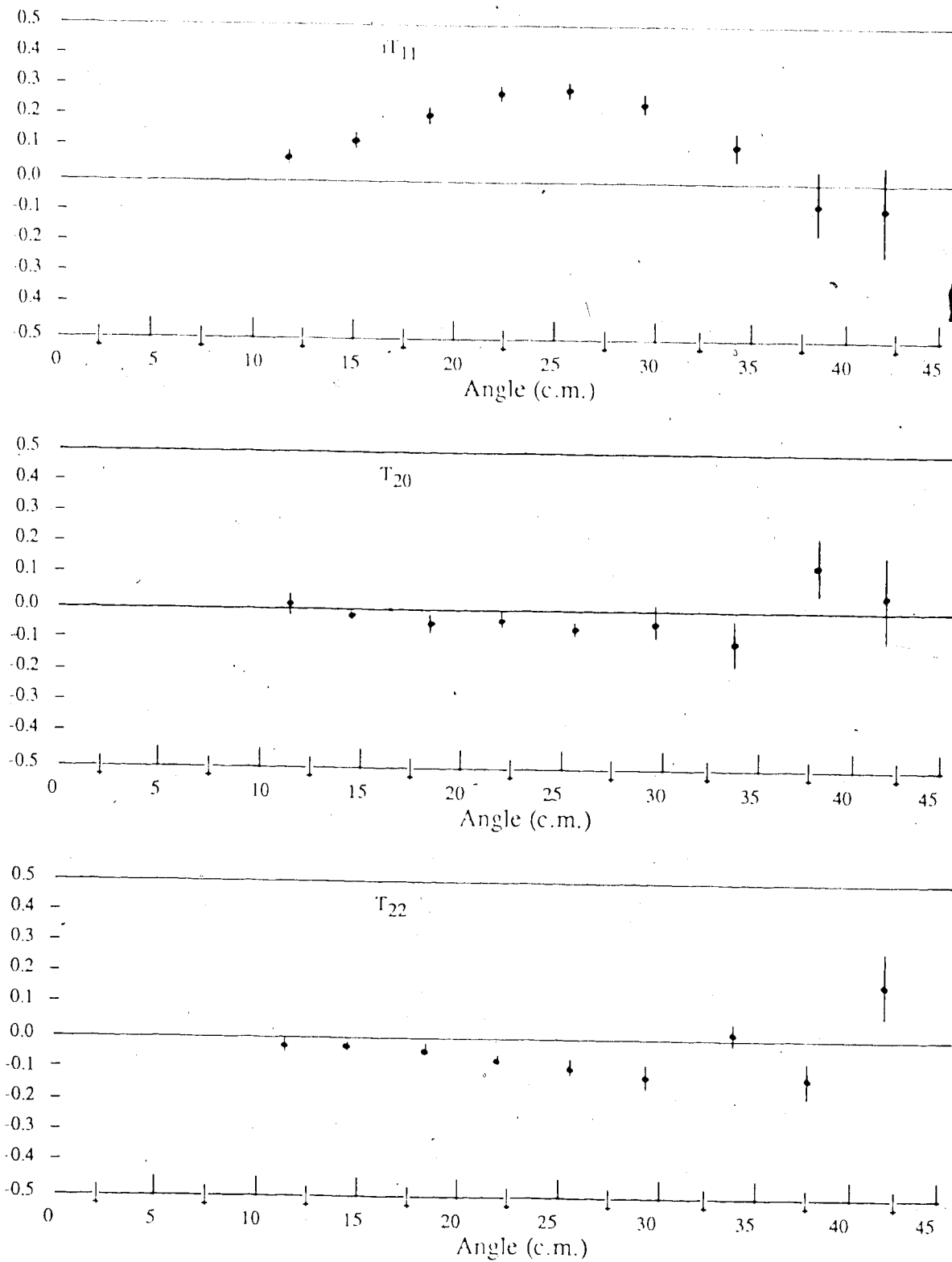


Figure IV-12 : d + Pb 191 MeV • Inclusive Scattering - 1.5 cm Fe Absorber

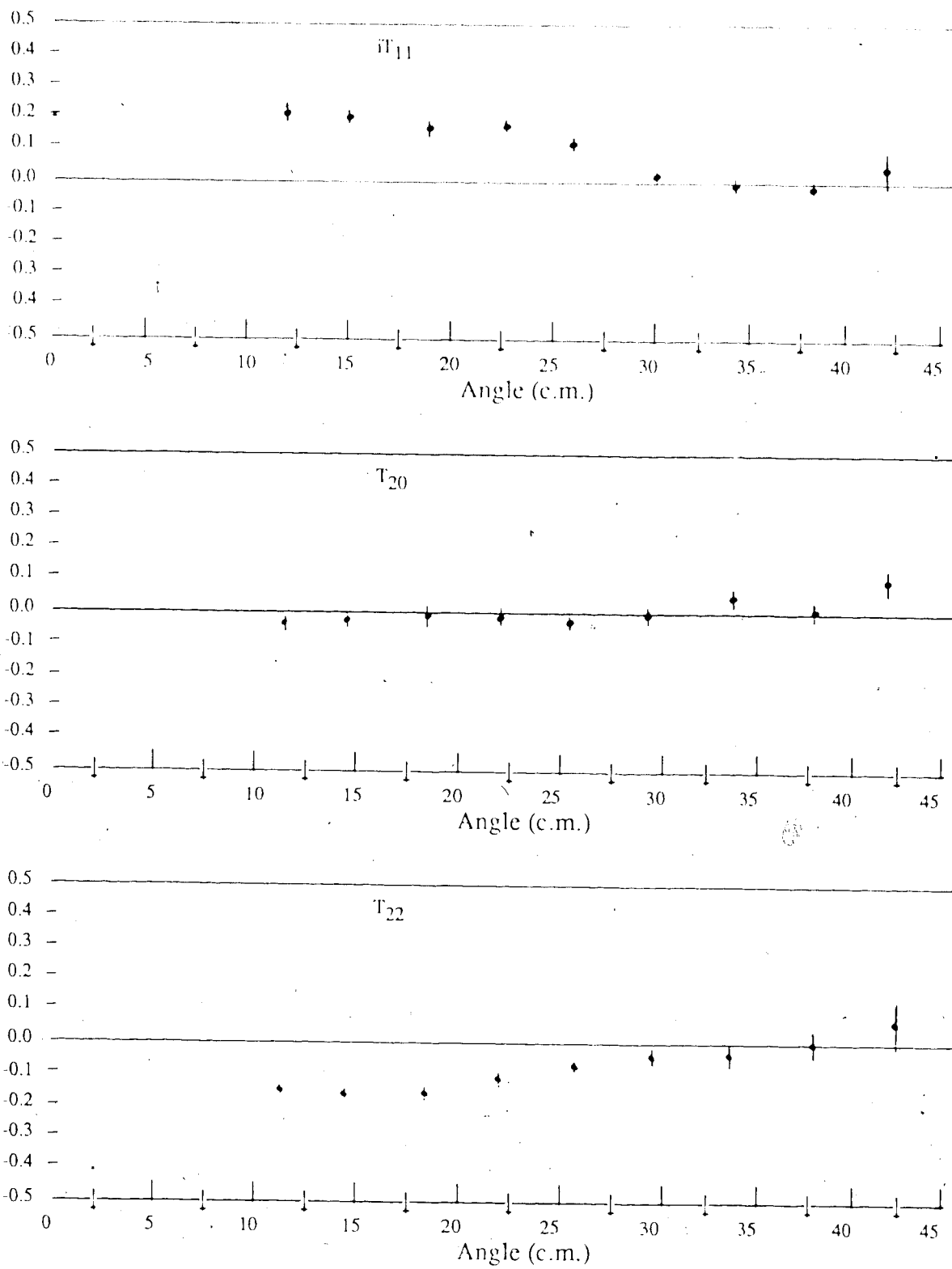


Figure IV-13: d + Pb 395 MeV • Inclusive Scattering - 5.5 cm Fe Absorber

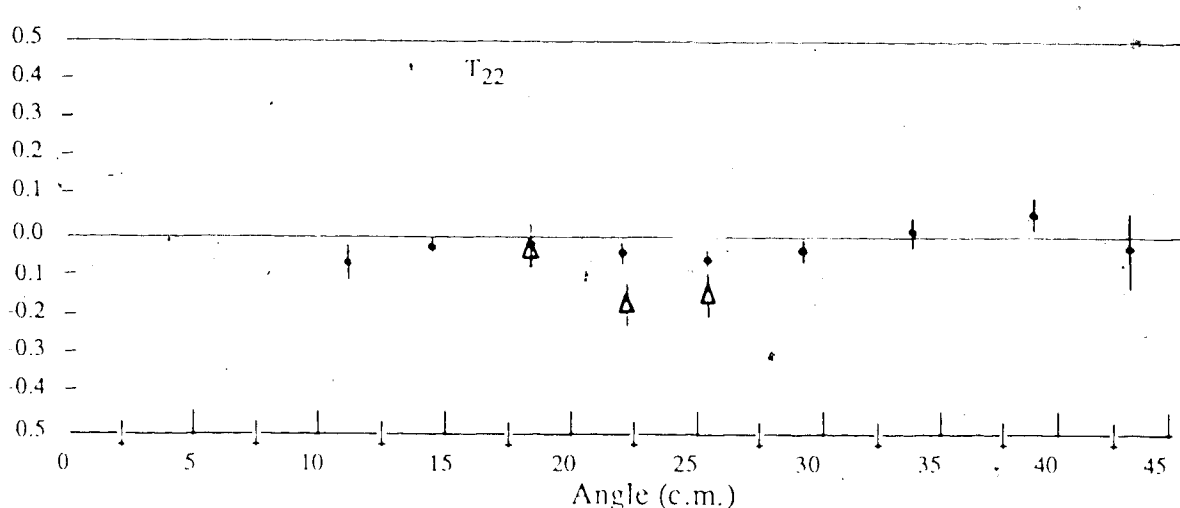
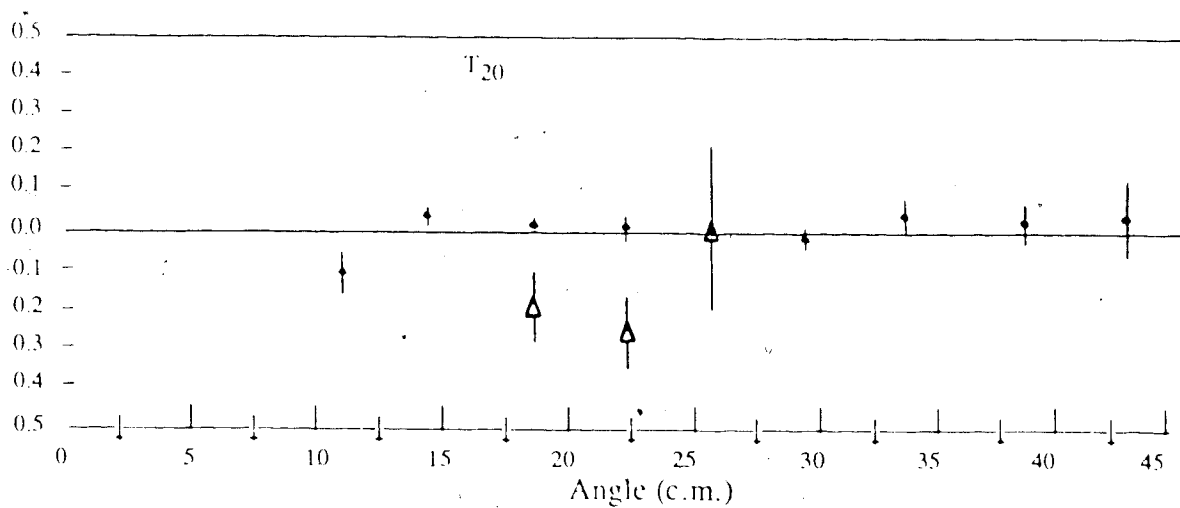
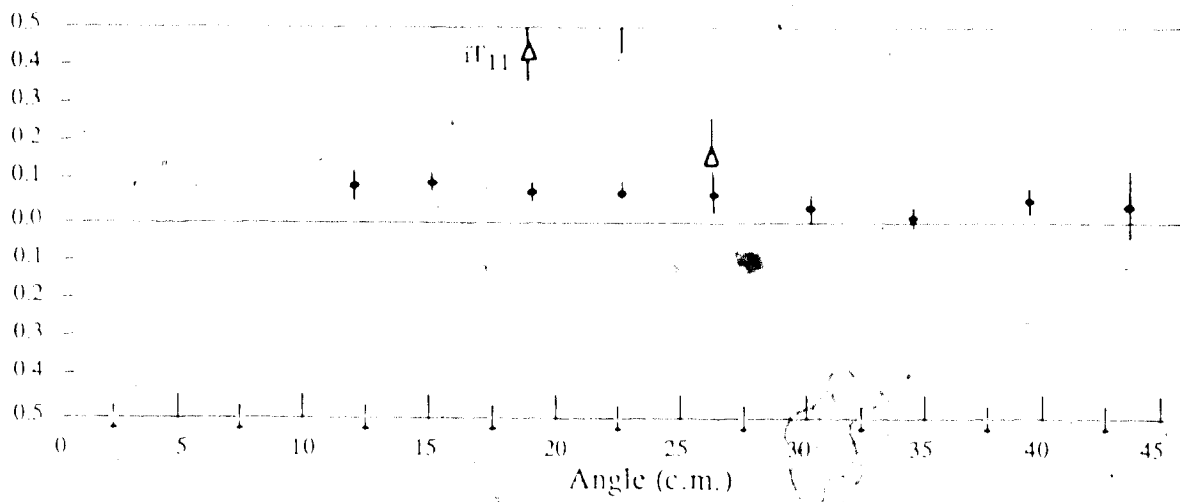


Figure IV-14: d + Li 191 MeV
 • Inclusive Scattering - No Absorber
 Δ Elastic Scattering

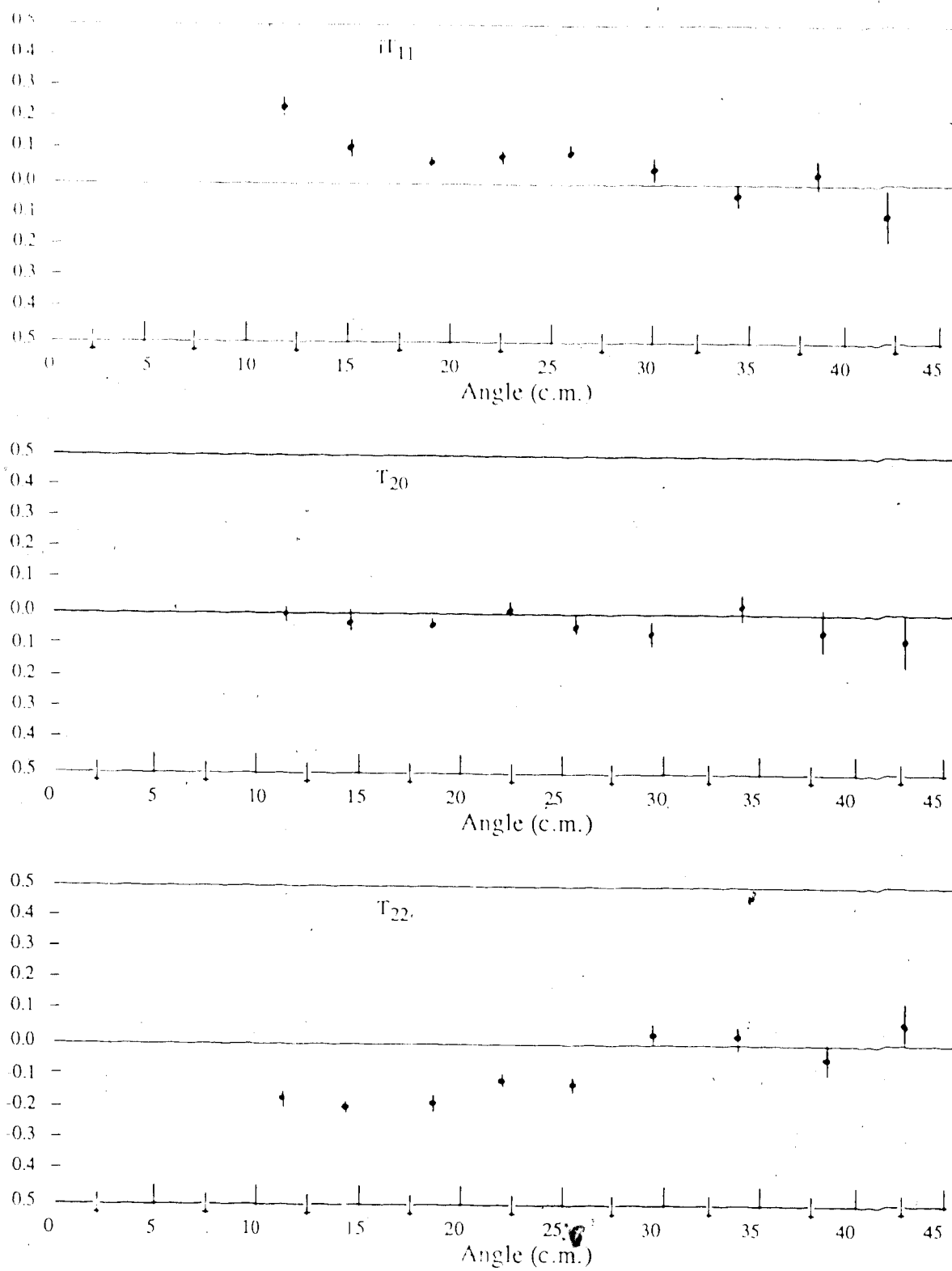


Figure IV-15: d + Li 395 MeV Inclusive Scattering - 5.5 cm Fe Absorber

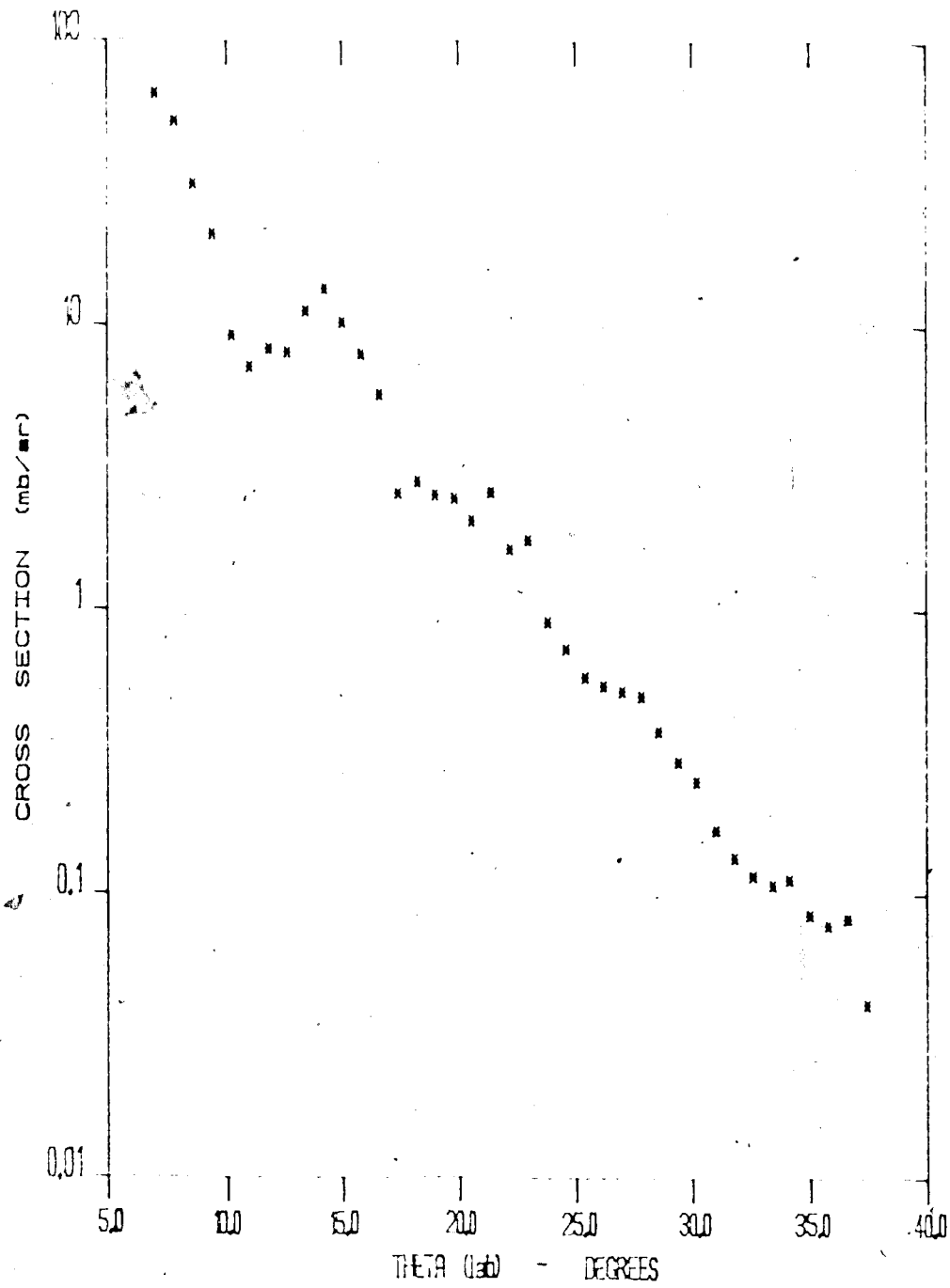


Figure IV 16 : $d + Ni$ 200 MeV, $d\sigma/d\Omega = 2^+$ State

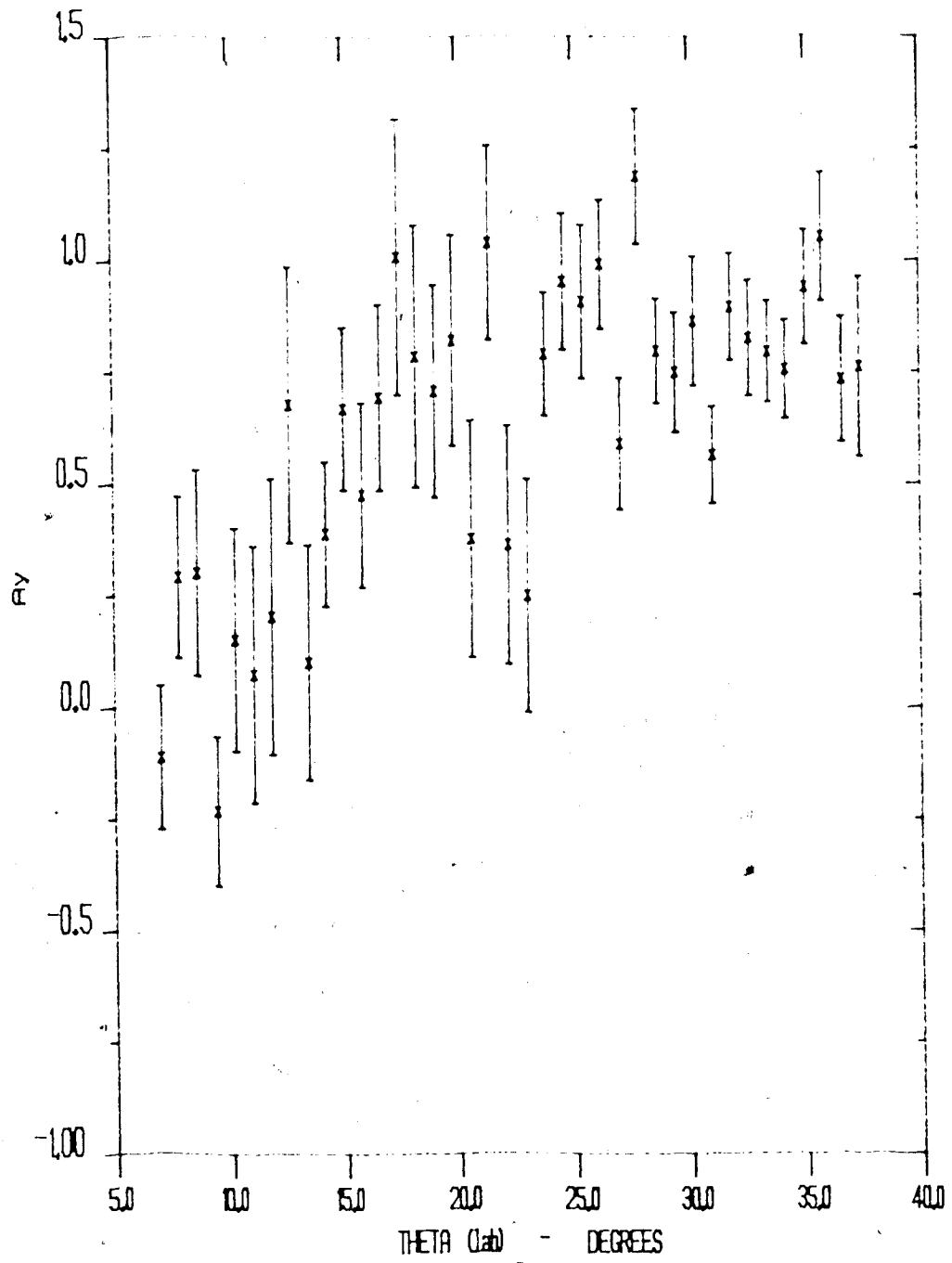


Figure IV-17: d + Ni 200 MeV, $A_y - 2^+$ State

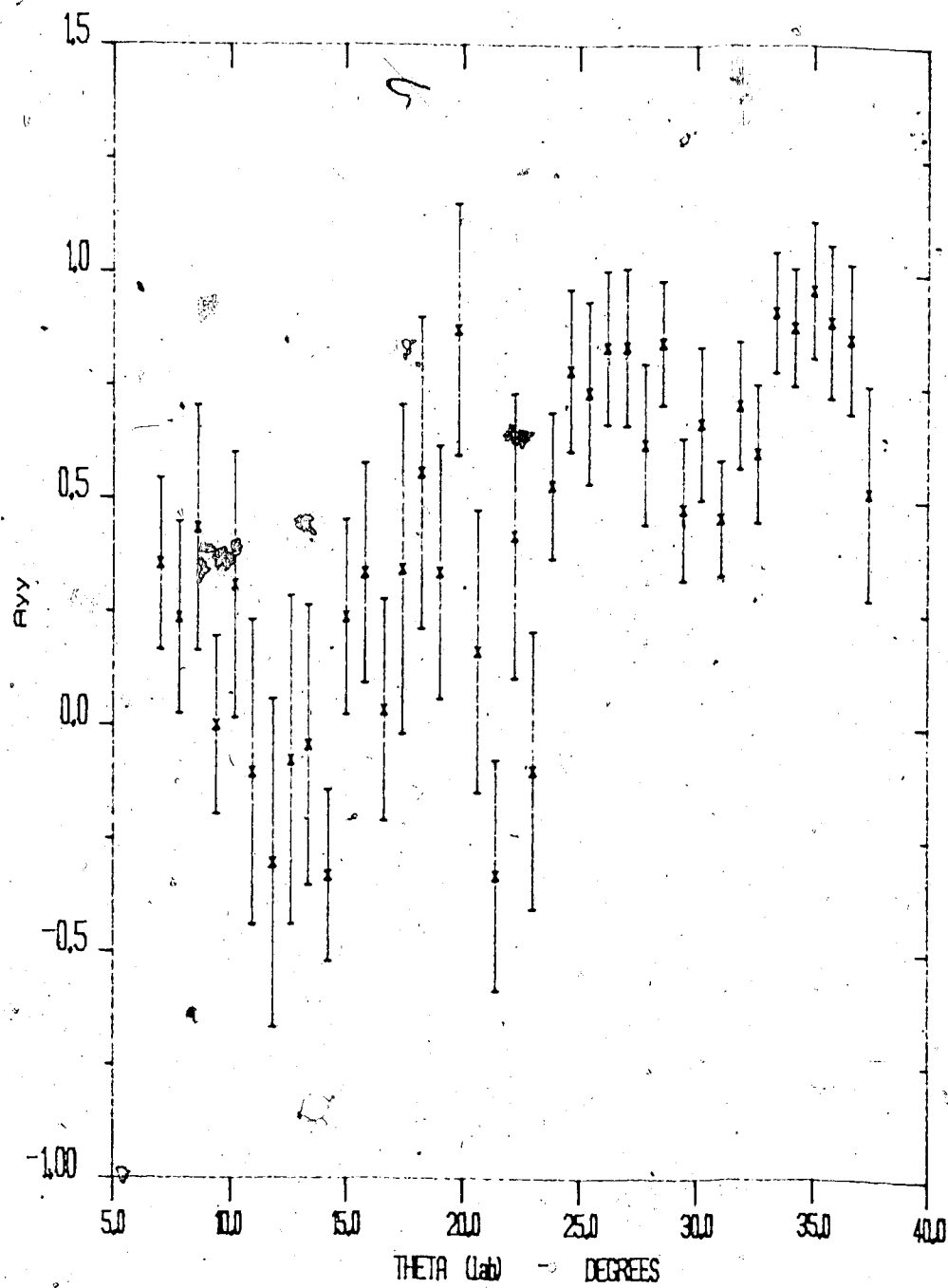


Figure IV-18 : d + Ni 200 MeV, A_{yy} - 2^+ State

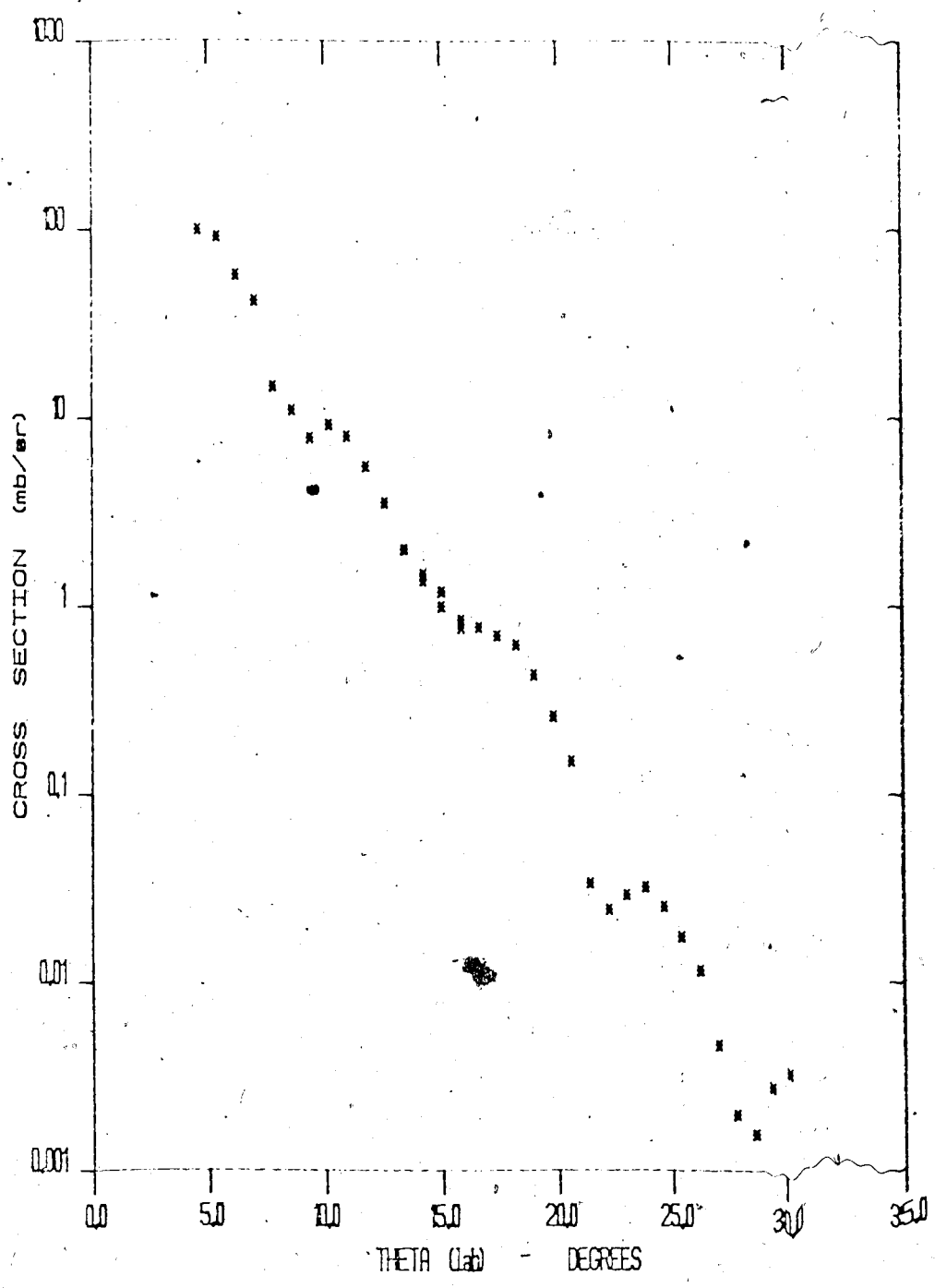


Figure IV-18: d + Ni 400 MeV, $\frac{d\sigma}{d\Omega}$ - 2^+ State

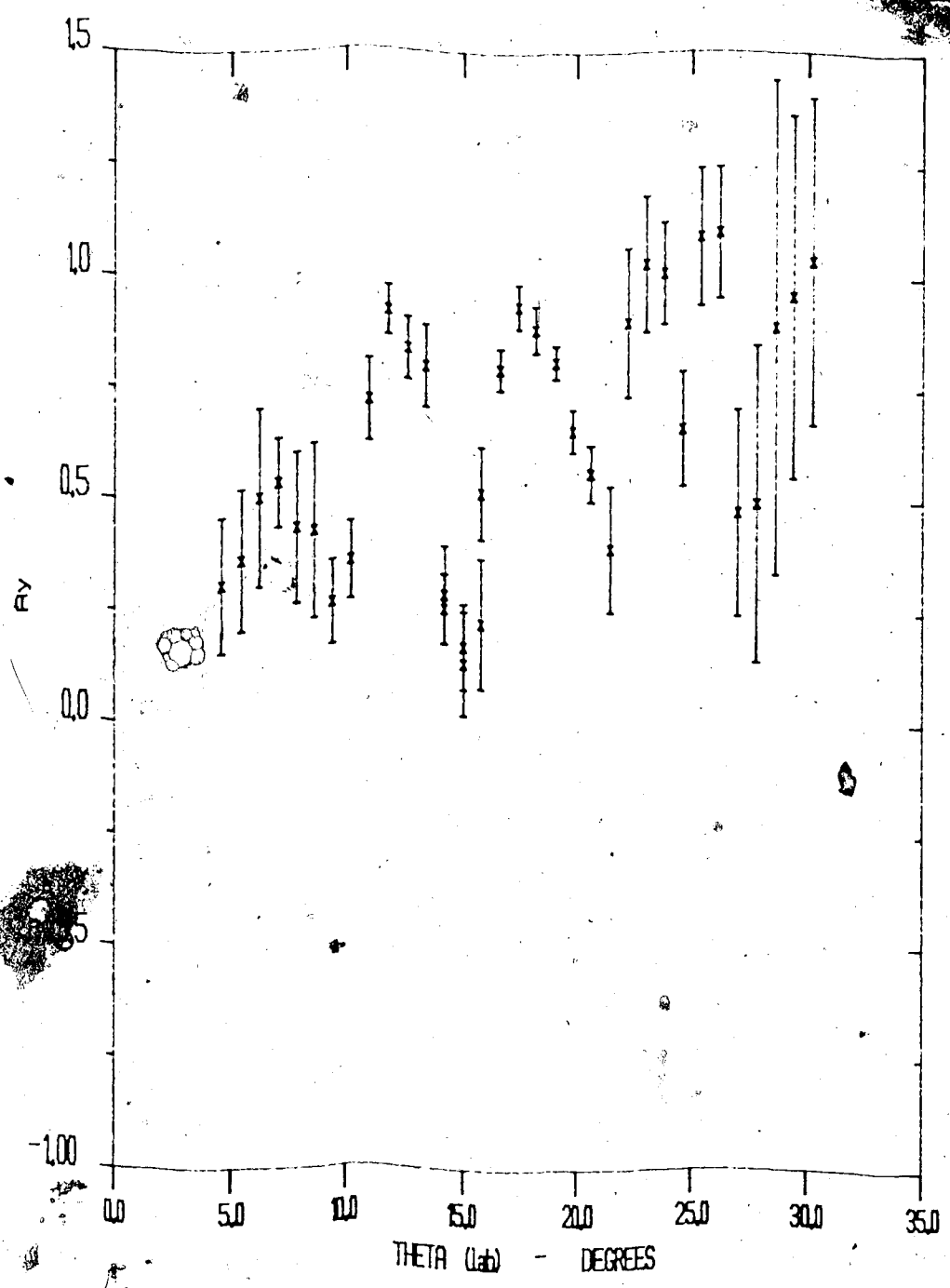


Figure IV-20 : d + Ni 400 MeV, $A_y - 2^+$ State

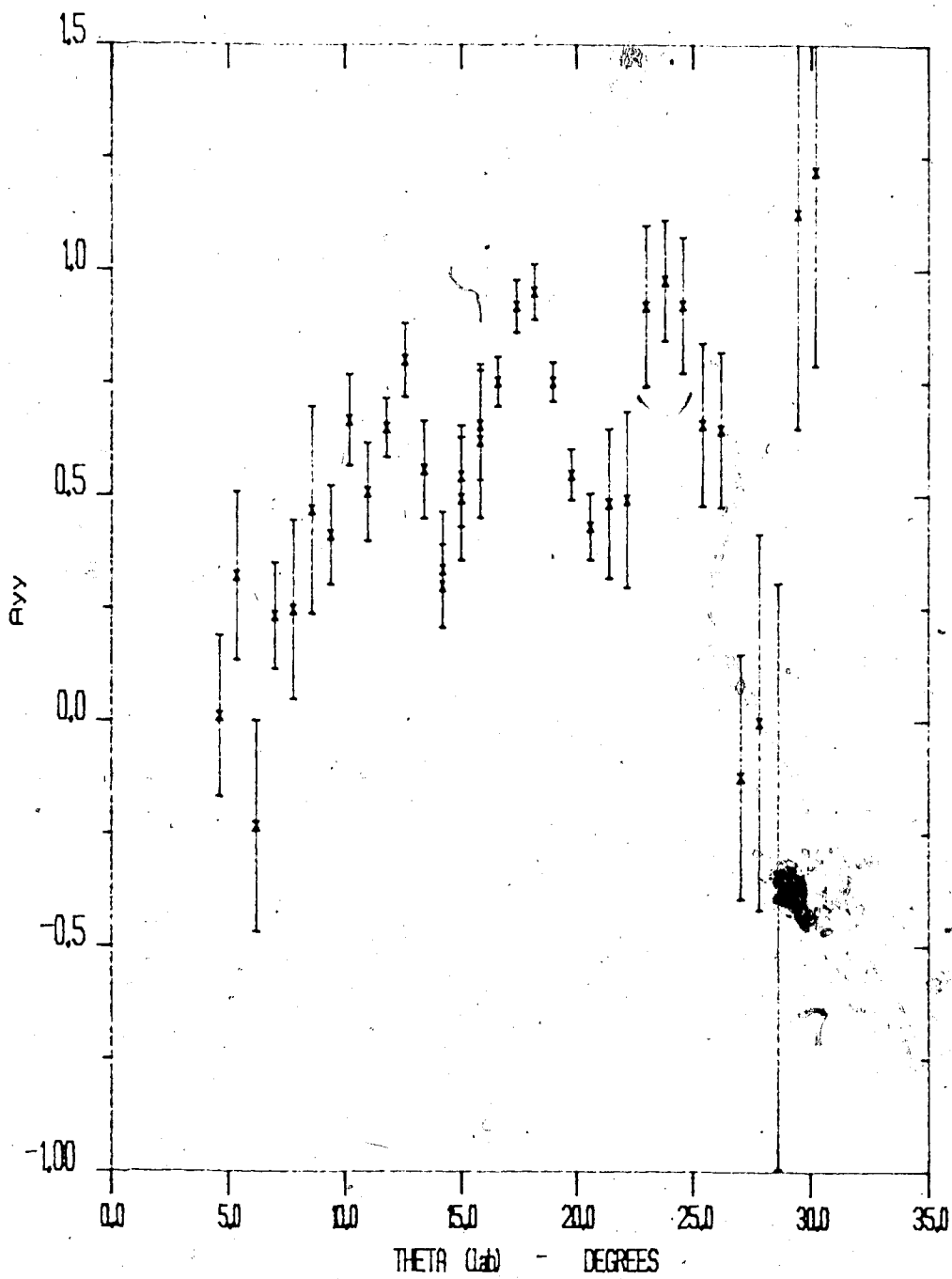


Figure IV-21 : $d + Ni$ 400 MeV, $A_{yy} - 2^+$ State

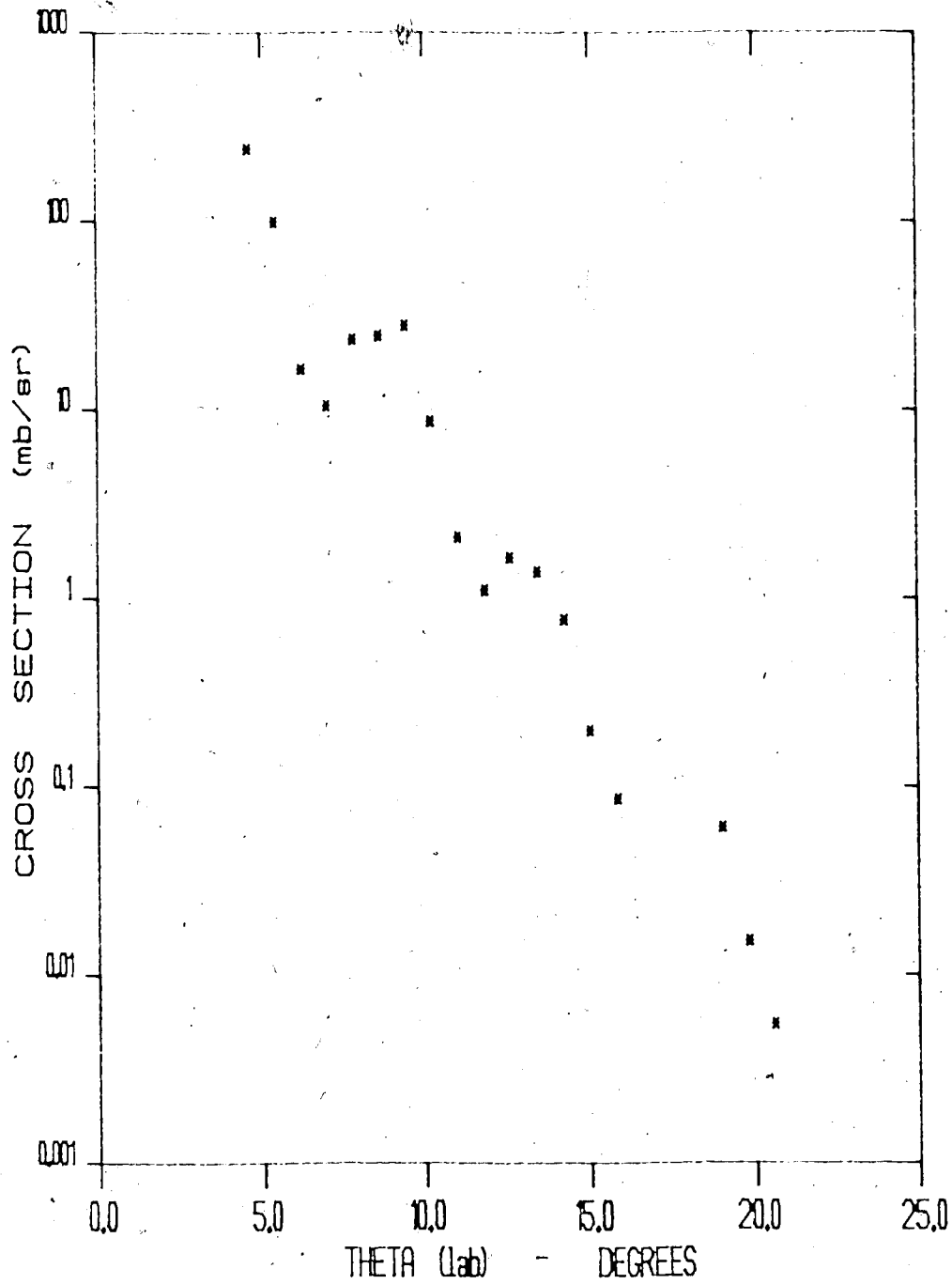


Figure IV-22 : $d + Ni$ 700 MeV, $d\sigma/d\Omega - 2^+$ State

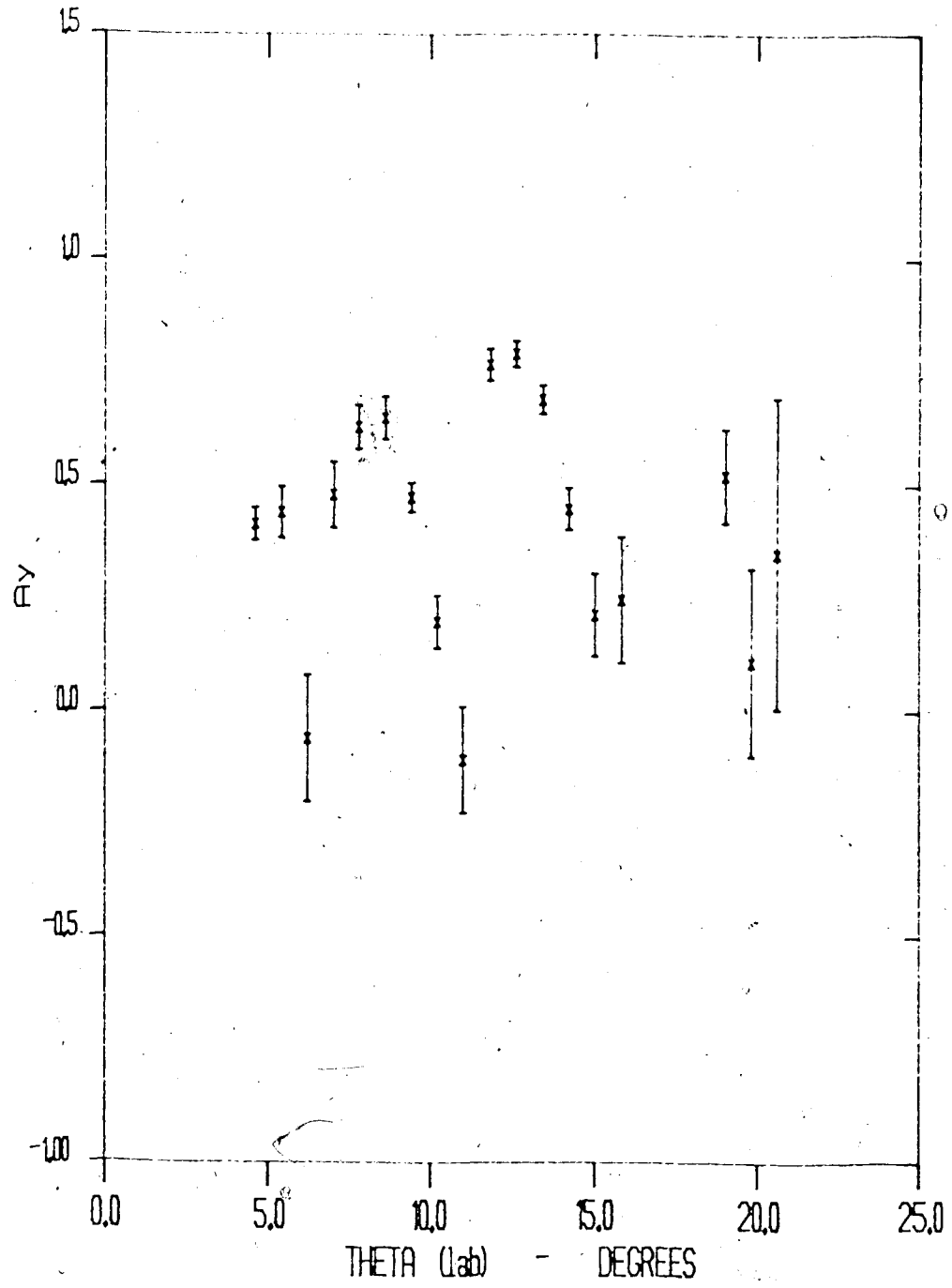


Figure IV-23: d + Ni 700 MeV, $A_y - 2^+$ State

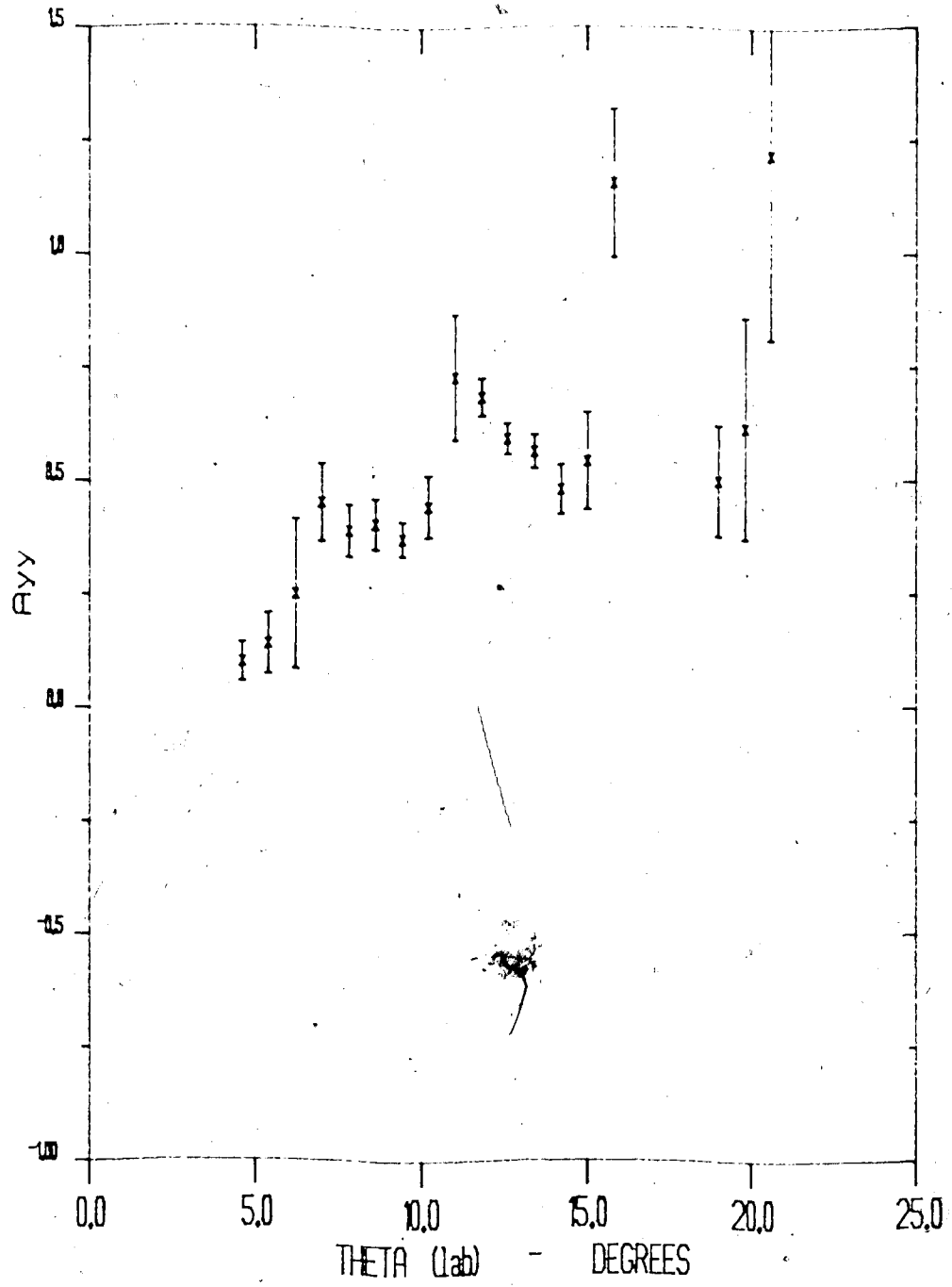


Figure IV-24: d + Ni 700 MeV, A_{yy} - 2⁺ State

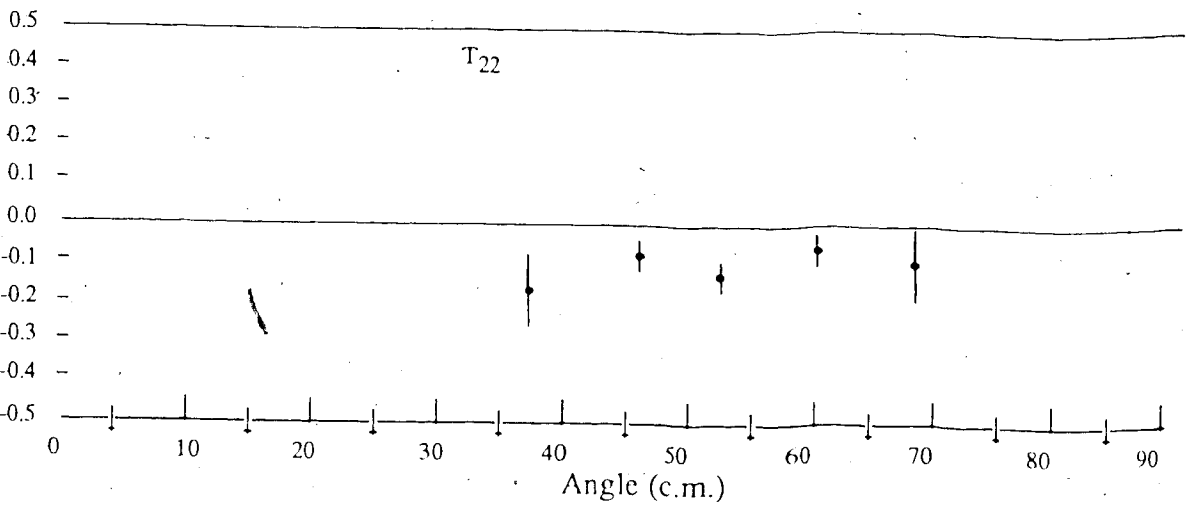
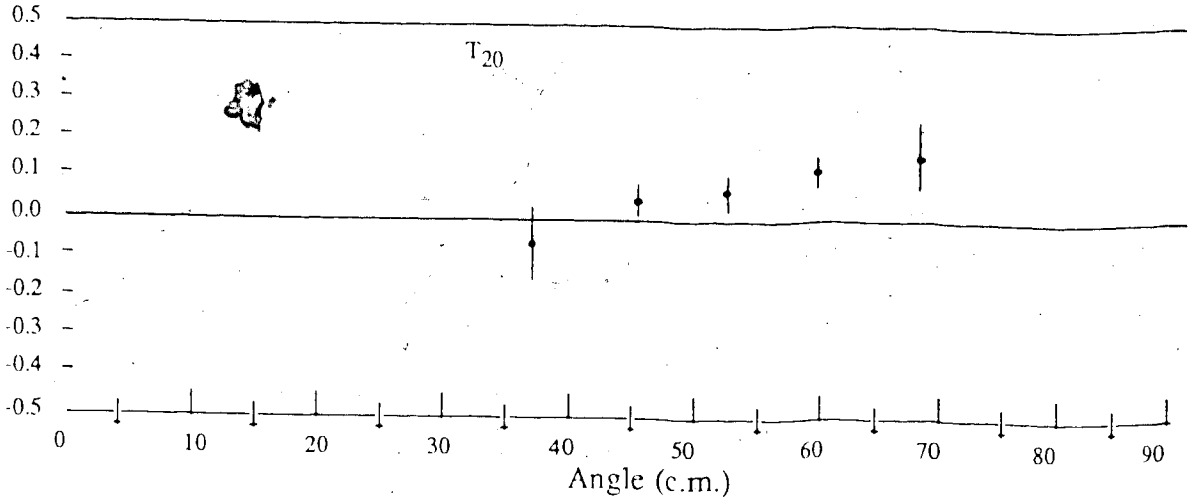
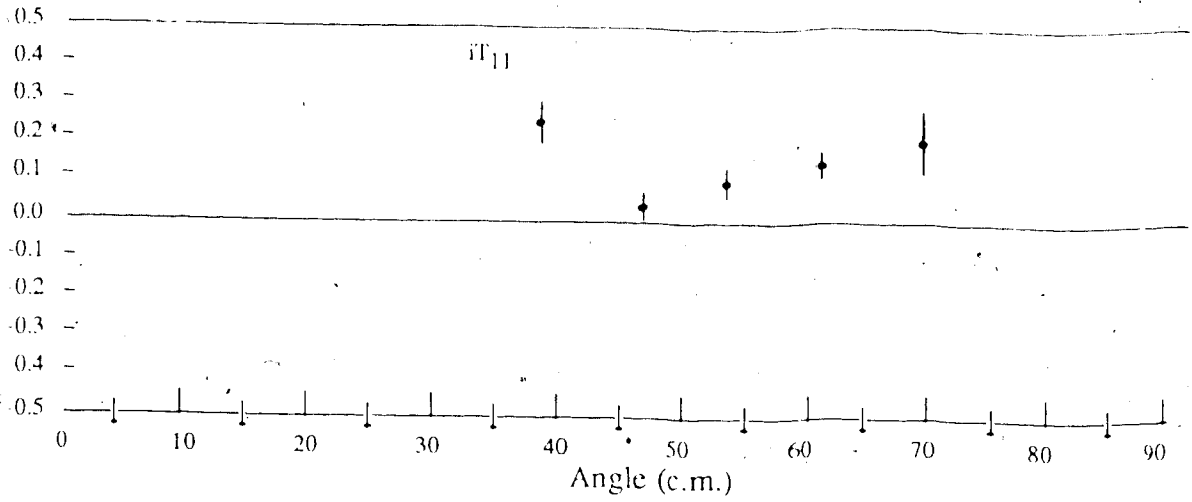


Figure IV-25 : d + d 191 MeV • Elastic Scattering

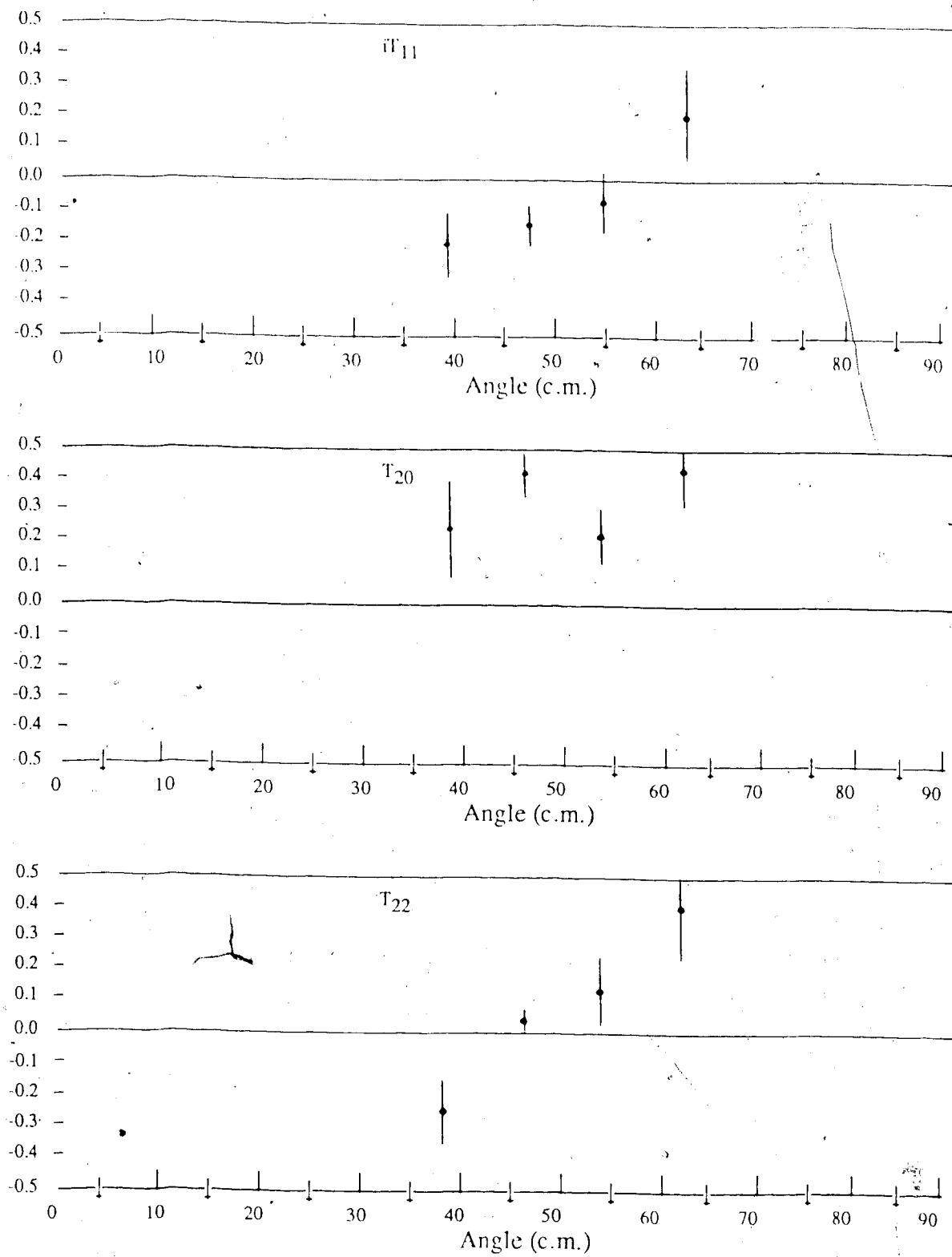


Figure IV-26: $d + d$ 395 MeV • Elastic Scattering

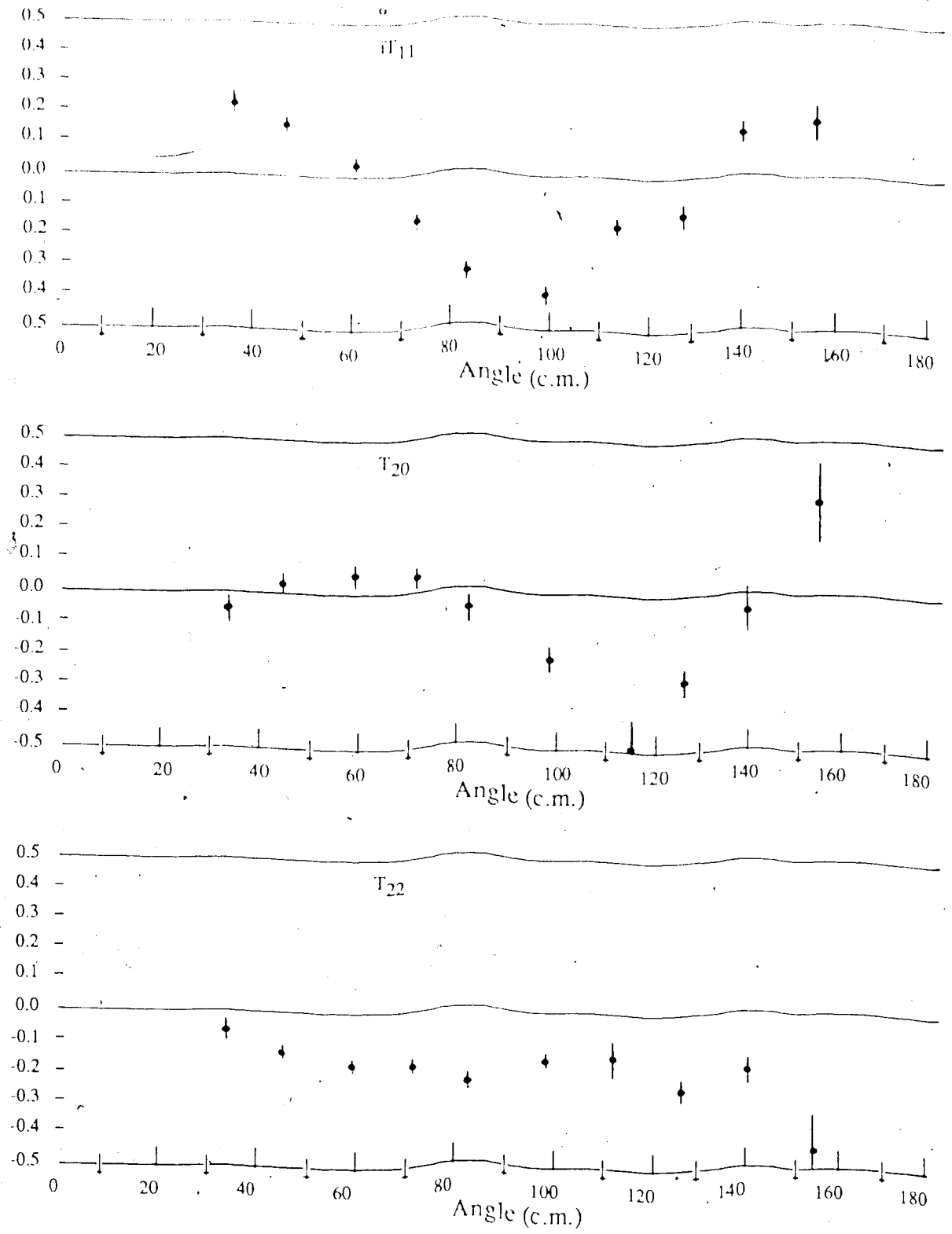


Figure IV-27 : d + p 191 MeV • Elastic Scattering

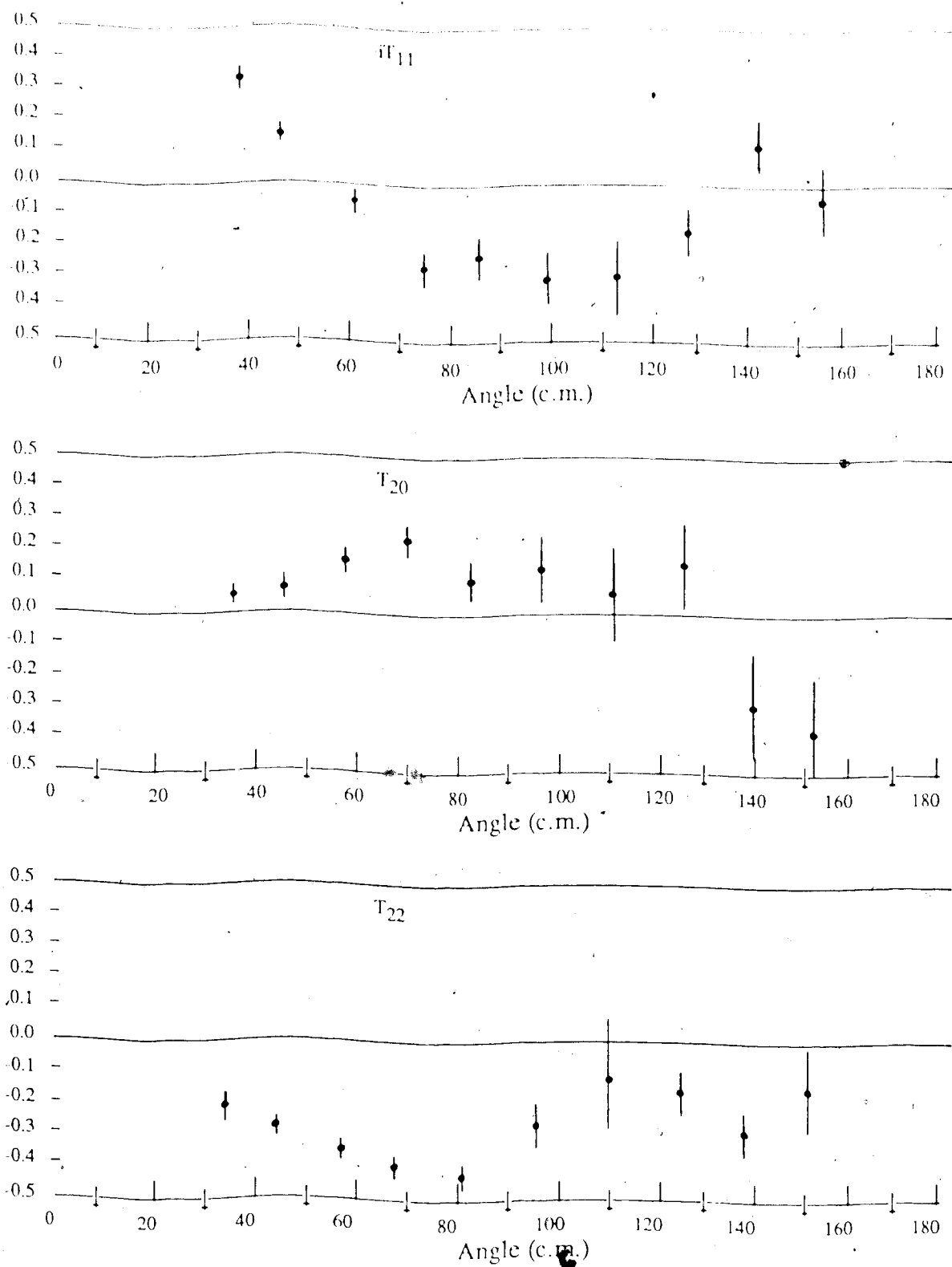


Figure IV-28 : $d + p$ 395 MeV • Elastic Scattering

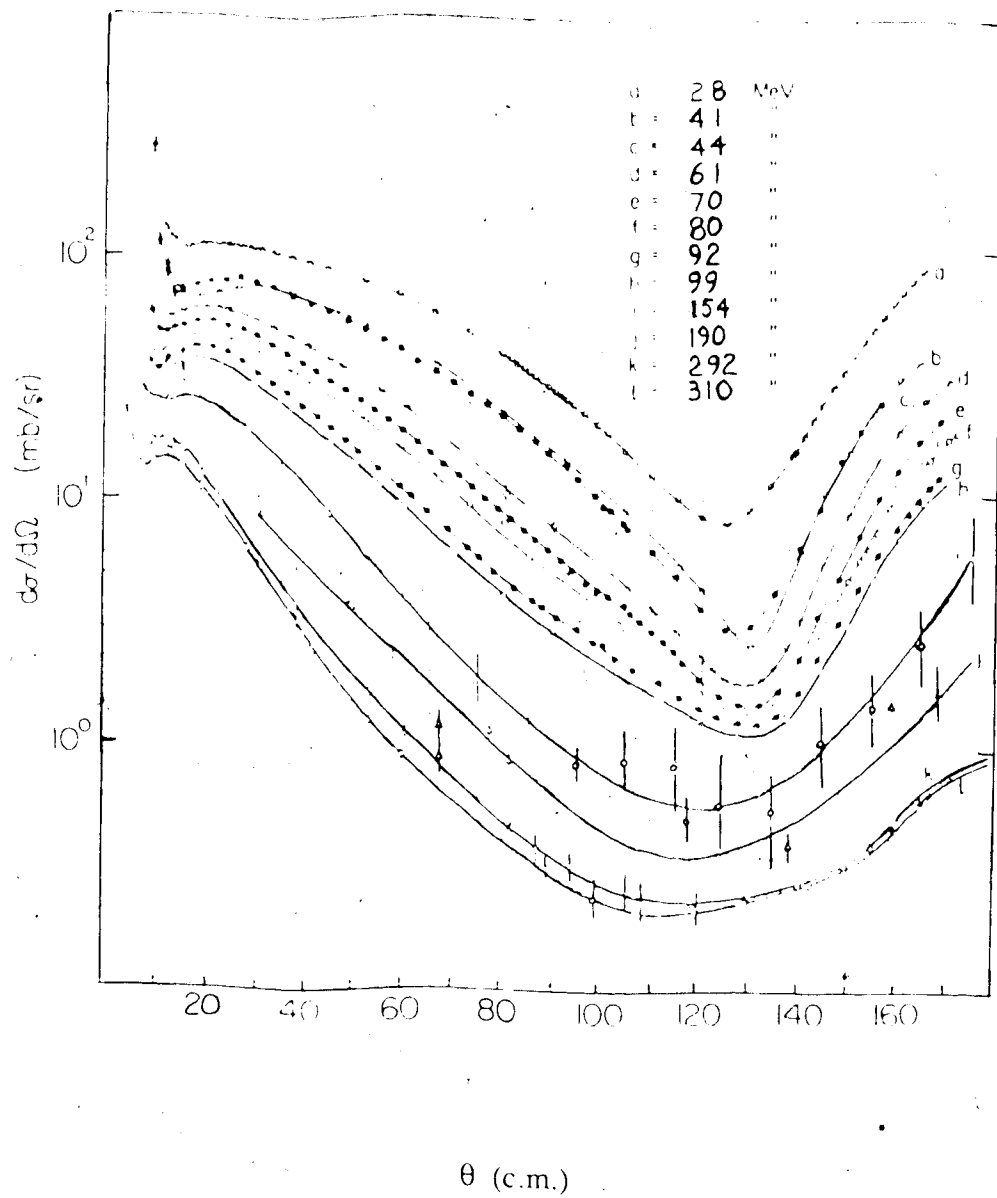


Figure IV-29 : d + p differential cross section for various energies.

Chapter V - Deuteron Tensor Polarimeters

In this chapter some aspects of low energy deuteron polarimeters, as well as the medium energy polarimeter currently under construction at the University of Alberta, will be discussed. A prerequisite to the design of a tensor polarimeter is an understanding of the method of determining initial polarization from the accumulated data. This topic is the first to be discussed.

I. Method of Determination of Deuteron Polarization

As shown in Chapter II, the possible components of spherical tensor polarization are t_{11} , t_{20} , t_{21} , and t_{22} . Three of these four polarizations may be determined unambiguously by measuring differential cross sections of scatterings off target nuclei as functions of ϕ and θ . The value of t_{21} will be determined except for its sign. Necessary for this measurement is the knowledge of the values of the tensor analyzing powers T_{11} , T_{20} , T_{21} , and T_{22} , for the range of θ which is to be used. As an example, from the last chapter it was seen that for the dp reaction, T_{20} is large between 85° and 148° . This fact suggests that this angular region is an appropriate θ range to use, and the values of the other asymmetries must be known for this region. The only necessary analyzing power not determined from the radiography experiment is T_{21} . An experiment is currently being planned to measure T_{21} by rotating the beam polarization axis in a magnetic field such that the t_{21} component is nonzero. If β is chosen such that $\text{Re}(t_{21})$ is nonzero, the term which contains T_{21} in the cross section expression 41-5 a) does not vanish. Measurement of T_{21} then becomes feasible.

The method of determining initial beam polarization begins with the most general cross section expression:

$$\sigma(\theta, \phi) = \sigma_0(\theta) \{1 + 2i\Gamma_{11}(\theta) \operatorname{Re}(it_{11}) + t_{20}T_{20}(\theta) + 2T_{21}(\theta) \operatorname{Re}(t_{21}) + 2T_{22}(\theta) \operatorname{Re}(t_{22})\}$$

If the detector used is rotated at an angle ϕ about the z axis, keeping the incident beam polarization fixed in space, the t_{kq} will be changed. With respect to the reaction plane, the spin system is rotated about the z axis by ϕ , the t_{kq} are transformed to \dagger_{kq} by the following:

$$t_{kq} = \dagger_{kq} e^{-iq\phi}$$

Upon substitution into the cross section equation, this leads to:

$$\sigma(\theta, \phi) = \sigma_0(\theta) \{1 + 2 \dagger_{11} T_{11}(\theta) \cos(\phi) + \dagger_{20} T_{20}(\theta) + 2 \dagger_{21} T_{21}(\theta) \sin(\phi) + 2 \dagger_{22} T_{22}(\theta) \cos(2\phi)\}$$

In a particular θ bin, the number of counts will follow the angular distribution

$$f(\phi) = (A/2\pi) (1 + 2 \dagger_{11} T_{11} \cos(\phi) + \dagger_{20} T_{20} + 2 \dagger_{21} T_{21} \sin(\phi) + 2 \dagger_{22} T_{22} \cos(2\phi)),$$

where A is assumed to be constant. Since the axis of polarization is at an arbitrary azimuthal angle, the phase ϕ_s must be incorporated in the above equation:

$$f(\phi) = [A/2\pi] [1 + 2 \dagger_{11} T_{11} \cos(\phi - \phi_s) + \dagger_{20} T_{20} + 2 \dagger_{21} T_{21} \sin(\phi - \phi_s) + 2 \dagger_{22} T_{22} \cos(2(\phi - \phi_s))]]$$

Use trigonometric identities to arrive at the following:

$$f(\phi) = [1/2\pi] [A + \Theta A + \Lambda A \cos(\phi) + B A \sin(\phi) + \Gamma A \cos(2\phi) - \Gamma A \sin^2(\phi) + \Xi A \sin(\phi) \cos(\phi)]$$

The new constants are defined as:

$$\Theta = \dagger_{20} T_{20}$$

$$\Lambda = (2 \dagger_{11} T_{11} \cos(\phi_s) - 2 \dagger_{21} T_{21} \sin(\phi_s))$$

$$B = (2 \dagger_{11} T_{11} \sin(\phi_s) + 2 \dagger_{21} T_{21} \cos(\phi_s))$$

$$\Gamma = 2 \dagger_{22} T_{22} \cos(2\phi_s)$$

$$\Xi = 4 \dagger_{22} T_{22} \sin(2\phi_s)$$

The next step in the procedure involves calculating several integrals of $f(\phi)$ with various trigonometric factors, then comparing them to equivalent sums of counts from the ϕ bins in the polarimeter:

$\int_0^{2\pi} f(\phi) d\phi = \sum_{\text{ev}} 1 = A(1 + \Theta) = N$, the total number of counts in the particular θ bin

$$\int_0^{2\pi} f(\phi) \cos(\phi) d\phi = \sum_{\text{ev}} \cos(\phi) = A \Lambda / 2 \quad \text{V-1 b)}$$

$$\int_0^{2\pi} f(\phi) \sin(\phi) d\phi = \sum_{\text{ev}} \sin(\phi) = A B / 2 \quad \text{V-1 c)}$$

$$\int_0^{2\pi} f(\phi) \cos^2(\phi) d\phi = \sum_{\text{ev}} \cos^2(\phi) = [2(\Theta + 1) + \Gamma] A / 4 \quad \text{V-1 d)}$$

$$\int_0^{2\pi} f(\phi) \sin^2(\phi) d\phi = \sum_{\text{ev}} \sin^2(\phi) = [2(\Theta + 1) - \Gamma] A / 4 \quad \text{V-1 e)}$$

$$\int_0^{2\pi} f(\phi) \cos(\phi) \sin(\phi) d\phi = \sum_{\text{ev}} \cos(\phi) \sin(\phi) = A \Xi / 8 \quad \text{V-1 f)}$$

In ed scattering where the electron is unpolarized, when only one photon exchange is involved, t_{11} is identically zero, and the constants become:

$$\Theta = t_{20} T_{20} \quad \text{V-2 a)}$$

$$\Lambda = -2 t_{21} T_{21} \sin(\phi_s) \quad \text{V-2 b)}$$

$$B = 2 t_{21} T_{21} \cos(\phi_s) \quad \text{V-2 c)}$$

$$\Gamma = 2 t_{22} T_{22} \cos(2\phi_s) \quad \text{V-2 d)}$$

$$\Xi = 4 t_{22} T_{22} \sin(2\phi_s) \quad \text{V-2 e)}$$

The axis of quantization, ξ , is also oriented at some polar angle β' relative to the beam direction. The tensor polarizations t_{20} , t_{21} , and t_{22} are not independent and are related by relative populations of spin projections as seen in Chapter II. Because t_{20} may then be reduced further in terms of β' and a tensor polarization ρ_{20} :

$$t_{20} = \rho_{20} [3\cos^2(\beta') - 1] / 2 \quad \text{V-3}$$

$$t_{21} = \sqrt{3/2} \rho_{20} \cos(\beta') \sin(\beta') \quad \text{V-4}$$

$$t_{22} = \sqrt{3/8} \rho_{20} \sin^2(\beta') \quad \text{V-5}$$

The unknown variables which remain to be determined are ρ_{20} , β' , and ϕ_s .

Combining equations V-2 b) and V-2 c), the value of ϕ_s is found to within a phase factor of π .

$$\tan(\phi_s) = -A \Lambda / A B$$

Combining equations V-2 b), 2 d), 3, and 5, leads to the expression for β' :

$$\tan(\beta') = -2 [\Gamma \Lambda / \Lambda A] [T_{21} \sin(\phi_s) / T_{22} \cos(2\phi_s)]$$

To determine the final parameter ρ_{20} , combine equations V-2 a), 2 b), 3, and 4:

$$\rho_{20} = -2A\Lambda / [2\sqrt{6} \Lambda \Theta \sin(\beta') \cos(\beta') T_{21} \sin(\phi_s) + A\Lambda T_{20} (3\cos^2(\beta') - 1)]$$

The tensors polarizations are then easily found, however due to the uncertainty in the phase of ϕ_s , the sign of \dagger_{21} will remain unknown.

The above treatment has been done for only one θ bin. To obtain the most statistics in order to reduce the errors in the calculated polarizations, the measurements should be taken over a θ region which has reasonably large T_{2q} . It is clear that as long as the error bars on a particular set of T_{2q} values are relatively constant, having greater values of T_{2q} will reduce the errors in the calculated polarizations. Therefore when calculating the polarizations, weighted sums are used in order that the regions of largest T_{2q} are represented most, in an effort to reduce such errors. This simple method involves redefining the above constants V-2 such that:

$$\Theta = \dagger_{20} \quad \text{V-6 a)}$$

$$\Lambda = -2 \dagger_{21} \sin(\phi_s) \quad \text{V-6 b)}$$

$$B = 2 \dagger_{21} \cos(\phi_s) \quad \text{V-6 c)}$$

$$\Gamma = 2 \dagger_{22} \cos(2\phi_s) \quad \text{V-6 d)}$$

$$\Xi = 4 \dagger_{22} \sin(2\phi_s) \quad \text{V-6 e)}$$

The sums V-1 must be calculated such that the values of T_{2q} are not treated as constants.

$$\sum_{ev} 1 = A (1 + \Theta T_{20}) = N, \text{ the total number of counts}$$

$$\sum_{ev} \cos(\phi) = A \Lambda T_{21} / 2 \quad \text{V-7 b)}$$

$$\sum_{ev} \sin(\phi) = A B T_{21} / 2 \quad \text{V-7 c)}$$

$$\Sigma_{eV} \cos^2(\phi) = [2(\Theta T_{20} + 1) + \Gamma T_{22}] A / 4 \quad \text{V-7 d)}$$

$$\Sigma_{eV} \sin^2(\phi) = [2(\Theta T_{20} + 1) - \Gamma T_{22}] A / 4 \quad \text{V-7 e)}$$

$$\Sigma_{eV} \cos(\phi) \sin(\phi) = A \Xi T_{22} / 8 \quad \text{V-7 f)}$$

Calculation of ρ_{20} , β' , and ϕ_S , is performed as in the manner demonstrated for a single θ bin.

2. Low Energy Deuteron Polarimeters

Measurements of deuteron tensor polarization have been successfully carried out at lower energies using several other analyzing reactions.

For example the low energy polarimeter at LNS utilizes the reaction $d(d,p)t$ at 380 keV, for which the spherical tensor polarization are known to an uncertainty of 6%. The target is deuterium absorbed in titanium 1.8 mg/cm² thick which is deposited on 10.5 mg/cm² of aluminum foil. The ratio of deuterium atoms to titanium atoms is 1.8.

Recoil protons between 3 and 4 MeV are counted by surface barrier silicon detectors at scattering angles of -120° , 0° , and $+120^\circ$. Measurement of beam tensor polarization involves the use of the 0° detector, where measurement of the vector polarization requires the $\pm 120^\circ$ detectors. The number of incident deuterons is determined by stopping the beam in a target foil backing which is electrically isolated. Current from this foil is then measured to give the deuteron flux. Considering equations II-6 and the ratio R_t of equation III-1, at 0° this ratio becomes:

$$R_t = \rho_{20} T_{20}(0^\circ) / 2$$

The value of $T_{20}(0^\circ)$ has been measured to be -0.669 ± 0.040 , so the beam tensor polarization ρ_{20} may then be readily determined. The uncertainty in this quantity is a direct result of the uncertainty in $T_{20}(0^\circ)$. It is interesting to note that estimates [12] have shown

values of $T_{20}(120^\circ) = -0.042 \pm 0.010$ and $T_{22}(120^\circ) = -0.053 \pm 0.015$.

With the value of $iT_{11}(120^\circ) = 0.175 \pm 0.007$, determination of vector polarization ρ_{10} involves the following calculation, again referring to equations II-6 and III-1:

$$N_{G1} = N(120^\circ)_1 + N(120^\circ)_{1+2}$$

$$N_{D1} = N(-120^\circ)_1 + N(-120^\circ)_{1+2}$$

$N(\theta)$ is the normalized number of counts in the detector at angle θ for beam polarization i .

And

$$L = [N_{G1}N_{D2}/N_{G2}N_{D1}]^{1/2}$$

$$R_V = L - 1/L = \sqrt{2} \rho_{10} iT_{11}$$

In a similar energy range the reaction ${}^3\text{He}(d,p){}^4\text{He}$ has also been used successfully. The first methods of measuring deuteron spherical tensor polarization at 2 - 9 MeV involved degrading the deuteron energy to ≈ 430 keV [13] where a $S_{3/2+}$ resonance exists.

It was then shown by Greubler et. al. [14] that the same reaction may be used to measure the cartesian tensor polarizations of deuterons of up to 15 MeV provided the ${}^3\text{He}$ gas density is high enough. At this higher energy the reaction cross section is much lower and in order to keep the figure of merit at a reasonable level it is necessary to increase the gas density. The measurement of the cartesian analyzing powers was done by placing four or more detectors at certain positions around the azimuth of the system. Using this method, all of the cartesian asymmetries could be measured. Once the asymmetries are known, a similar method is employed in order to determine initial beam polarizations.

The ${}^3\text{He}(d,p){}^4\text{He}$ reaction has further been shown to be operable in the energy range from 20 to 27 MeV [15]. It has been used in a polarimeter which measures t_{20} for recoil deuterons in ed elastic scattering in this energy range. This polarimeter consists of front scintillation counters to monitor deuteron flux and rear scintillation counters to detect

recoil protons exiting near 0° . There are also 2 front end wire chambers, and an energy counter which is placed behind the rear scintillator. The axially symmetric energy counter is composed of 4 segments to monitor the effects of other polarization components. There is also a proton veto counter at the extreme rear of the apparatus which cuts out higher energy protons from other sources, and a Ta deuteron stopper before the rear scintillator which eliminates noninteracting deuterons.

Incident deuterons of energy between 20 and 27 MeV pass through the front end counters and are energy degraded to approximately 6 MeV. In this analyzing reaction, $T_{20}(0^\circ)$ reaches a local minimum of -1.3 at this energy. The efficiency of this polarimeter reaches a maximum of about 1.2×10^{-4} at 23 MeV, and has a figure of merit of 8.6×10^{-3} .

The obvious problems of finding reactions with sufficiently large cross sections and analyzing powers at energies greater than 27 MeV are the limiting factors in the design of medium energy tensor polarimeters. There have been other attempts made at performing the measurements on deuterons of up to 60 MeV by degrading the incident energy, however this results in a rapidly decreasing efficiency.

Measurements of spherical tensor analyzing powers for dp scattering have been made at the Indiana University Cyclotron Facility [16] at 80 MeV. These asymmetries are shown in Figure V-1. Note that the T_{20} values seen at 120° reach a local minimum of -0.6. For a polarimeter built utilizing this reaction as a basis, at 80 MeV the efficiency would be 6×10^{-3} using a target 0.6 g/cm^2 thick, and would have a figure of merit for T_{20} as large as 3.2×10^{-2} .

3. Medium Energy Deuteron Polarimeter

The basis for the high efficiency, medium energy deuteron polarimeter is the

relatively large values of T_{20} for dp scattering between 80 and 191 MeV. As seen in the last chapter, the values of T_{20} dips to -0.6 as is negative between 85° and 148° in the c.m. frame. Kinematics of the $d(p,p)d$ reaction show that in the lab frame, the corresponding deuteron scattering angles are between 25° and 30° . Possible scattered deuteron energies range from 40 MeV to 120 MeV. The recoil proton may exit the reaction at angles between 16° and 46° with energies between 163 and 80 MeV. Figure V-2 is a table of dp kinematics.

It is also necessary to use liquid hydrogen for the polarimeter to have a high figure of merit. Based on the estimated size of the deuteron beam spot from the ed scattering and the range of 200 MeV deuterons in liquid hydrogen, the dimensions of the target are to be 10 cm in diameter and 25 cm long. With these target dimensions it is possible that the lower energy deuterons from the scattering may not have sufficient energy to exit the target. Alpha particles should have no difficulty passing through the target.

The kinematics of the reaction determine the physical requirements of the polarimeter. It must cover as much of the entire azimuthal angle as possible, and between 16° and 46° of the polar angle. It is in the lower region of these angles that the deuteron may not escape the target, and the proton is the sole particle to be detected. Because of resolution considerations, and range limitations of the low energy deuterons from the scattering, the polarimeter must be constructed such that a minimum of mass exists between the target and the detecting apparatus.

A calorimeter is to be incorporated into the polarimeter in order to determine the energy of the scattered particles. This energy measurement is necessary in to determine elastic scattering events, as well as to assist in reduction of errors in measured quantities by kinematical overdetermination. A thin scintillator placed before the energy counters is to be used in dE/dx measurements for particle identification in ambiguous kinematical situations.

A Monte Carlo simulation of events from dp scattering in the polarimeter has been carried out. The detailed design of the polarimeter used for this simulation will not be discussed here, however some of the important results will be noted. The input parameters for the program are ρ_{20} and β' .

Incident Deuteron energy of 120 MeV with an energy spread of 4 % was used with the liquid hydrogen target described above. The deuteron loses energy as it traverses the target. In this energy region the cross section for the dp reaction increases with decreasing energy, therefore the majority of the reactions occur in the downstream region of the target. Figure V-3 shows a plot of deuteron energy at the scattering point. The energies of the particles leaving the target are calculated from the kinematics, and the particles are tracked through the polarimeter. Distributions of all scattering events and all detected events are shown in Figure V-4. The probability of multiple scattering is taken into account for the deuterons, and has been shown in Figure V-5.

The particle then traverses through the remainder of the polarimeter which includes various target insulating layers, 2 cylindrical argon - methane wire chambers, the AE scintillator, and the calorimeter. Energy loss, straggling, and multiple scattering are taken into account for each part of the apparatus.

Preliminary tests have been performed for a 50,000 event run. In this simulation ρ_{20} and β' were set to 0.80 and 75° respectively. The analysis gave $\rho_{20} = 0.828 \pm 0.030$, and $\beta' = 73.1^\circ \pm 1.3^\circ$ however in the ed scattering experiment to be performed, the statistics will be much more limiting than in this test.

Inelastic scattering events which are not detectable from the recorded kinematics might have the effect of reducing the analyzing powers. Figure V-5 shows an energy spectrum of the $d(p,p)np$ reaction at 80 MeV, and from this graph the proportions of elastic, inelastic, and breakup events may be seen. Figure V-5 also shows the tensor analyzing powers for these different kinematic regions. Note that the analyzing powers for

the inelastic events are of the same sign as that of elastic scattering and are generally 50 to 100 % of the elastic values. Hence inclusion of a small amount of inelastic scattering is expected to have a small effect [17].

Resolution in the azimuthal angle must be sufficient to separate $\cos(\phi)$, $\cos(2\phi)$, and no $\cos(\phi)$ dependences. If the ϕ bin size is the order of 10° , ϕ resolution of 1° or 2° will be sufficient. This value is comparable to the multiple scattering expected to take place within the polarimeter.

It must be noted that the relationships between the analyzing powers and the incident deuteron energy have not yet been experimentally measured at all energies, however the energy dependence is expected to be minimal. Upon reexamination of Figure V-1, it is seen that the asymmetries are relatively unchanged from the 191 MeV case which is justification for the assumption of small analyzing power energy dependence. Note also that the values of the analyzing powers for the 395 MeV case are very different from the 191 MeV data, which suggests strong energy dependence somewhere above 200 MeV. Further data will be collected in order to completely investigate the energy dependence.

Upon completion of construction and testing, the Alberta High Efficiency Deuteron Polarimeter (AHED Polarimeter) will be taken to LNS for calibration. The AHED polarimeter will then be taken to the Bates Linear Accelerator Center for the electron deuteron scattering experiment to separate the deuteron charge and quadrupole form factors.

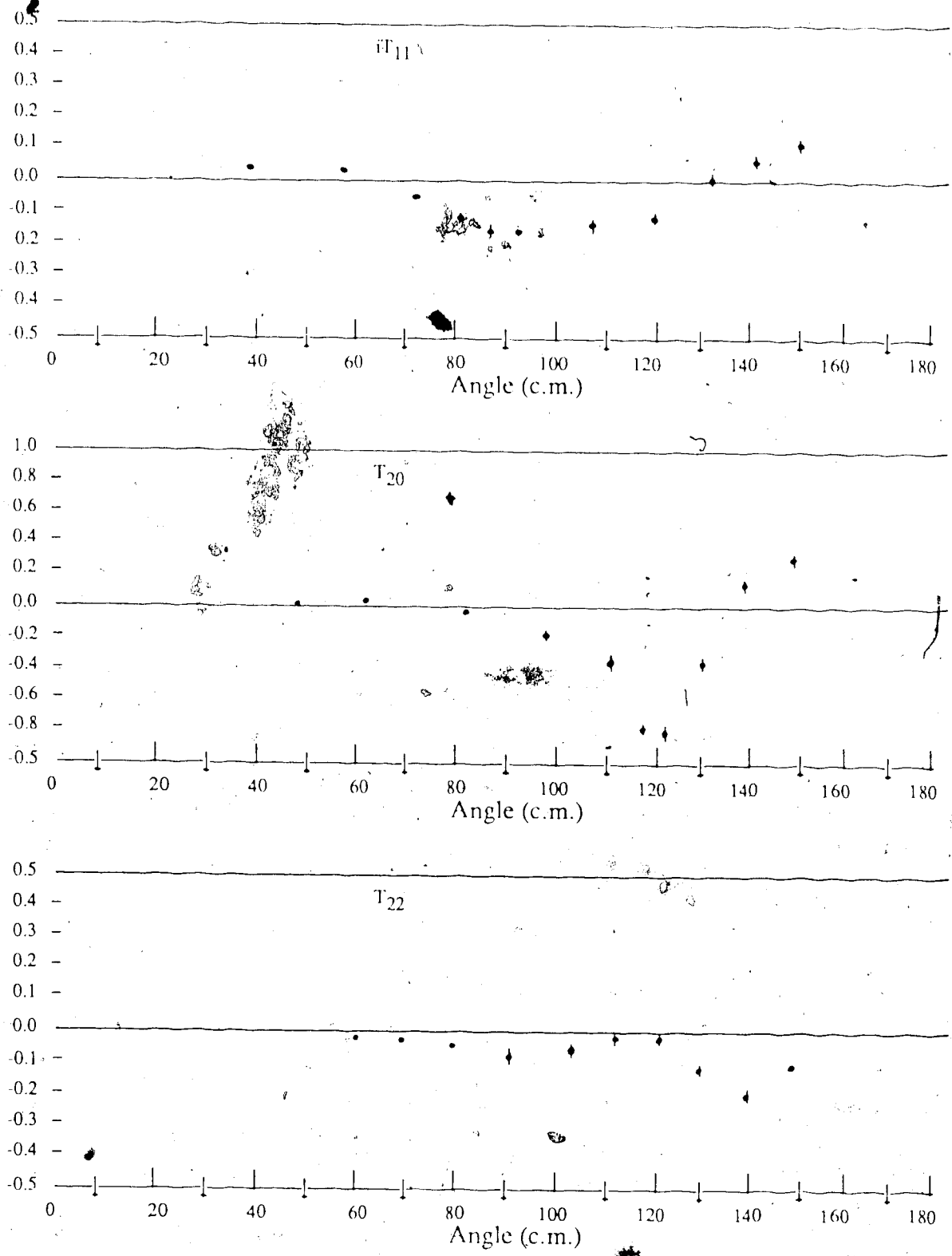


Figure V-1 : d + p 80 MeV • Elastic Scattering

$d + p \rightarrow d + p$ 200 MeV deuteron kinetic energy

θ c.m.	<u>Deuteron</u>		<u>Proton</u>	
	θ lab	E lab	θ lab	E lab
50	15.87	168.1	63.99	31.94
55	17.34	161.9	61.42	38.12
60	18.79	155.3	58.86	44.70
65	20.19	148.4	56.31	51.62
70	21.54	141.2	53.77	58.83
75	22.84	133.7	51.23	66.27
80	24.07	126.1	48.71	73.88
85	25.23	118.4	46.20	81.61
90	26.31	110.6	43.70	89.41
95	27.28	102.8	41.20	97.20
100	28.14	95.07	38.72	104.9
105	28.87	87.45	36.25	112.6
110	29.44	80.02	33.78	120.0
115	29.83	72.81	31.33	127.2
120	30.01	65.89	28.88	134.1
125	29.94	59.31	26.45	140.7
130	29.57	53.13	24.02	146.9
135	28.87	47.37	21.59	152.6
140	27.76	42.11	19.18	157.9
145	26.20	37.36	16.77	162.6
150	24.13	33.17	14.36	166.8
155	21.48	29.57	11.96	170.4
160	18.22	26.58	09.56	173.4
165	14.35	24.23	07.17	175.8
170	09.93	22.55	04.78	177.5

Figure V-2: $d + p$ elastic scattering kinematics

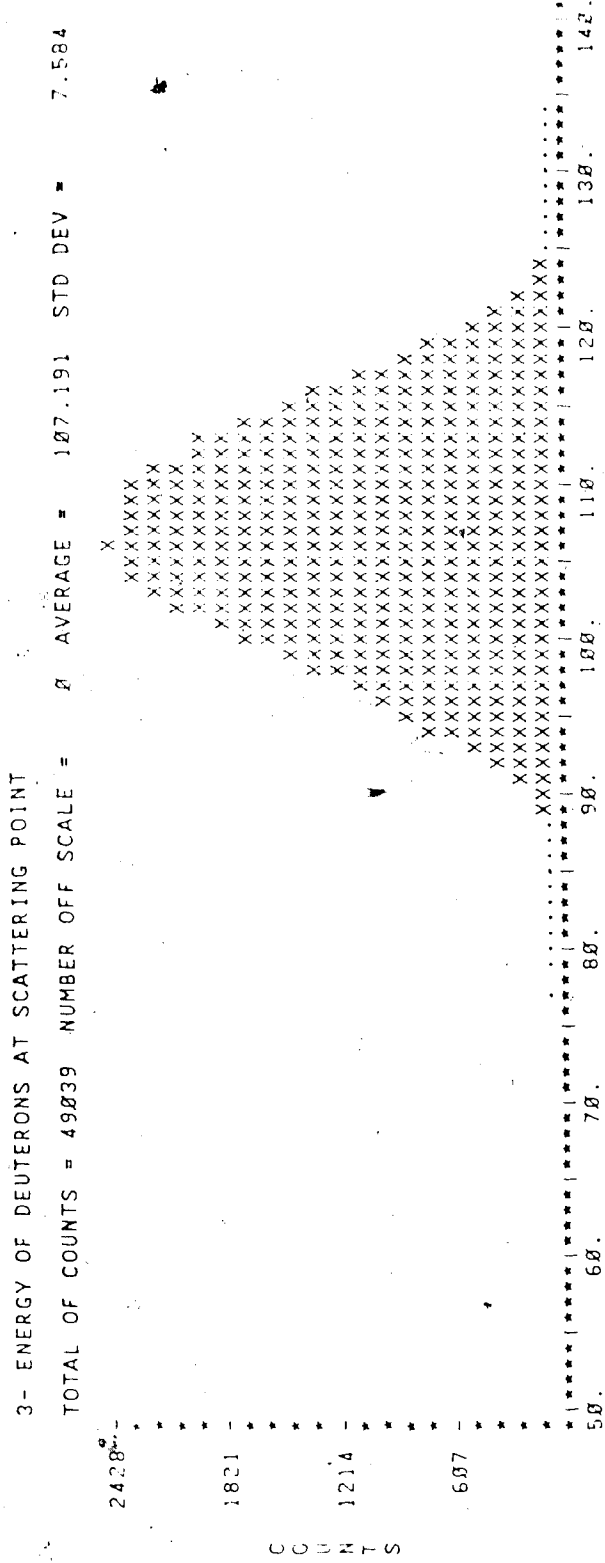
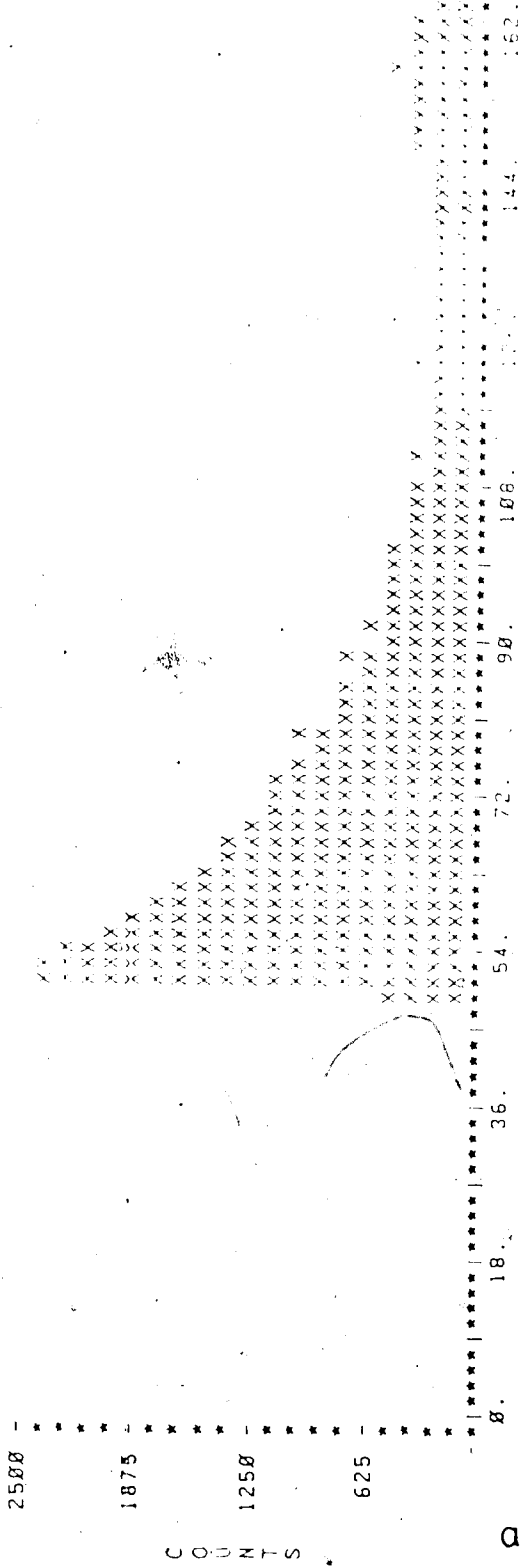


Figure V-3 : Deuteron energy distribution at the scattering point. Mean incident deuteron energy = 120 MeV.

TOTAL OF COUNTS = 49039 NUMBER OFF SCALE = 0 AVERAGE = 86.807 STD DEV = 33.975



TOTAL OF COUNTS = 43739 NUMBER OFF SCALE = 0 AVERAGE = 81.268 STD DEV = 27.445

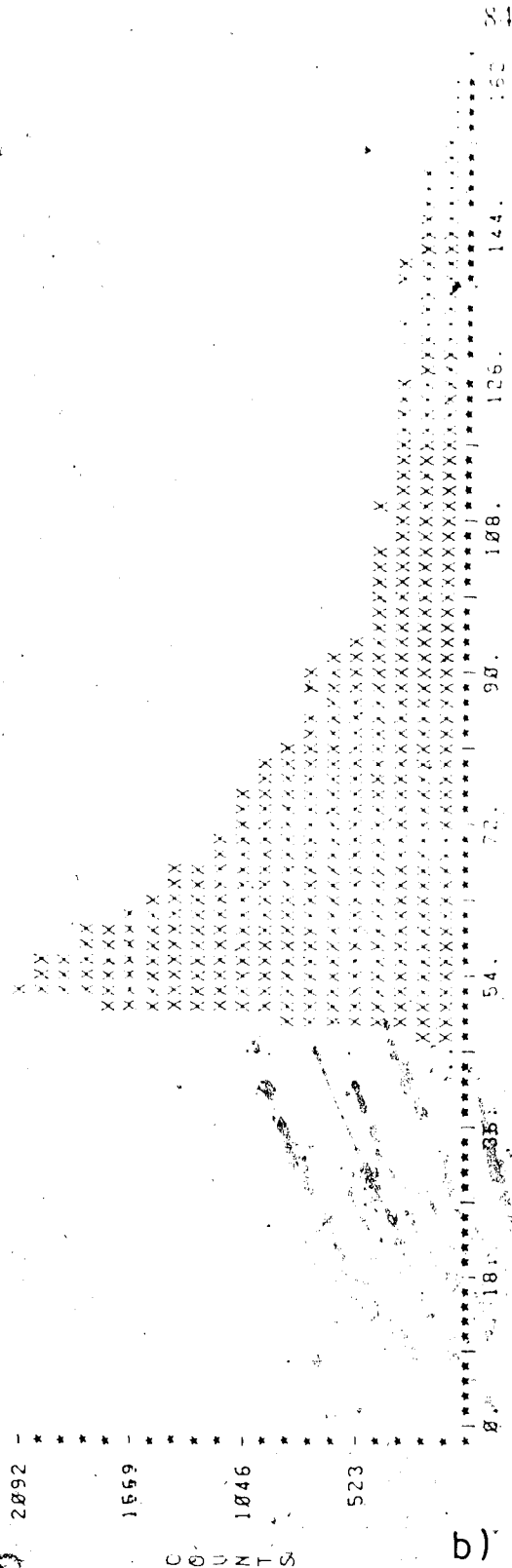


Figure V-4 : a) Distribution of all scattered particles as a function of θ (c.m.)
 b) Distribution of all detected events as a function of θ (c.m.)

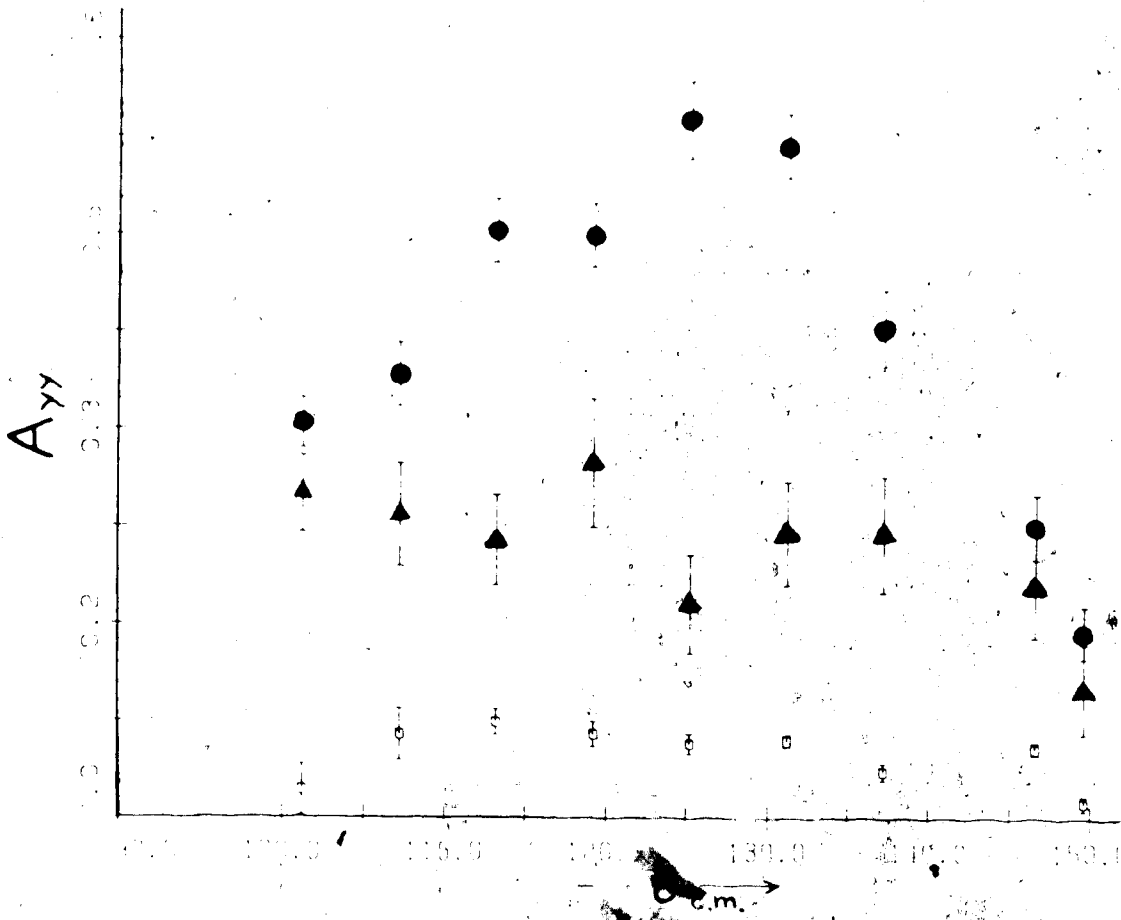
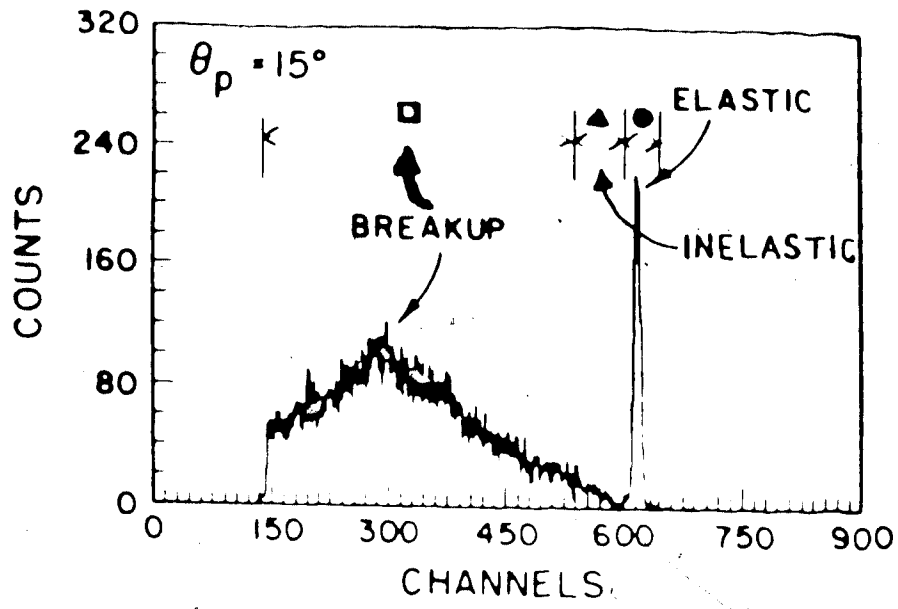


Figure V-5 : $d + p \quad 80 \text{ MeV}$
 a) Inclusive proton spectrum for a laboratory proton angle = 15° .
 b) A_{yy} for breakup, inelastic, and elastic events.

Bibliography

Jackson D.G., **Nuclear Reactions**, Muthuen & Co. Ltd. (London) 1970

Roy, R., and Nigam, B.P., **Nuclear Physics**, John Wiley and Sons (London) 1967

Yuan & Wu, **Methods of Experimental Physics**, Volume 5, Part A, Academic Press
(New York and London) 1961.

Robson, B. A., **The Theory of Polarization Phenomenon**, Clarendon Press
(Oxford) 1974

References

1. Jackson D.G., Nuclear Reactions, (Muthuen & Co. Ltd., London, 1970)
2. Goldfarb, L.J.B., Nuclear Physics, 7(1958)622
3. Lakin, W., Physical Review 98(1955)139
4. Proc. Third Int. Polarization Symp., ed. H.H. Barschall and W. Haeblerli (Univ. of Wisconsin Press, Madison, 1971)
5. Arvieux, J. et al., Nuclear Physics, A431(1984)613
6. Arvieux, J., Polarisation Proton Ion Sources, ed. A. D. Krisch and A.T.M. Lin, AIP Conference Proceedings, 80(1982) 185
7. Duchazeaubeneix, J.C., Radiographie par Diffusion Nucleaire de Protons d'Energies Intermediaires, These pour Obtenir le Titre de Docteur d'Universite, L'Universite de Paris Sud, Centre d'Orsay, 5 Fevrier '82.
8. Energy loss and range values available through Fortran program "Handbook" at the University of Alberta Nuclear Research Center, Edmonton, Alberta. This program is based upon the Bethe-Bloch equation. See Yuan & Wu, Methods of Experimental Physics, Volume 5, Part A, Academic Press - New York and London, 1961.
9. Ensembles de Detection Magnetique du Laboratoire National Saturne, Cycle de Seminars, sur less Equipments de Spectrometrie, Saclay - Mars a Juin 1980, Commissariat a l'Energie Atomique - Institut National de Physique Nucleaire at de Physique des Particules.
10. Nguyen Van Sen, et al., Elastic Scattering of Polarized Deuterons from ^{16}O at 200, 400, and 700 MeV, 6th International Symposium on Polarization Phenomenon in Nuclear Physics, Osaka, Japan, 26 - 30 Aug., 1985.
11. Nguyen Van Sen, et al., Physics Letters 156B (1985) 185

12. Arvieux, J., Calcul de la Polarisation du Faisceau de Déutons de Saturne II, LNS Internal Report LNS/071, 25 Nov. 1982
13. McIntyre, L.C., and Haeberli, W., Nuclear Physics A91 (1967) 369
14. Greubler, W., et al., Nuclear Inst. and Meth., 203 (1982) 235
15. Holt, R.J., et al., Phys. Rev. Lett., 43 (1979) 1229
16. IUCF Scientific and Technical Report, Jan. 1, 1983 to Dec. 31, 1983
17. Boudard, A., Mesure du Pouvoir d'Analyse T_{20} de la Diffusion Elastique Arrière dp dans la Région d'Excitation du Δ et Analyse Théorique de cette Réaction, Thèse pour Obtenir le Grade de Docteur d'Etat, L'Université de Paris Sud, Centre d'Orsay, 8 décembre '83.
18. Roy, R., and Nigam, B.P., Nuclear Physics, John Wiley and Sons (London) 1967

Appendix I

1. Deuteron Properties

mass	$m_D = 1875.587 \text{ MeV}$
spin - parity	$J^\pi = 1^+$
binding energy	$E_B = -2.225 \text{ MeV}$
magnetic dipole moment	$\mu_D = 0.8574 \text{ N.M.}$
electric quadrupole moment	$Q_D = 2.860 \times 10^{-27} \text{ cm}^2$

2. Deuteron Form Factors

The reaction cross section for ed scattering is given by:

$$d\sigma/d\Omega = (d\sigma/d\Omega)_{\text{MOTR}} [A(q) + B(q) \tan^2(\theta/2)]$$

$$A(q) = F_C^2(q) + 8\eta^2 F_Q(q) / 9 + 2\eta F_M^2(q) / 3$$

$$B(q) = 4\eta (1 + \eta) F_M^2(q) / 3$$

where $\eta = (q / 2m_D)^2$, and

$$F_C(q) = [G_{Ep} + G_{En}] \int_0^\infty r^2 [\Psi_S^2(r) + \Psi_D^2(r)] j_0(qr/2) dr$$

$$F_Q(q) = \{ 2 [G_{Ep} + G_{En}] / (8/9)^{1/2} \eta \} \int_0^\infty r^2 \Psi_D(r) [\Psi_S(r) - \Psi_D(r) / \sqrt{8}] j_2(qr/2) dr$$

$$F_M(q) = 2 [G_{Mp} + G_{Mn}] \int_0^\infty r^2 [\Psi_S^2(r) - \Psi_D^2(r) / 2] j_0(qr/2) dr$$

$$+ [G_{Mp} + G_{Mn}] \int_0^\infty r^2 [\Psi_S(r) \Psi_D(r) / \sqrt{2} - \Psi_D^2(r) / 2] j_2(qr/2) dr$$

$$+ \{ 3 [G_{Ep} + G_{En}] / 2 \} \int_0^\infty r^2 \Psi_D^2(r) [j_0(qr/2) + j_2(qr/2)] dr$$

where $\Psi_S(r), \Psi_D(r)$ are deuteron S and D state wave functions

$G_{Ep}, G_{En}, G_{Mp}, G_{Mn}$ are proton and neutron electric and magnetic form factors. They are also functions of q .

$j_l(qr/2)$ are the spherical Bessel functions

Appendix 2

1. Relations between Cartesian and Spherical Tensors

$$T_{10} = \sqrt{3/2} A_z$$

$$T_{1\pm 1} = \pm(-\sqrt{3}/2) (A_x \pm i A_y)$$

$$T_{20} = A_{zz}/\sqrt{2}$$

$$T_{2\pm 1} = \pm(-1/\sqrt{3}) (A_{xz} \pm i A_{yz})$$

$$A_x = (-1/\sqrt{3}) (T_{11} - T_{1-1})$$

$$A_y = (i/\sqrt{3}) (T_{11} + T_{1-1})$$

$$A_z = (\sqrt{2/3}) T_{10}$$

$$A_{xx} = \sqrt{3} (T_{22} + T_{2-2}) / 2 - T_{20} / \sqrt{2}$$

$$A_{yy} = -\sqrt{3} (T_{22} + T_{2-2}) / 2 - T_{20} / \sqrt{2}$$

$$A_{xy} = A_{yx} = -i \sqrt{3} (T_{22} - T_{2-2}) / 2$$

$$A_{xz} = A_{zx} = -\sqrt{3} (T_{21} - T_{2-1}) / 2$$

$$A_{yz} = A_{zy} = i \sqrt{3} (T_{22} + T_{2-2}) / 2$$

$$A_{zz} = \sqrt{2} T_{20}$$

2. Relations between Tensor Polarization and Deuteron Form Factors for ed Scattering

$$t_{20} = - \{ 8\eta^2 F_Q^2 / 9 + 8\eta F_C F_Q \sqrt{3} + 2\eta F_M^2 [1/2 + (1 + \eta) \tan^2(\theta/2)] / 3 \} / \sqrt{2} C$$

$$t_{2\pm 1} = \pm 2\eta (\kappa - \eta) F_M F_Q \tan(\theta/2) / \sqrt{2} C$$

$$t_{2\pm 2} = -\eta F_M^2 / 2\sqrt{3} C$$

where $\kappa = |\mathbf{p}| / m_D$

\mathbf{p} = incident electron momentum

m_D = deuteron mass

$$C = A(q) + B(q) \tan^2(\theta/2)$$

θ = scattering angle

Appendix 3

1. Rotation of Spherical Tensors

Rotation of spherical tensors is accomplished using Wigner D -matrices in a manner analogous to the rotation of the spherical harmonics. The transformation of ρ_{kq} to a rotated frame in which it becomes t_{kq} is the following [18]:

$$t_{kq} = \sum_{q'} \rho_{kq'} D_{q'q}^{(k)}$$

The matrix D is given in terms of the Euler angles Θ, β , and ϕ :

$$D_{q'q}^{(k)}(\Theta, \beta, \phi) = e^{-iq'\Theta} e^{-iq\beta} d_{q'q}^{(k)}(\phi)$$

where

$$d_{q'q}^{(k)}(\phi) = \sum_n (-1)^n [C_1/C_2(n)] [\cos(\phi/2)]^{2k+q-q'-2n} [-\sin(\phi/2)]^{2n+q'-q}$$

C_1 and $C_2(n)$ are given by:

$$C_1 = [(k+q)!(k-q)!(k+q)!(k-q)]^{1/2}$$

$$C_2(n) = (k-q'-n)!(k+q-n)!(n)!(q'-q+n)!$$

In the case of transforming ρ_{k0} through angles β and ϕ ,

$$D_{0q}^{(k)}(0, \beta, \phi) = (-1)^q [4\pi / (2k+1)]^{1/2} Y_{kq}(\beta, \phi)$$

where Y_{kq} are the spherical harmonics. The t_{kq} become:

$$t_{kq}(\beta, \phi) = \rho_{k0} (-1)^q [4\pi / (2k+1)]^{1/2} Y_{kq}(\beta, \phi)$$

The case of $\phi = 180^\circ$ rotation leads to the equations of Chapter II:

$$t_{00} = 1$$

$$t_{10} = \rho_{10} \cos(\beta)$$

$$i t_{11} = \rho_{10} \sin(\beta) e^{i\phi} / \sqrt{2}$$

$$t_{20} = \rho_{20} (3 \cos^2(\beta) - 1) / 2$$

$$t_{21} = -i \sqrt{3/2} \rho_{20} \sin(\beta) \cos(\beta) e^{i\phi}$$

$$t_{22} = -\sqrt{3/8} \rho_{20} \sin^2(\beta) e^{i2\phi}$$

Appendix 4

1. Parity Conservation in the Determination of Reaction Cross Section

As was stated in Chapter II, the reaction cross section for deuteron elastic scattering may be written:

$$\sigma(\theta) = \sigma_0(\theta) \sum_{kq} t_{kq} T_{kq}^*$$

Conservation of parity requires the analyzing tensors to be invariant under 180° rotation of the system about \mathbf{n} . As seen in the preceding appendix, spherical tensors transform as follows:

$$T_{kq} = \sum_{q'} T_{kq'} D_{q'q}^{(k)}$$

For this 180° rotation,

$$D_{q'q}^{(k)} = (-1)^{k-q'} \delta_{q',-q},$$

and

$$\begin{aligned} T_{kq} &= \sum_{q'} T_{k-q'} (-1)^{k-q'} \delta_{q',-q} \\ &= T_{k-q} (-1)^{k+q} \end{aligned}$$

From the property of the spherical tensors

$$T_{k-q} = (-1)^q T_{kq}^* \tag{A-4.1}$$

T_{kq} may be written

$$T_{kq} = (-1)^k [(-1)^q T_{k-q}]$$

Since $T_{kq}^\dagger = (-1)^q T_{k-q}$,

$$T_{kq} = (-1)^k T_{kq}^\dagger \tag{A-4.2}$$

From equations A-4.1 and A-4.2, the following relations may be found:

$$T_{00} = (-1)^0 T_{00}^* = T_{00}^* \quad \Rightarrow \quad T_{00} \text{ real}$$

$$T_{10} = (-1)^1 T_{10}^* = -T_{10}^*$$

$$T_{10}^* = (-1)^0 T_{10} = T_{10} \quad \Rightarrow \quad T_{10} = 0$$

$$T_{11} = (-1)^1 T_{11}^* = -T_{11}^*$$

$$T_{11}^* = (-1)^1 T_{1-1}^* = -T_{1-1} \quad \Rightarrow \quad T_{1-1} = T_{11}, \text{ imaginary}$$

$$T_{20} = (-1)^2 T_{20}^* = T_{20}^*$$

$$T_{20} = (-1)^0 T_{20} = T_{20} \quad \Rightarrow \quad T_{20} \text{ real}$$

$$T_{21} = (-1)^2 T_{21}^* = T_{21}^*$$

$$T_{21}^* = (-1)^1 T_{2-1} = -T_{2-1} \quad \Rightarrow \quad T_{21} = -T_{2-1}, \text{ real}$$

$$T_{22} = (-1)^2 T_{22}^* = T_{22}^*$$

$$T_{22}^* = (-1)^2 T_{2-2} = T_{2-2} \quad \Rightarrow \quad T_{22} = T_{2-2}, \text{ real}$$

Now the cross section may be written:

$$\sigma(\theta) = \sigma_0(\theta) \sum_{kq} t_{kq} T_{kq}^*$$

$$= \sigma_0(\theta) \sum_{kq} [\text{Re } t_{kq} \text{Re } T_{kq} - \text{Im } t_{kq} \text{Im } T_{kq}]$$

$$\sigma(\theta) = \sigma_0(\theta) [1 + 2 \text{Im } t_{11} \text{Im } T_{11}(\theta) + \text{Re } t_{20} \text{Re } T_{20}(\theta) + 2 \text{Re } t_{21} \text{Re } T_{21}(\theta) + 2 \text{Re } t_{22} \text{Re } T_{22}(\theta)]$$

This may also be written as in Chapter II:

$$\sigma(\theta) = \sigma_0(\theta) [1 + 2i T_{11}(\theta) \text{Re } it_{11} + t_{20} T_{20}(\theta) + 2 T_{21}(\theta) \text{Re } t_{21} + 2 T_{22}(\theta) \text{Re } t_{22}]$$

Appendix 5

1. Calculation of Analyzing Powers using Least Squares Fit

The ratios of Chapter III, R_α ($\alpha = 0, v, t$), are found using the method of least squares demonstrated here. To obtain the analyzing powers from these ratios, they must be multiplied by the appropriate constant. Recall the ratios

$$R_\alpha = S_{f\alpha} / S_f, \quad \text{where } S_{f\alpha} = \sum_i \epsilon_{\alpha i} F_i N_i, \quad \text{and } S_f = \sum_i F_i N_i.$$

The statistical errors in these ratios are given by

$$\Delta R_\alpha^2 = \sum_i (\partial R_\alpha / \partial N_i)^2 \Delta N_i^2$$

$$\text{where } (\partial R_\alpha / \partial N_i) = [\epsilon_{\alpha i} F_i S_f - F_i S_{f\alpha}] / S_f^2, \quad \text{and } \Delta N_i = \sqrt{N_i}.$$

Now

$$\begin{aligned} \Delta R_\alpha^2 &= \sum_i \{ [F_i^2 S_f^2 + F_i^2 S_{f\alpha}^2 - 2 \epsilon_{\alpha i} F_i^2 S_{f\alpha}] / S_f^4 \} N_i \\ &= \{ S_{f2} (S_f^2 + S_{f\alpha}^2) - 2 S_f S_{f\alpha} S_{f2\alpha} \} / S_f^4 \end{aligned}$$

$$\text{where } S_{f2} = \sum_i F_i^2 N_i \quad \text{and} \quad S_{f2\alpha} = \sum_i \epsilon_{\alpha i} F_i^2 N_i.$$

$$\text{Since } S_{f\alpha} = R_\alpha S_f,$$

$$\begin{aligned} \Delta R_\alpha^2 &= \{ S_{f2} (S_f^2 + R_\alpha^2 S_f^2) - 2 S_f^2 R_\alpha S_{f2\alpha} \} / S_f^4 \\ &= \{ S_{f2} (1 + R_\alpha^2) - 2 R_\alpha S_{f2\alpha} \} / S_f^2 \end{aligned}$$

and finally

$$\Delta R_\alpha = \{ S_{f2} (1 + R_\alpha^2) - 2 R_\alpha S_{f2\alpha} \}^{1/2} / S_f^2.$$

χ^2 for R_t is given by

$$\chi^2 = \sum_j \{ [R_{tj} - (A_{20} + A_{22} \cos_j(2\phi))] / \Delta R_{tj} \}^2 \quad \text{where } j \text{ refers to the } \phi \text{ bin, and } A_{20},$$

A_{22} are constants proportional to T_{20} and T_{22} .

The value of χ^2 must be minimized with respect to A_{20} and A_{22} :

$$\partial \chi^2 / \partial A_{20} = 0$$

$$\partial \chi^2 / \partial A_{22} = 0$$

Solving these equations gives

$$A_{22} = (S_1 S_{xy} - S_x S_y) / (S_1 S_x^2 - S_x S_x)$$

$$A_{20} = (S_y - A_{22} S_x) / S_1$$

$$\text{where } S_1 = \sum_j (1 / \Delta R_{tj}^2),$$

$$S_x = \sum_j (\cos_j(2\phi) / \Delta R_{tj}^2),$$

$$S_{xy} = \sum_j (R_{tj} \cos_j(2\phi) / \Delta R_{tj}^2),$$

$$S_x^2 = \sum_j (\cos_j^2(2\phi) / \Delta R_{tj}^2),$$

$$S_{xy} = \sum_j (R_{tj} / \Delta R_{tj}^2).$$

The statistical errors in A_{20} and A_{22} are given by

$$(\Delta A_{2q})^2 = \sum_j (\partial A_{2q} / \partial R_{tj})^2 \Delta R_{tj}^2,$$

and

$$\Delta A_{20} = [S_x^2 / (S_1 S_x^2 - S_x S_x)]^{1/2},$$

$$\Delta A_{22} = [S_1 / (S_1 S_x^2 - S_x S_x)]^{1/2}.$$

The correlation of errors of A_{20} and A_{22} are given by the value EC:

$$EC = [1 / (\Delta A_{20}) (\Delta A_{22})] \sum_j (\partial A_{20} / \partial R_{tj}) (\partial A_{22} / \partial R_{tj}) \Delta R_{tj}^2$$

The A_{2q} are related to the T_{2q} by

$$T_{20} = 2\sqrt{2} A_{20} |\rho_{20} / (\rho_{20})_{\max}|,$$

$$T_{22} = (2\sqrt{3}) A_{22} |\rho_{20} / (\rho_{20})_{\max}|.$$

The calculations for the vector part require the same procedure as for the tensor analyzing powers, however for R_v the value of χ^2 is given by

$$\chi^2 = \sum_j \{ [R_{vj} - (A_{22} \cos_j(\phi))] / \Delta R_{vj} \}^2$$